Supporting Information

BODIPY Analogues: Synthesis and Photophysical studies of difluoro Boron complexes from 2-Aminotropone Scaffolds through *N,O*-Chelation

Bibhuti Bhusana Palai,[§] Ramachandra Soren[§] and Nagendra K. Sharma*

School of Chemical Sciences, National Institute of Science Education and Research (NISER), Jatani-752050, Odisha, India.
& HBNI-Mumbai, Mumbai-India

*Corresponding author. Tel.: 0674-249-4141; fax: +91 (674) 2494004; E-mail: nagendra@niser.ac.in

§Authors have contributed equally

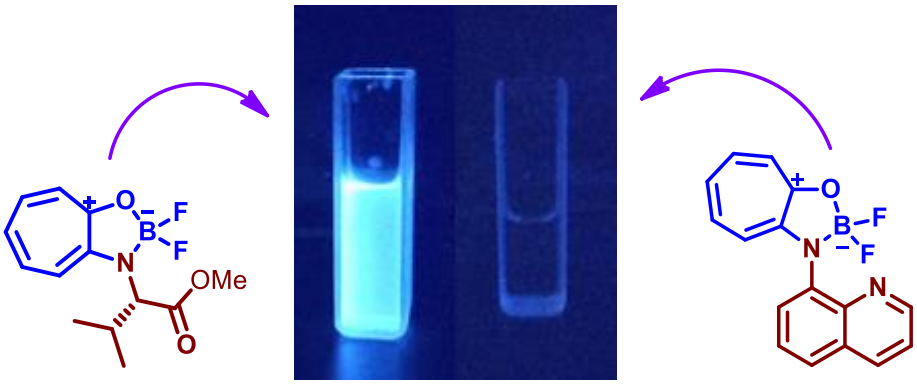

Contents

1. General Information

All required materials and solvents were purchased from commercial suppliers and used without any further purification unless noted. Anhydrous dichloromethane was freshly prepared by distilling over Calcium hydride. Reactions were monitored by thin layer chromatography, visualized by UV and Ninhydrin. Column chromatography was performed in 100-200 mesh silica. FT-IR spectra were recorded on Thermo Scientific Nicolet iS5N FT-NIR spectrometer. Mass spectra were obtained from Bruker micrOTOF-Q II Spectrometer and the samples were prepared in methanol and injected in methanol and water mixture. NMR spectra were recorded on Bruker AV- 400 at room temperature (^{1}H: 400 MHz, ^{13}C: 100.6 MHz, ^{11}B:128 MHz, ^{19}F:377 MHz). ^{1}H, ^{13}C, ^{11}B and ^{19}F NMR chemical shifts were recorded in ppm, downfield from tetramethyl silane. Splitting patterns are abbreviated as: s, Singlet; d, doublet; dd, doublet of doublet; app d, apparent doublet; app dd, apparent doublet of doublet; t, triplet; q, quartet; dq, doublet of quartet; m, multiplet. The crystal data of all peptide were collected on a Rigaku Oxford diffractometer at 293 K respectively. Absorption spectra were obtained using Jasco V-730 spectrometer. Fluorescence spectra were obtained from Perkin-Elmer LS-55 using Xenon lamp. All spectroscopic measurements were carried out with spectroscopic grade, non-degassed solvents and at 20°C. Relative fluorescence quantum yields were determined by comparing with quinine sulfate quantum yield in 0.1 M H_2SO_4 (0.54). The obtained values were substituted in the equation given below.

$$\phi_x = \phi_r \mathrm{x} \frac{F_x}{F_r} \mathrm{x} \frac{1-10^{-A_r}}{1-10^{A_x}} \mathrm{x} \frac{\eta_x^2}{\eta_x^2}$$

Absolute fluorescence quantum yields of **3a, 3c**, **3f, 3h** and **3i** in methanol (excited at 384 nm), of these dyes are measured by Edinburgh instrument FLS 920 using intergrating sphene according to the definition of fluorescence efficiency. The photostabilities of dyes **3a, 3c** and

3h were studied by continuous irradiation with a UV lamp in 265 nm wavelength under 4W LED in methanol.

All reagents were purchased from commercial suppliers and used without further purification. The reaction was monitored by analytical TLC plates. The column chromatography was performed with Rankem silica gel (100-200 mesh). HRMS's were analyzed with Agilent Q-TOF 6500. All computational data for compound (**3a, 3a-OH, 3b, 3h, 3i**) has been calculated using Gaussian 09 software and B3LYP/6-31+G* level of theory in vacuum.

Cyclic voltammograms of 1 mM **3a**, **3h** and **3i** were measured in acetonitrile solution, containing 0.1 M TBAPF6 as the supporting electrolyte, glassy carbon electrode as a working electrode, Pt wire as a counter electrode, and silver electrode as reference electrode at 100 mV s^{-1} of scanning rate at room temperature.

2. ^{1}H, ^{13}C NMR (400MHz, $CDCl_3$) and HRMS of Aminotropone **(2a)**

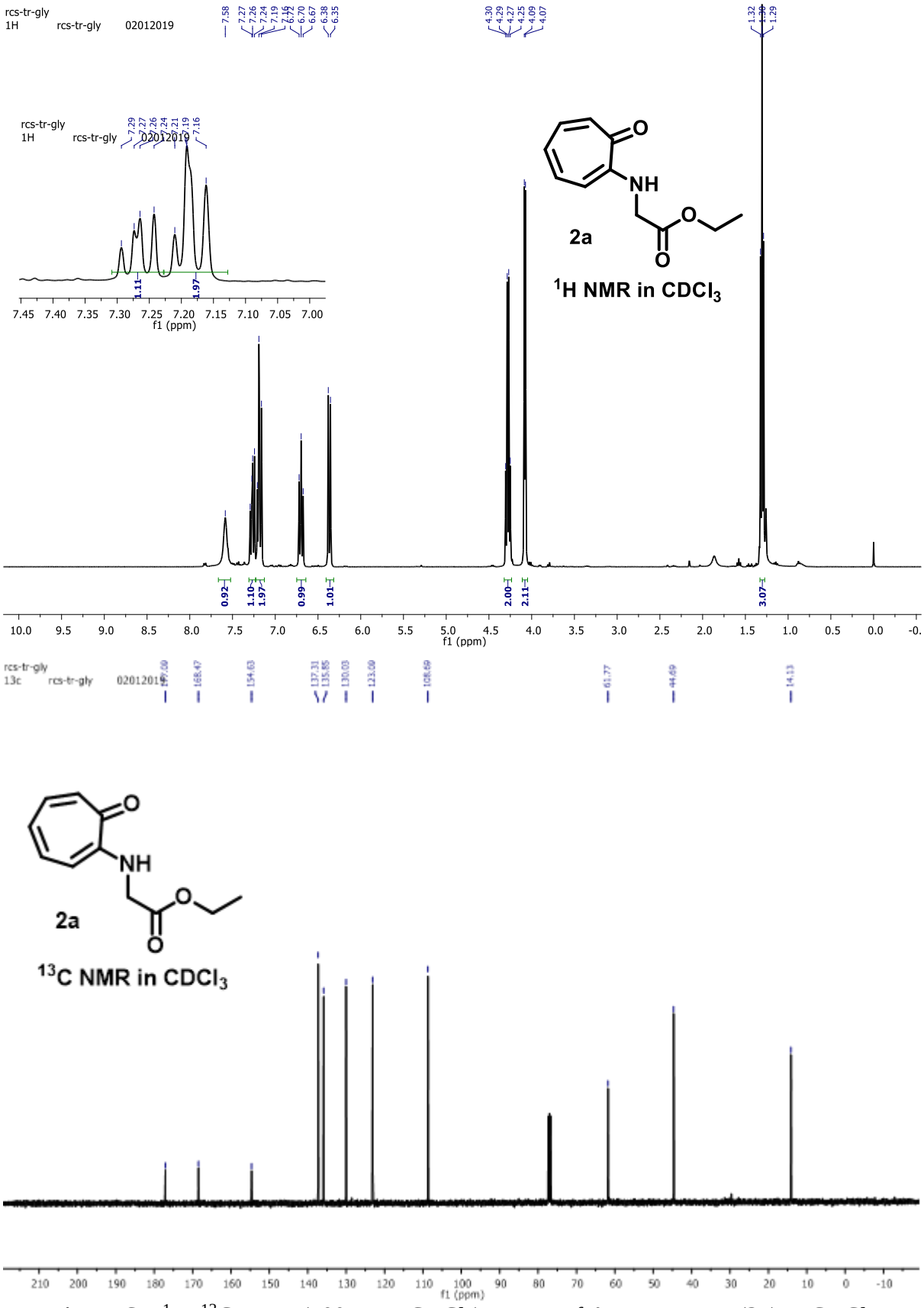

Figure S1. ^{1}H, ^{13}C NMR (400MHz, $CDCl_3$) spectra of Aminotropone **(2a)** in $CDCl_3$

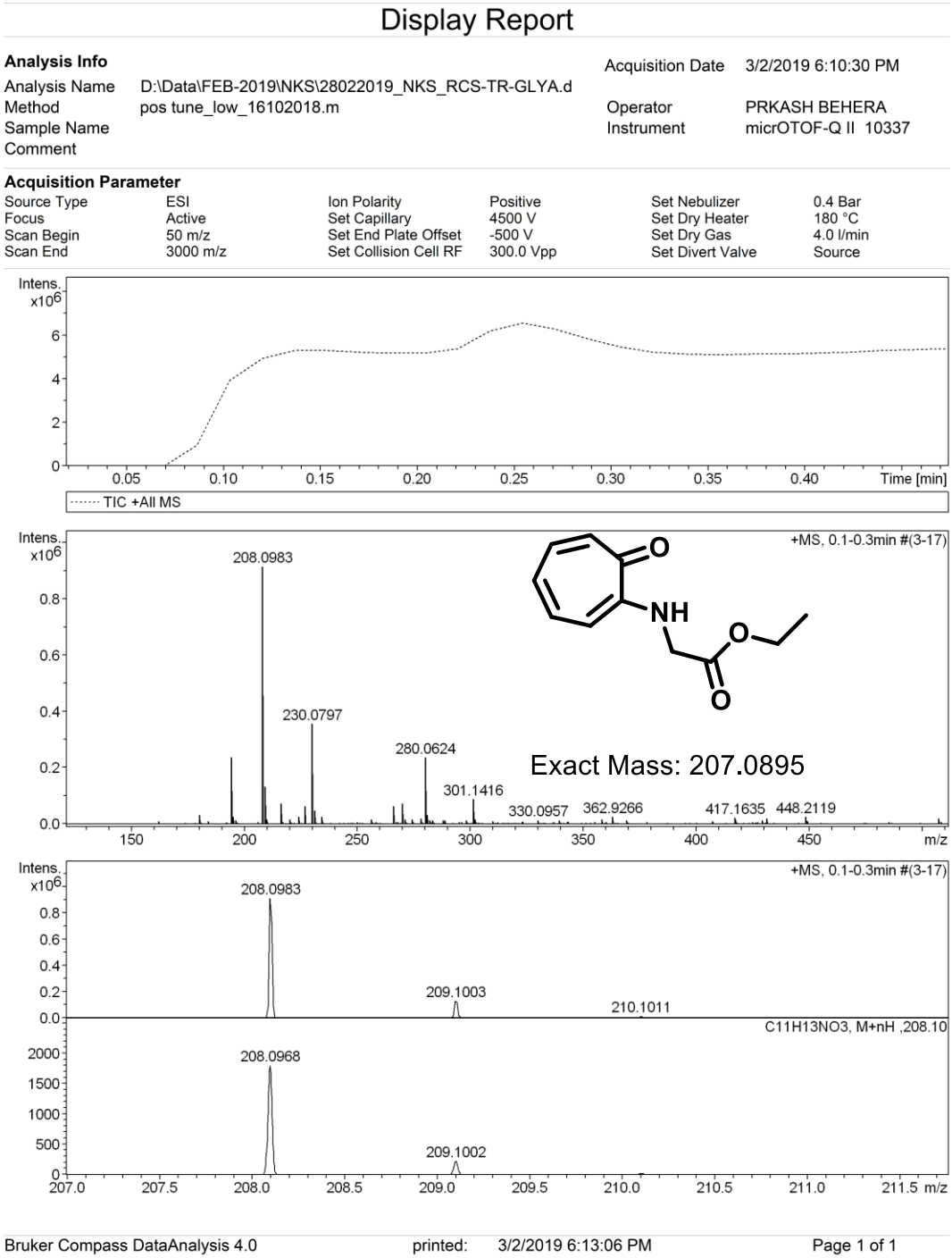

Figure S2. ESI/HRMS spectra of Aminotropone **(2a)**

3. ^{1}H, ^{13}C NMR (400MHz, $CDCl_3$) and HRMS of Aminotropone **(2b)**

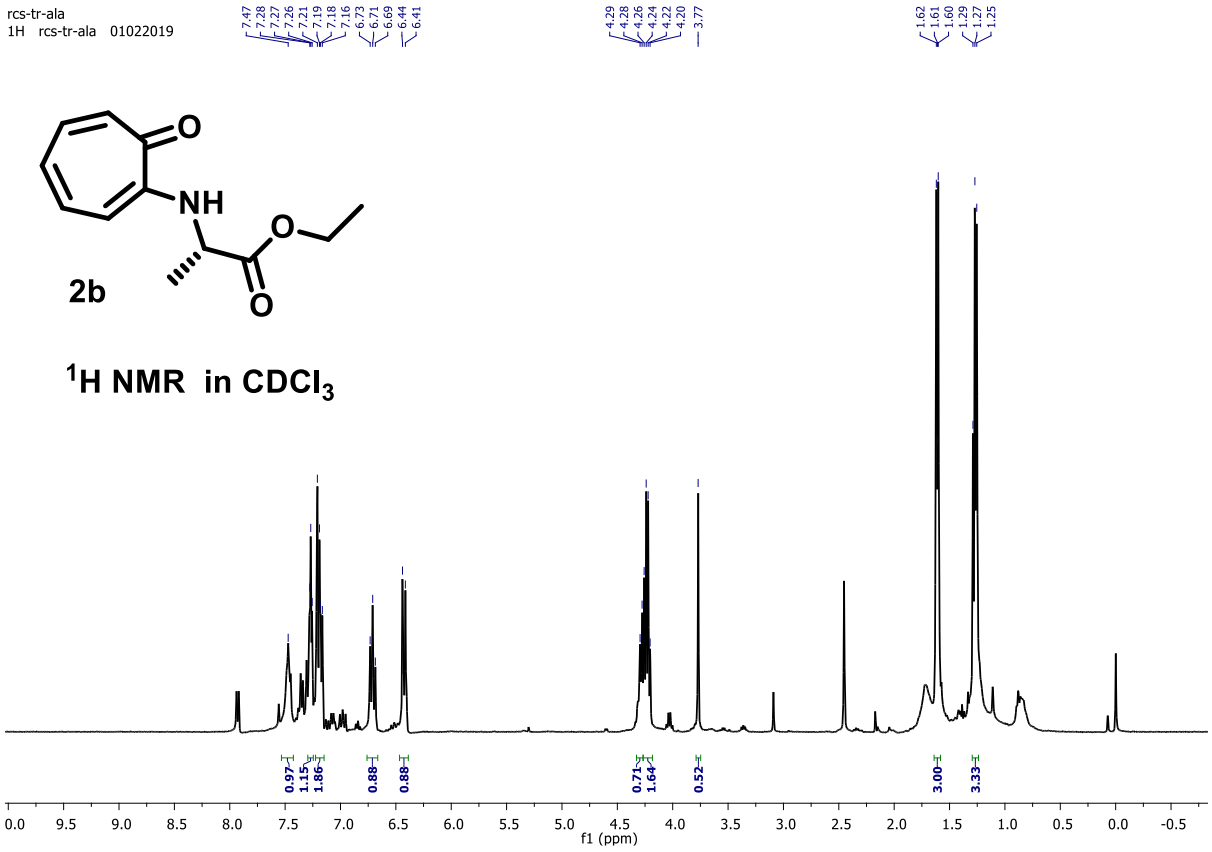

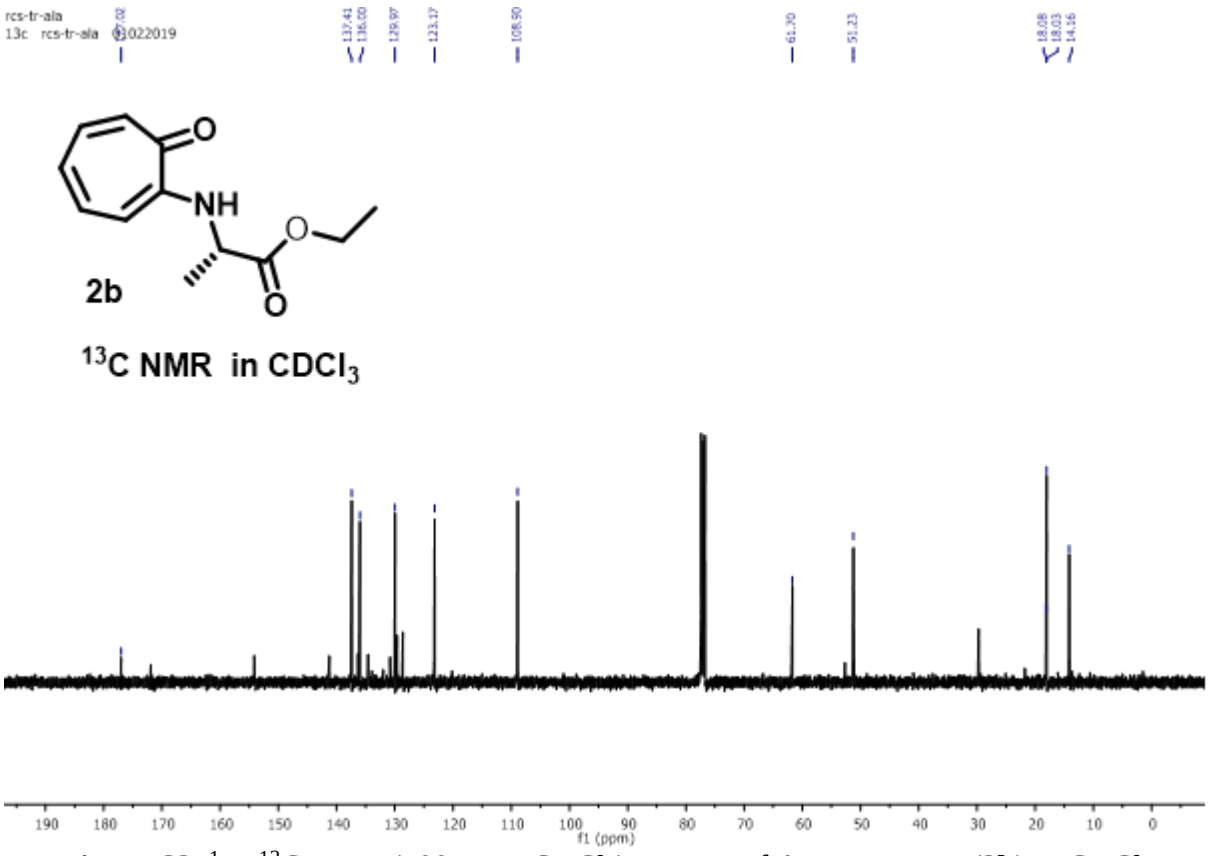

Figure S3. ^{1}H, ^{13}C NMR (400MHz, $CDCl_3$) spectra of Aminotropone **(2b)** in $CDCl_3$

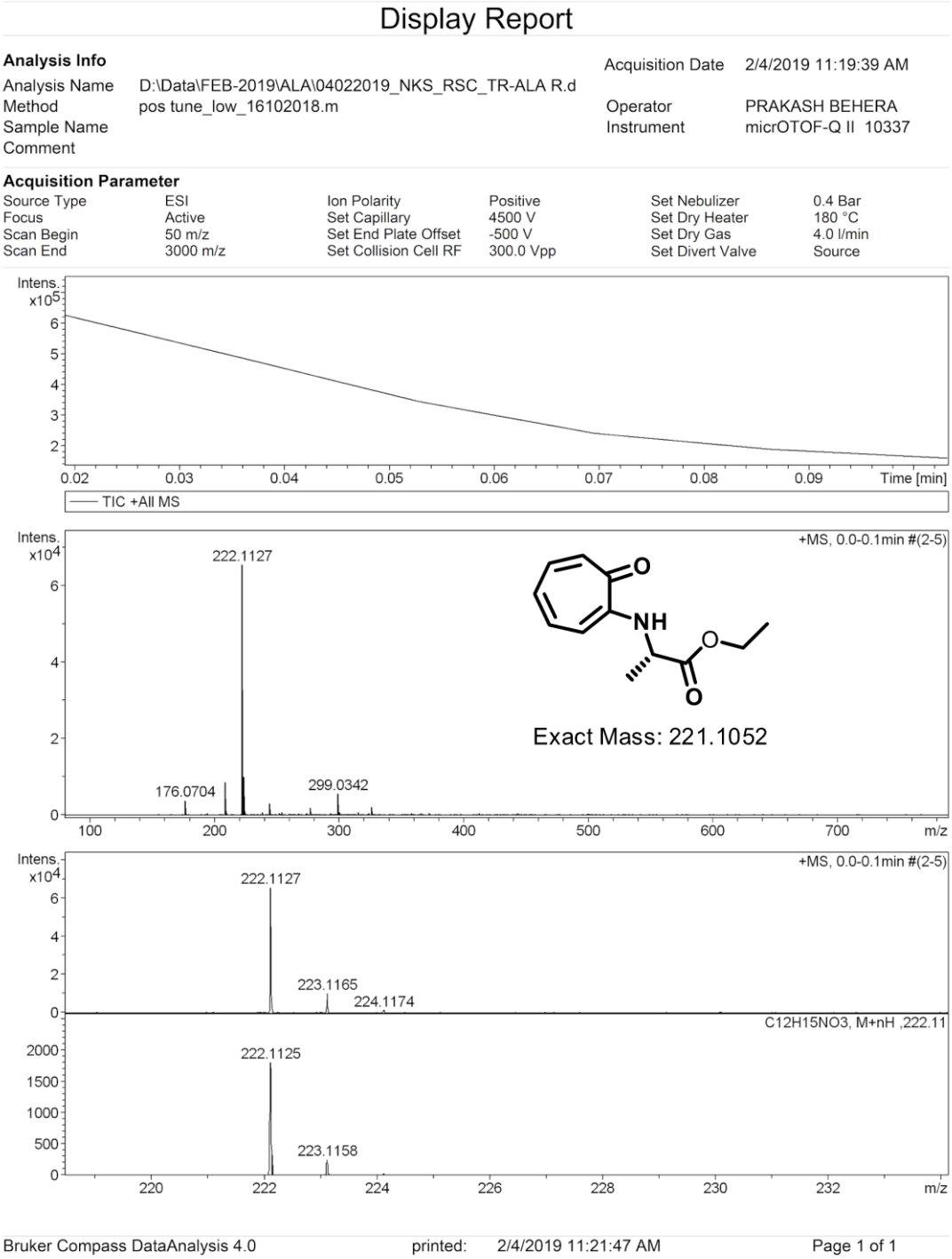

Figure 4. ESI/HRMS spectra of Aminotropone **(2b)**

4. ^{1}H, ^{13}C NMR (400MHz, $CDCl_3$) and HRMS of Aminotropone **(2c)**

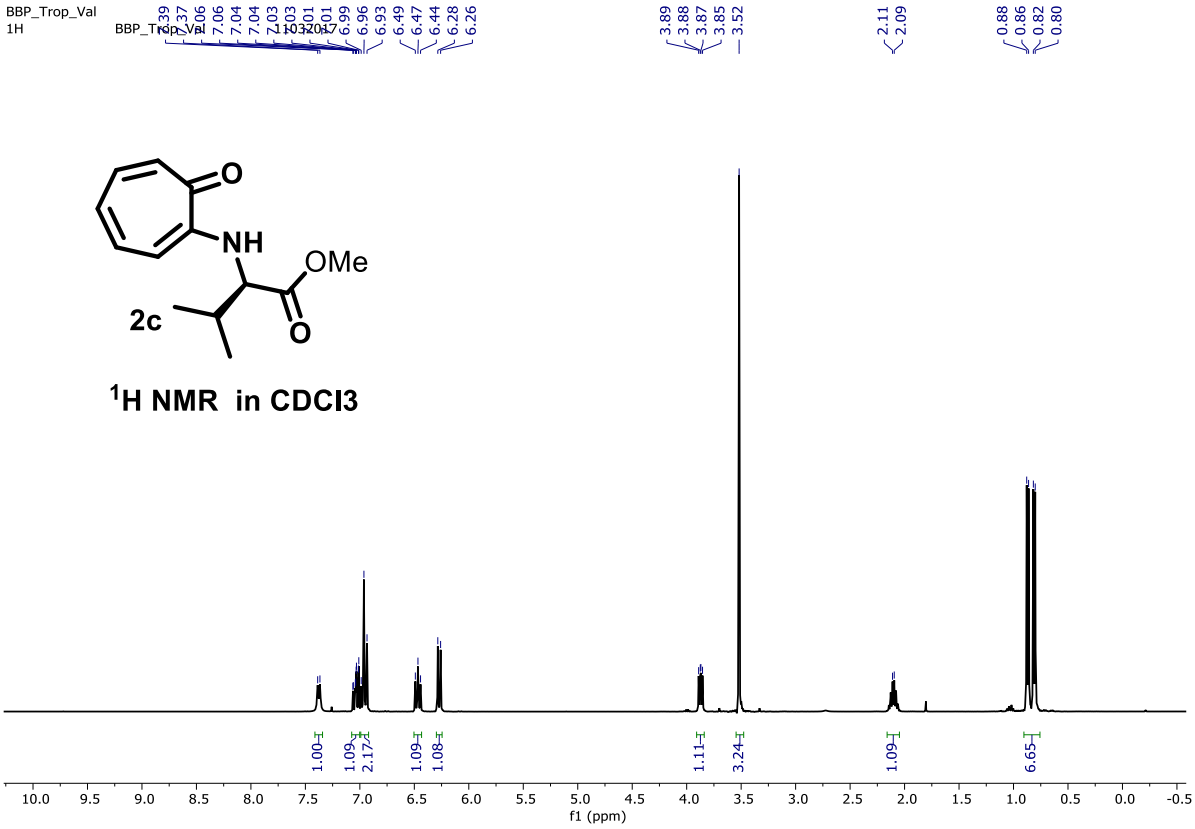

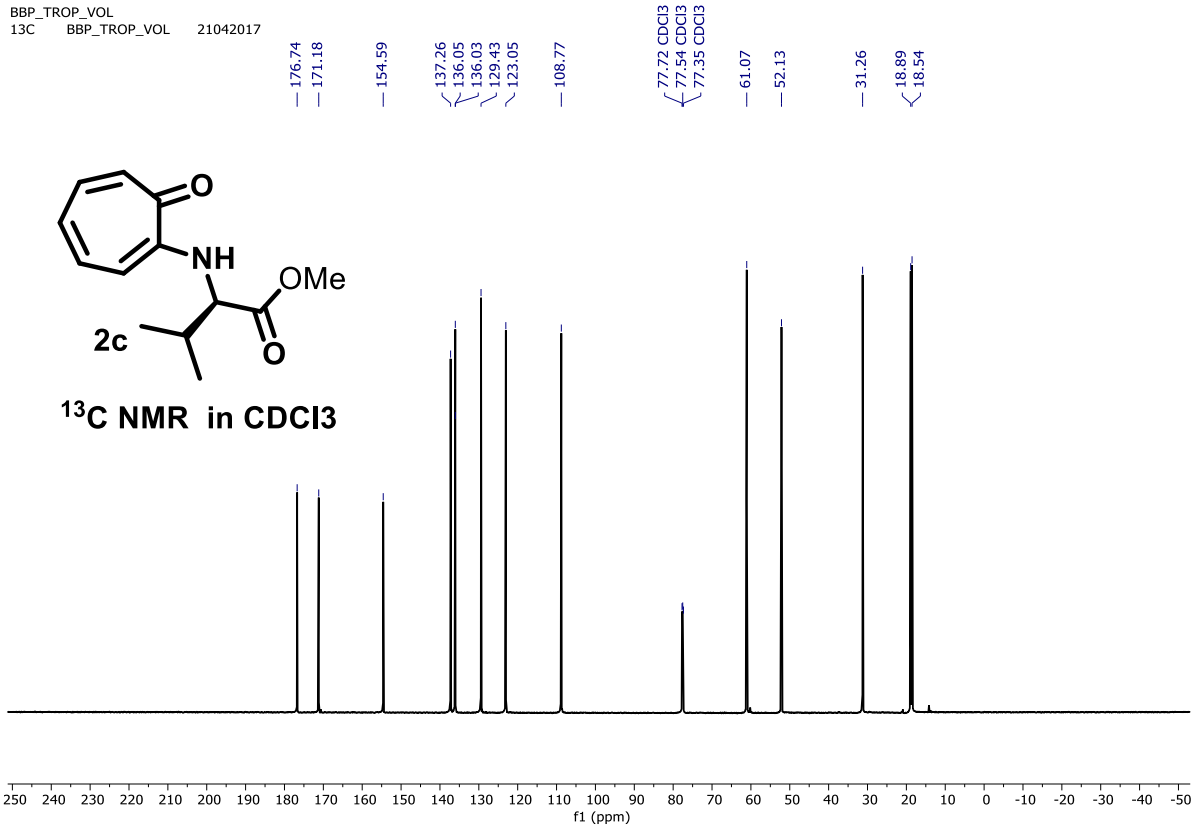

Figure S5. ^{1}H, ^{13}C NMR (400MHz, $CDCl_3$) spectra of Aminotropone **(2c)** in $CDCl_3$

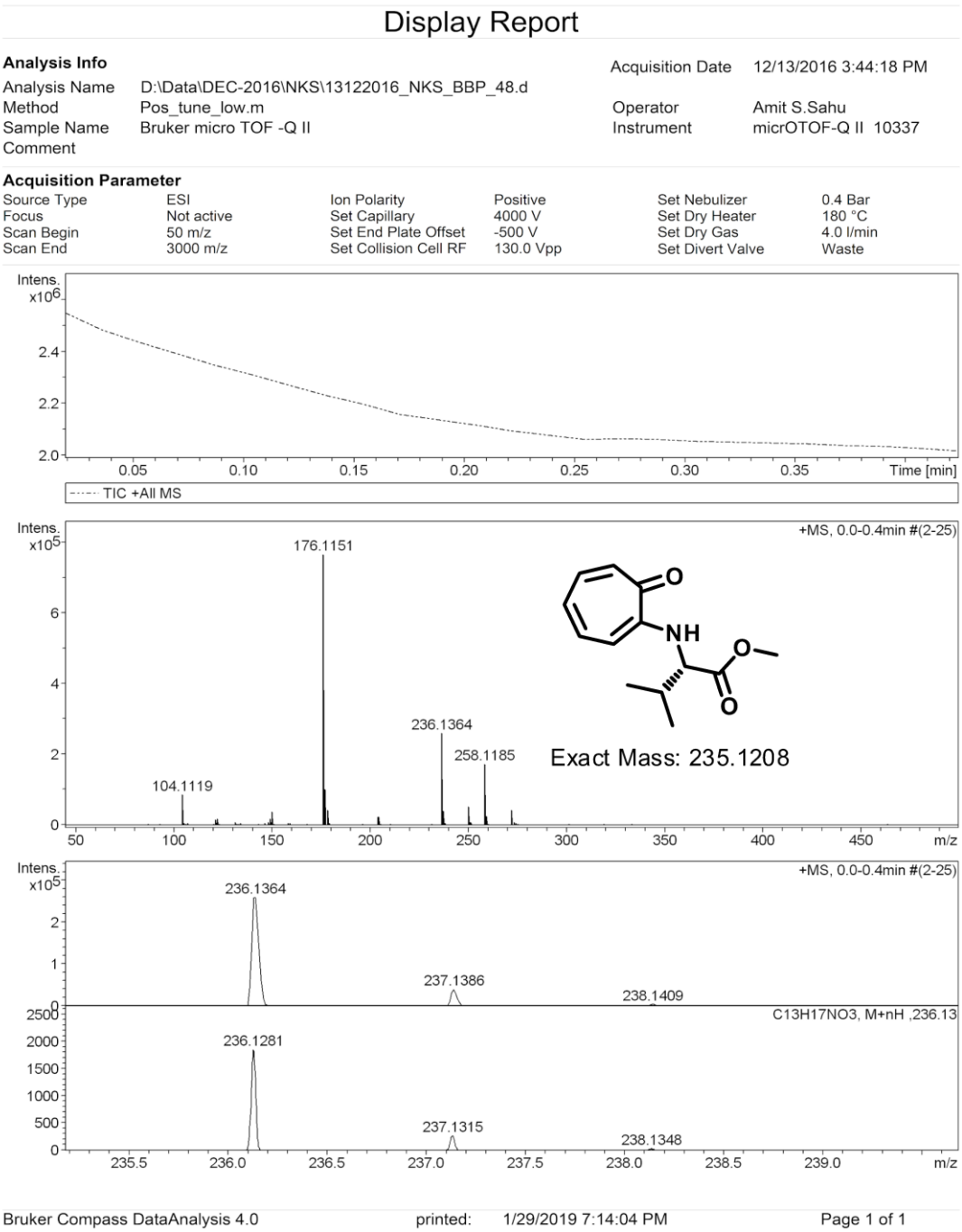

Figure S6. ESI/HRMS spectra of Aminotropone **(2c)**.

5. ^{1}H, ^{13}C NMR (400MHz, $CDCl_3$) of Aminotropone **(2d)**

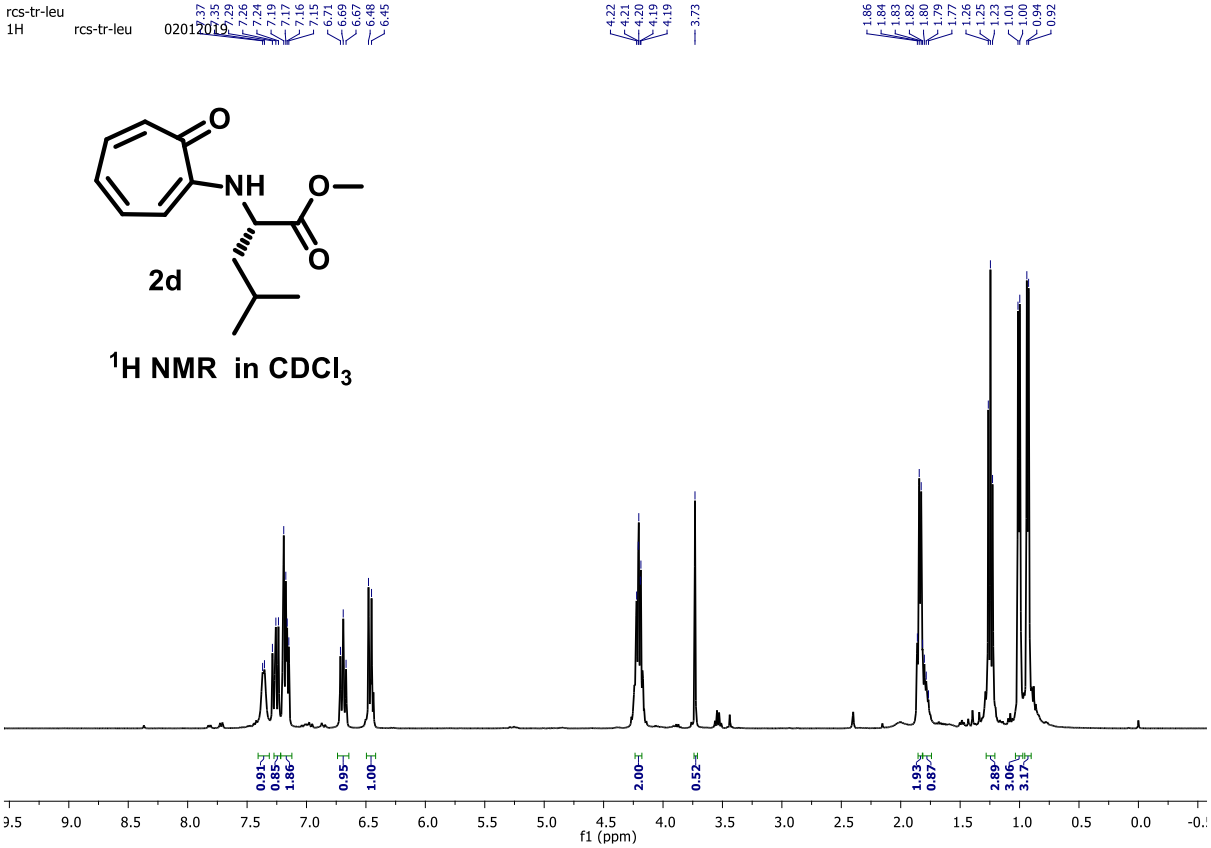

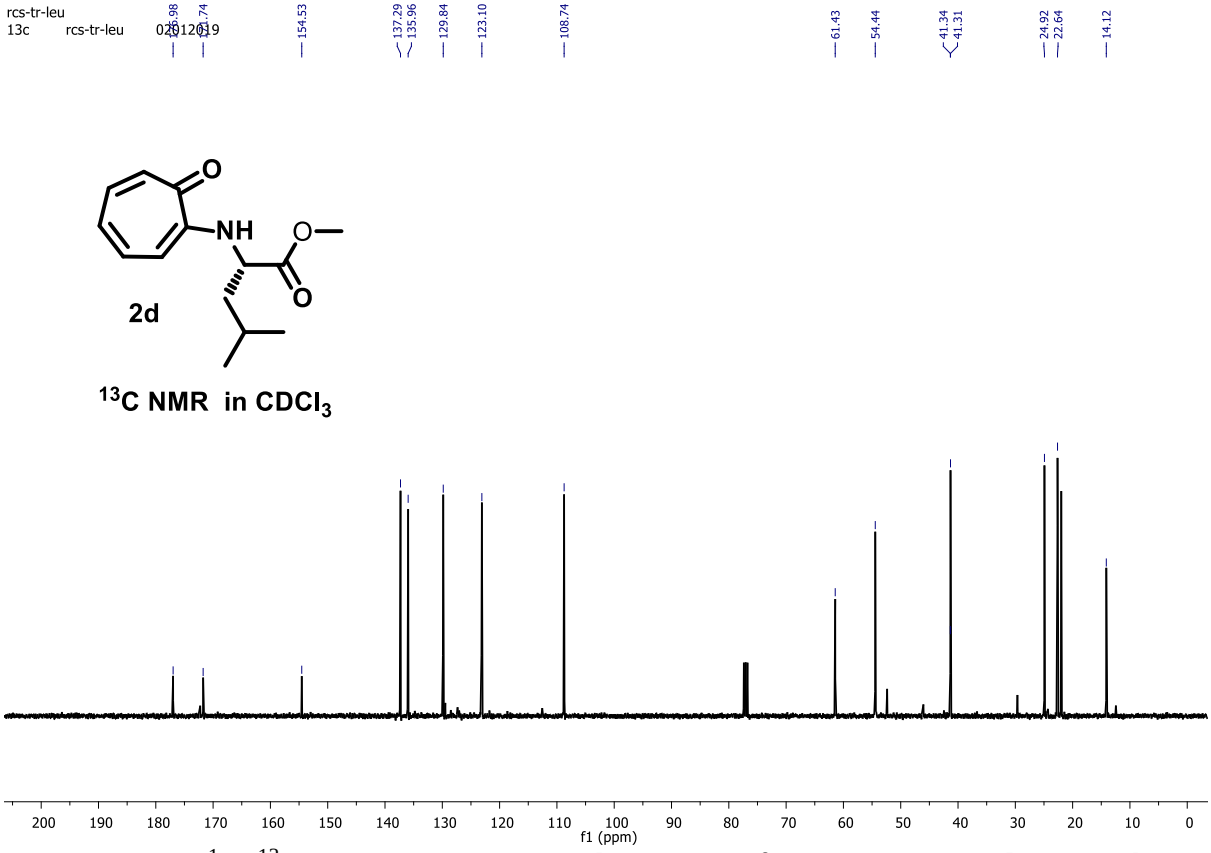

Figure S7. ^{1}H, ^{13}C NMR (400MHz, $CDCl_3$) spectra of Aminotropone **(2d)** in $CDCl_3$

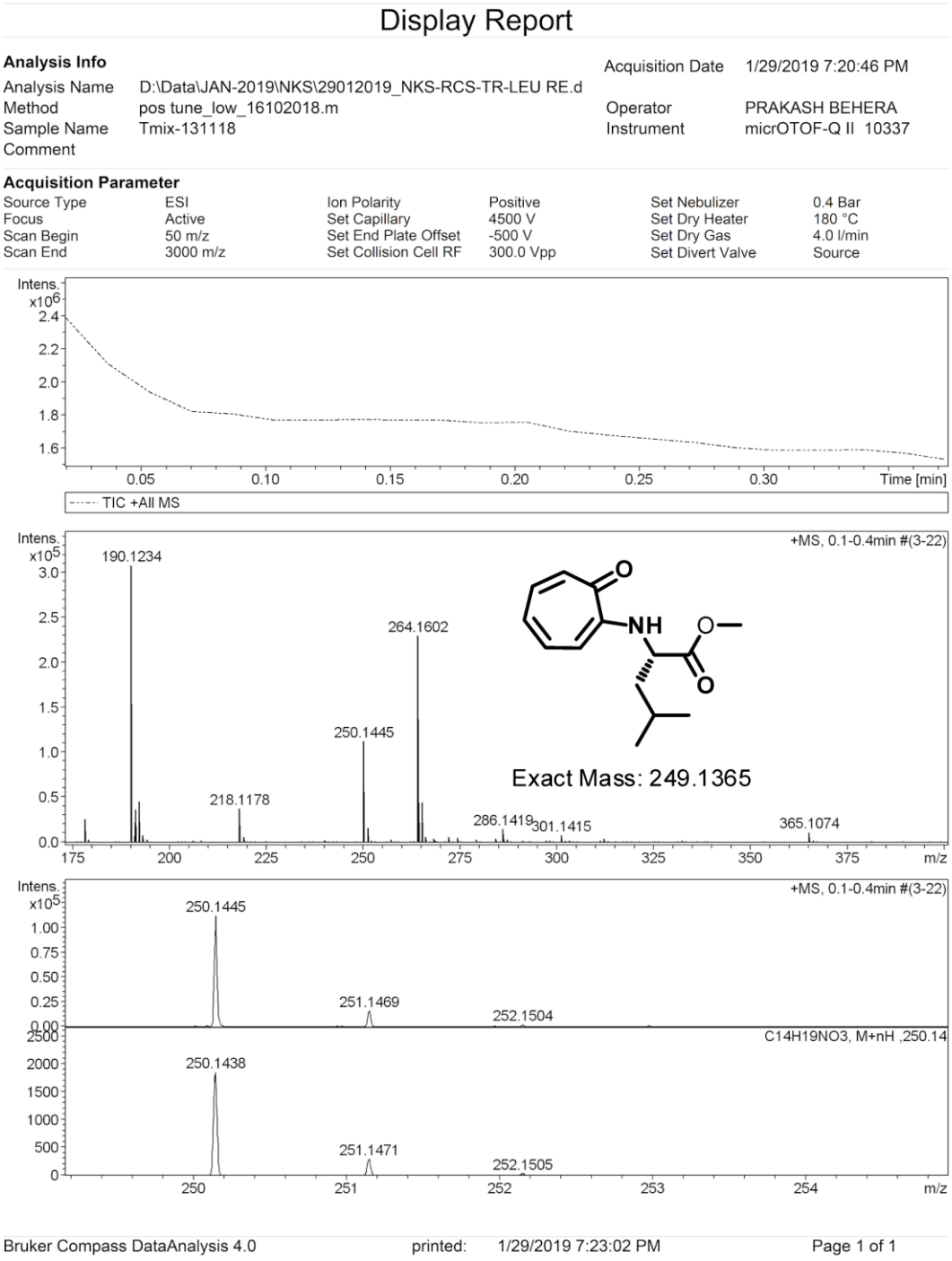

Figure S8. ESI/HRMS spectra of Aminotropone **(2d)**

6. ^{1}H, ^{13}C NMR (400MHz, $CDCl_3$) and HRMS of Aminotropone **(2e)**

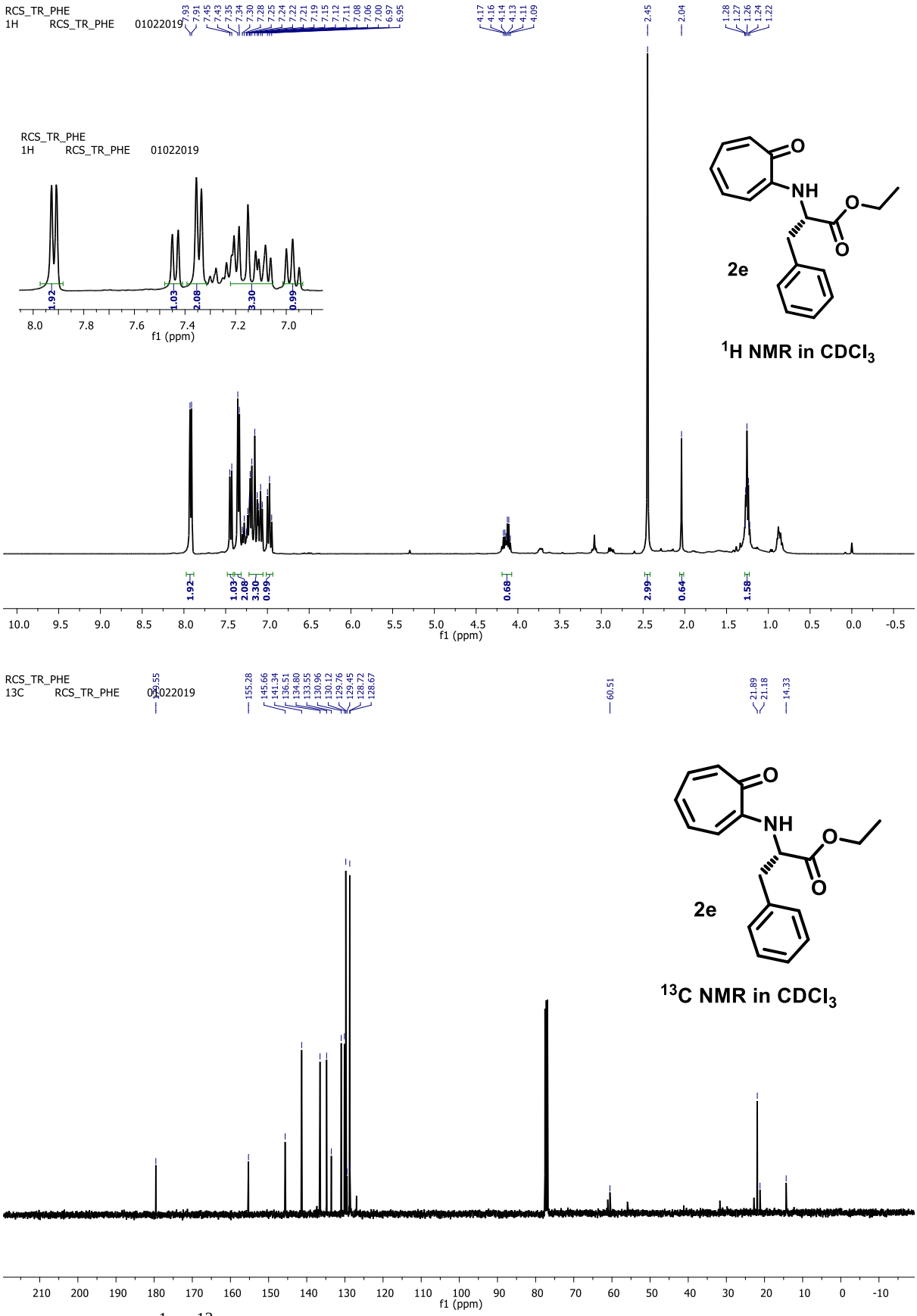

Figure S9. ^{1}H, ^{13}C NMR (400MHz, $CDCl_3$) spectra of Aminotropone **(2e)** in $CDCl_3$

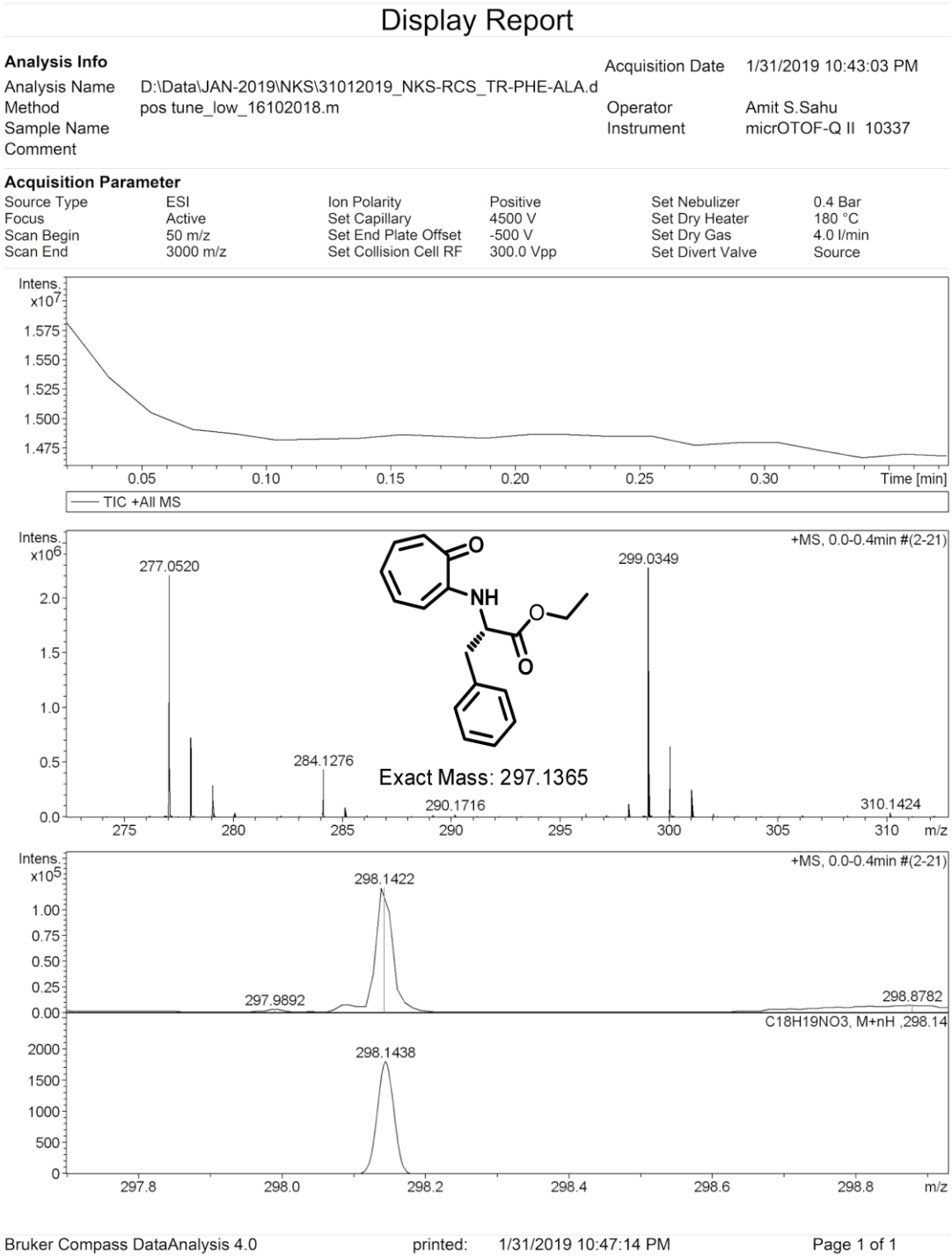

Figure S10. ESI/HRMS spectra of Aminotropone **(2e).**

7. NMR (^{1}H, ^{13}C) and HRMS of Aminotropone **(2f)**

8.

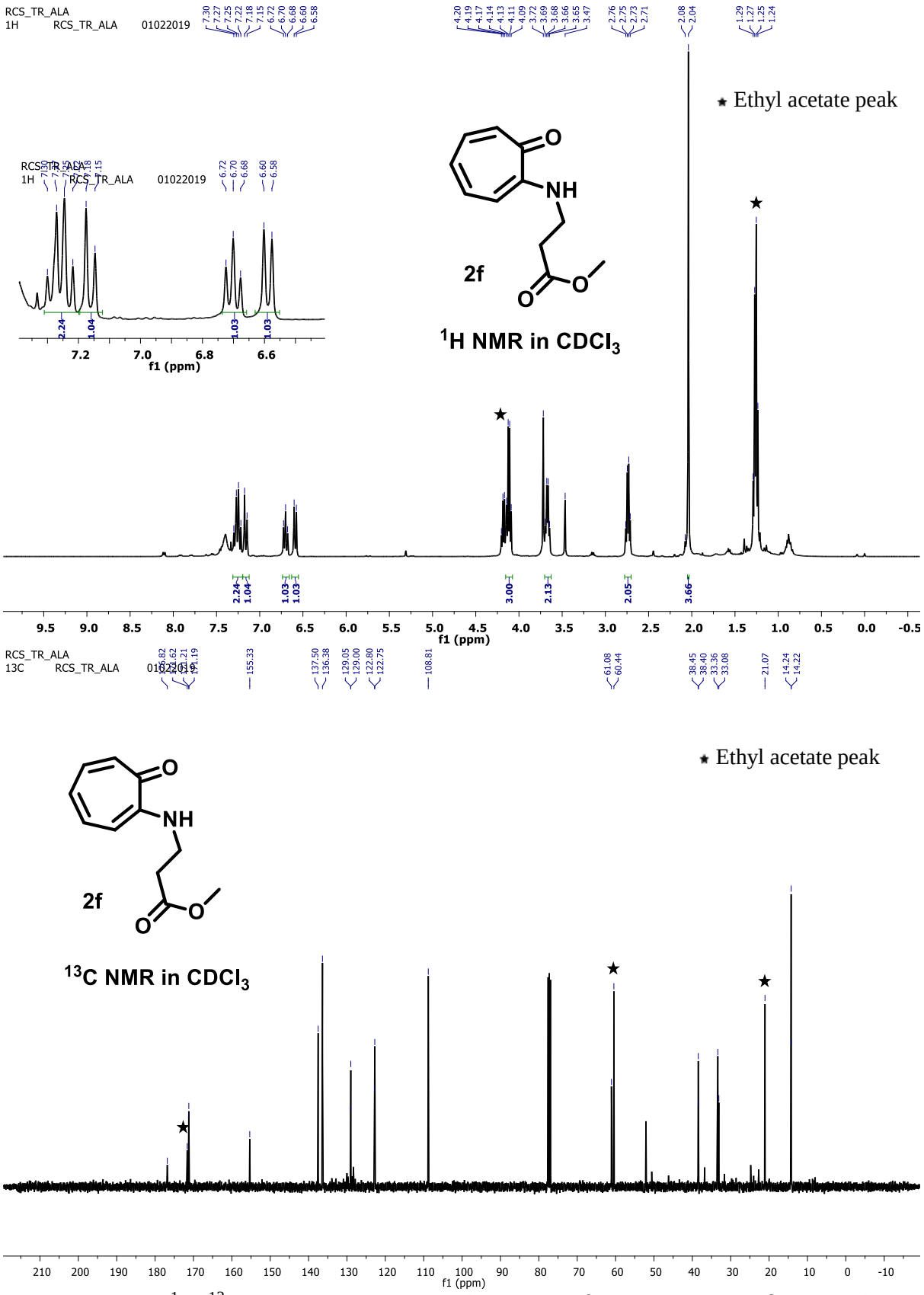

Figure S11. ^{1}H, ^{13}C NMR (400MHz, $CDCl_3$) spectra of Aminotropone **(2f)** in $CDCl_3$

Display Report

Analysis Info

Analysis Name	D:\Data\JAN-2019\NKS\31012019_NKS-RCS_TR-B-ALA.d	Acquisition Date	1/31/2019 10:37:16 PM
Method	pos tune_low_16102018.m	Operator	Amit S.Sahu
Sample Name		Instrument	micrOTOF-Q II 10337
Comment			

Acquisition Parameter

Source Type	ESI	Ion Polarity	Positive	Set Nebulizer	0.4 Bar
Focus	Active	Set Capillary	4500 V	Set Dry Heater	180 °C
Scan Begin	50 m/z	Set End Plate Offset	-500 V	Set Dry Gas	4.0 l/min
Scan End	3000 m/z	Set Collision Cell RF	300.0 Vpp	Set Divert Valve	Source

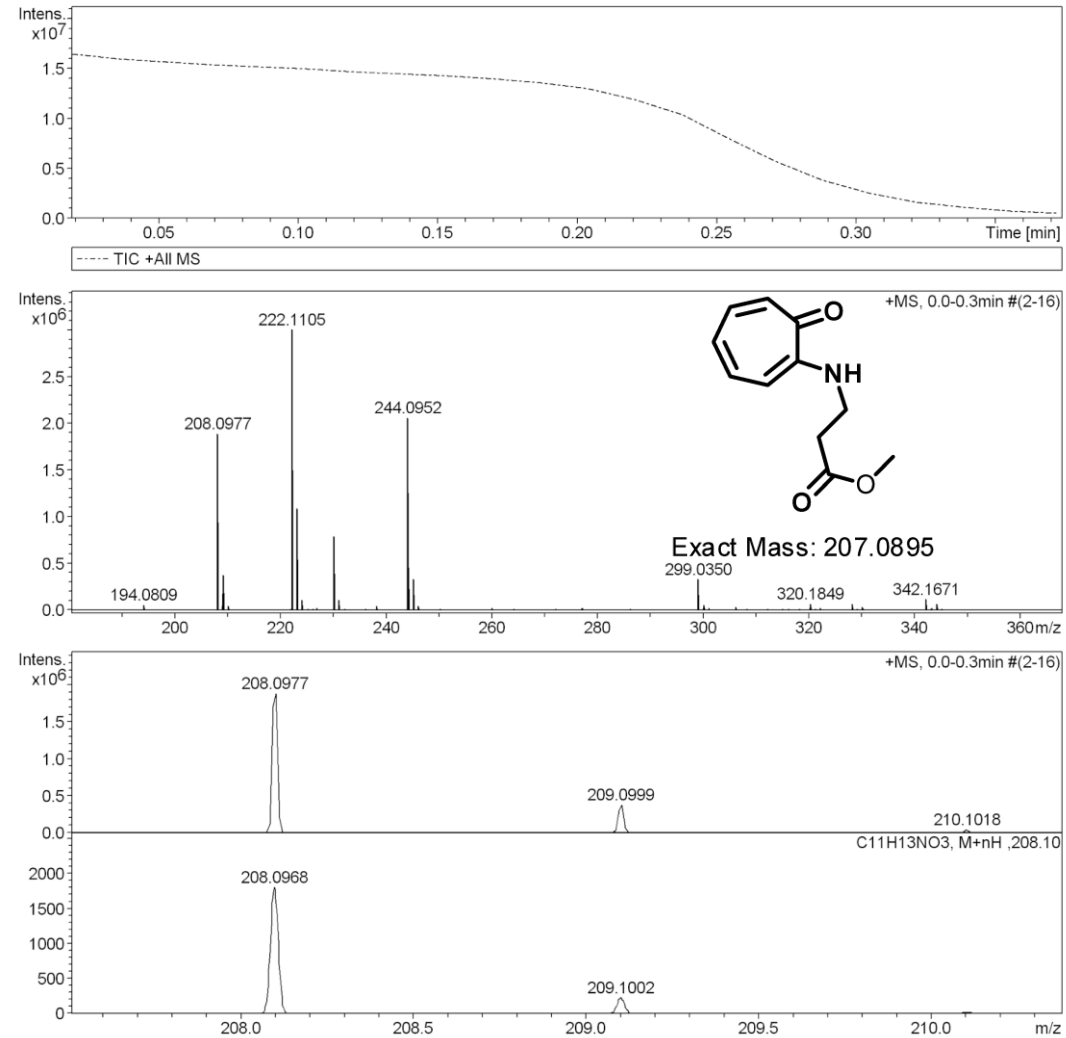

Bruker Compass DataAnalysis 4.0 printed: 1/31/2019 10:40:57 PM Page 1 of 1

Figure S12. ESI/HRMS spectra of Aminotropone **(2f)**

9. NMR (^{1}H, ^{13}C) and HRMS of Aminotropone **(2g)**

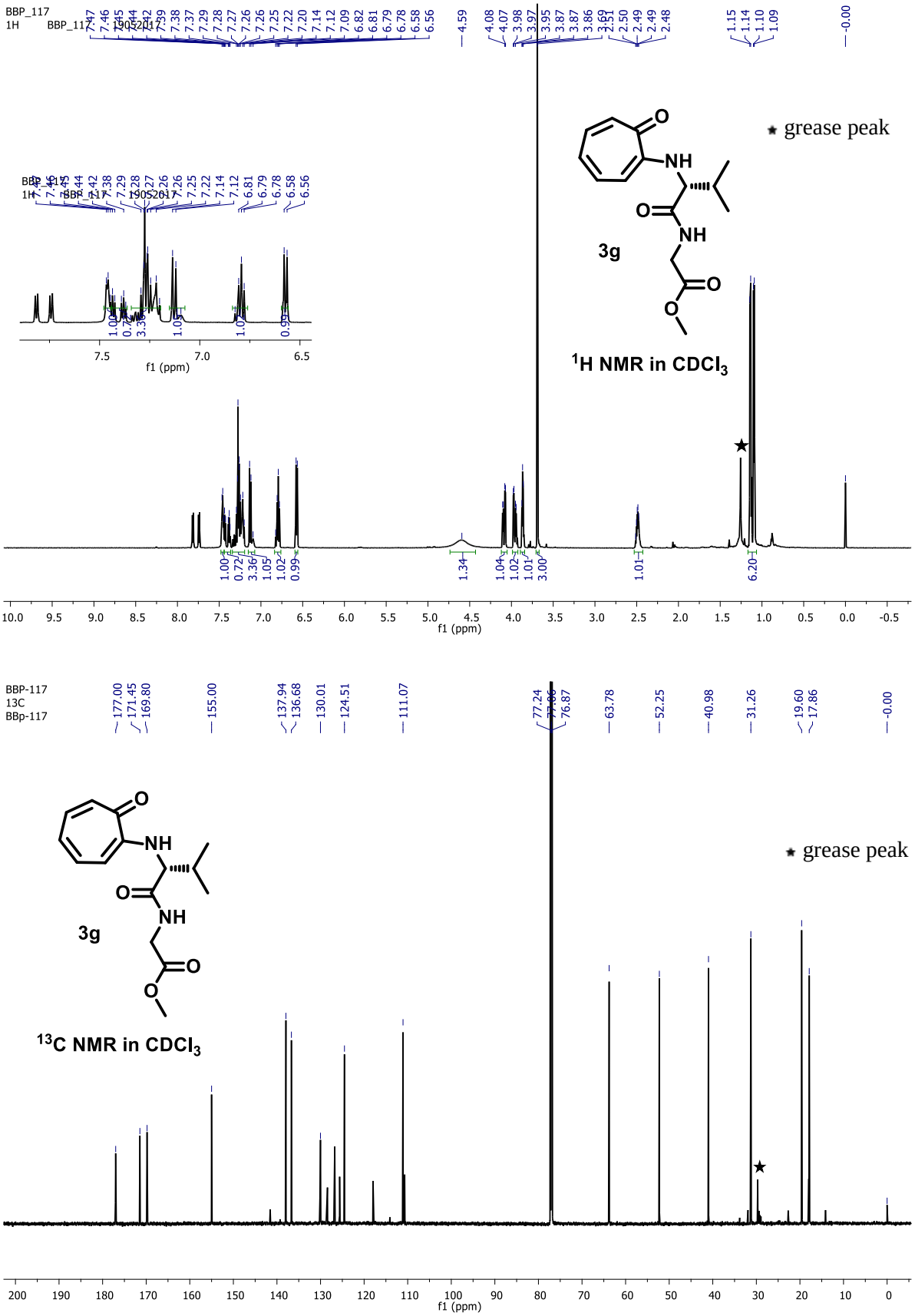

Figure S13. ^{1}H, ^{13}C NMR (700MHz, $CDCl_3$) spectra of Aminotropone **(2g)** in $CDCl_3$

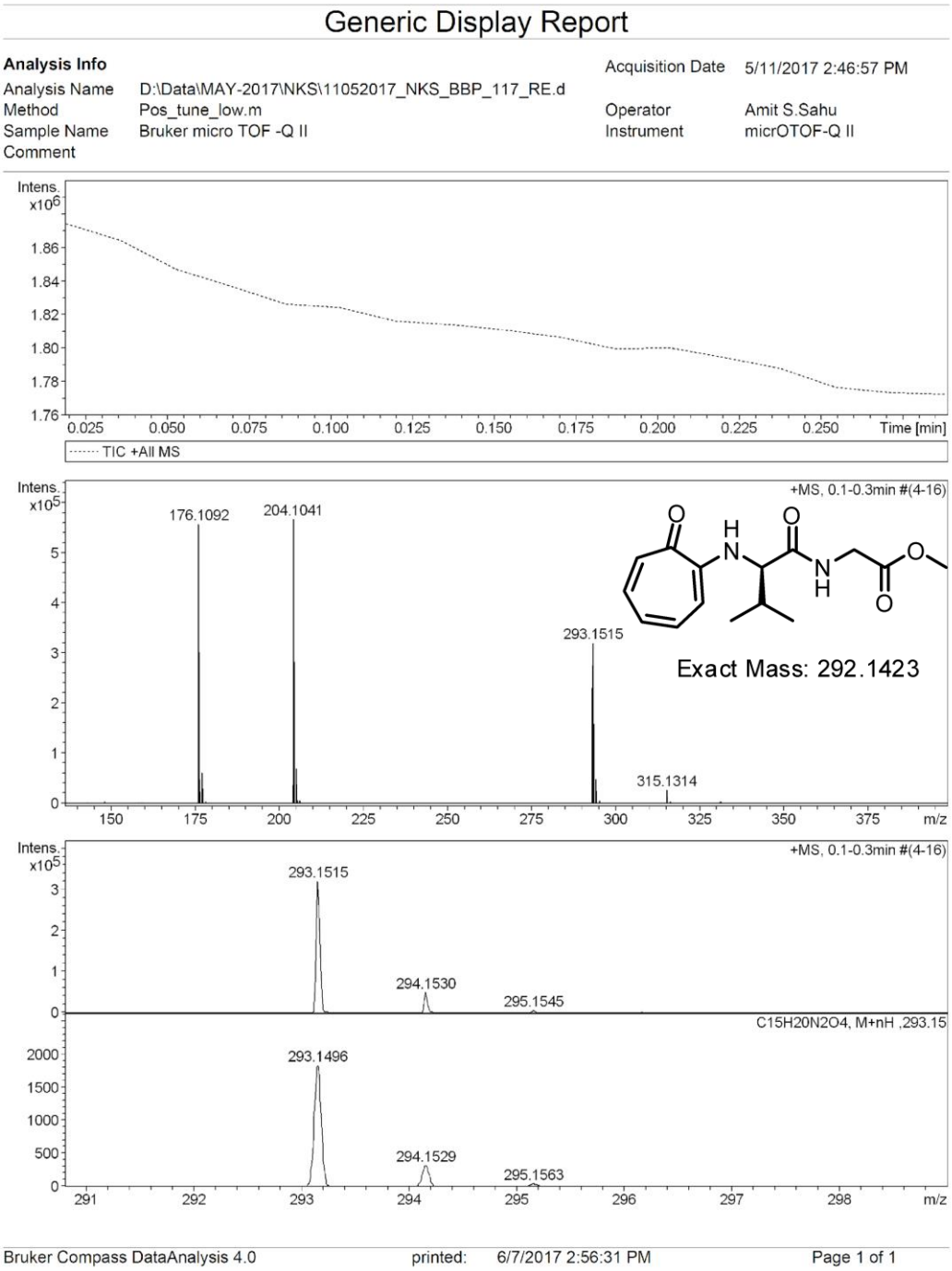

Figure S14. ESI/HRMS spectra of Aminotropone **(2g)**

10. NMR (^{1}H, ^{13}C) and HRMS of Aminotropone **(2h)**

11.

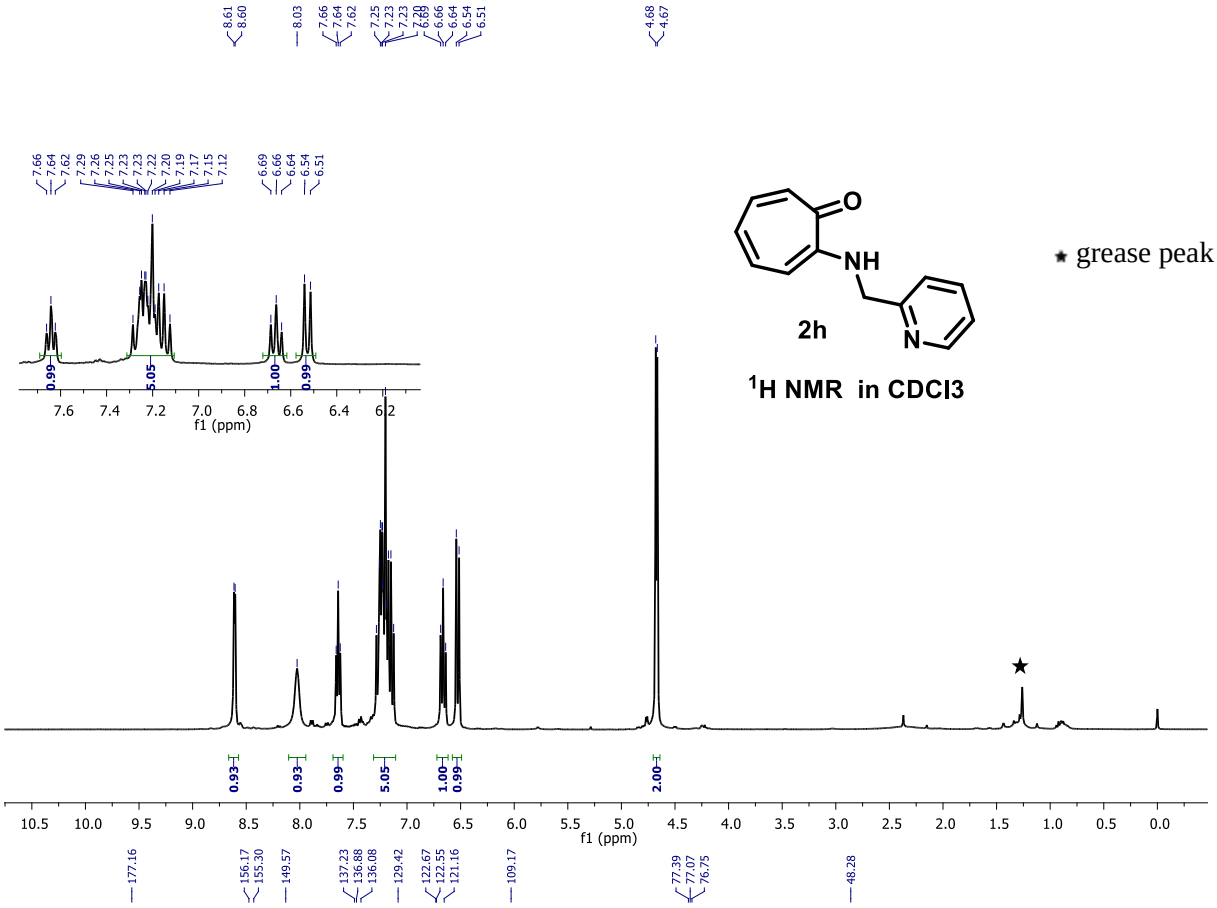

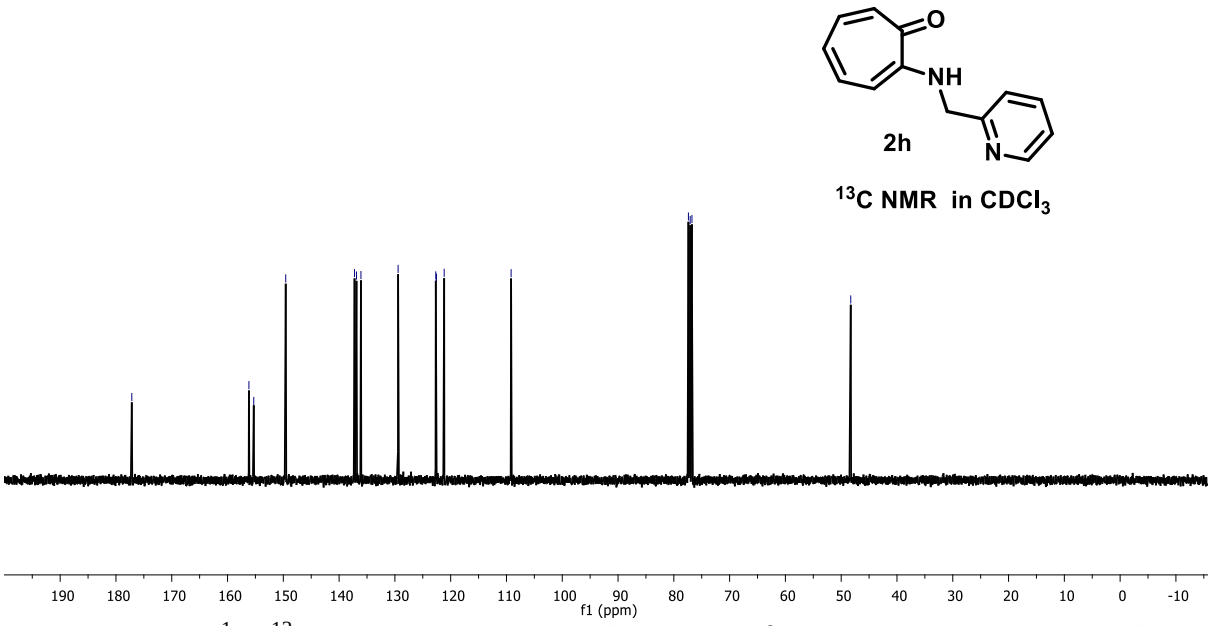

Figure S15. ^{1}H, ^{13}C NMR (400MHz, $CDCl_3$) spectra of Aminotropone **(2g)** in $CDCl_3$

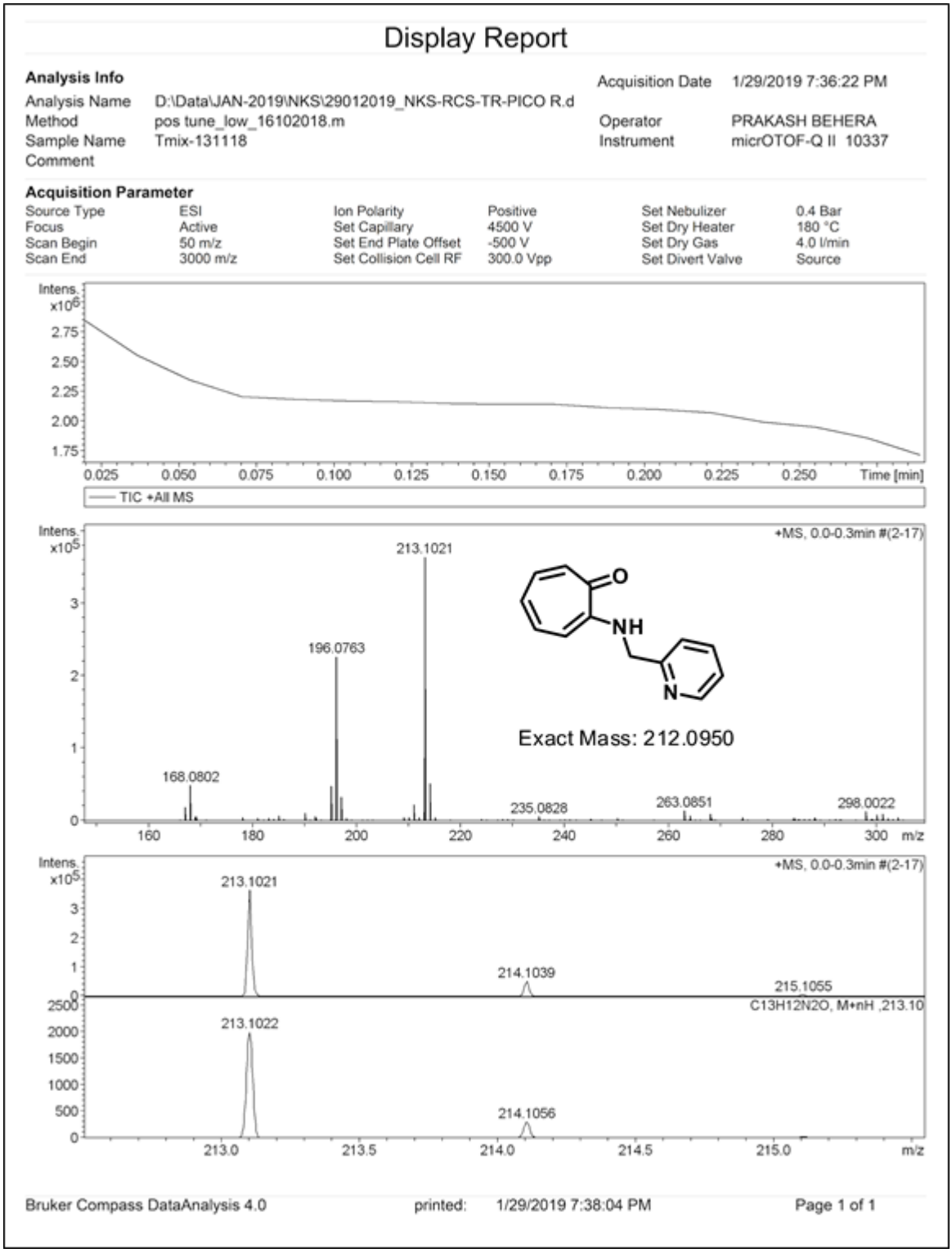

Figure S16. ESI/HRMS spectra of Aminotropone **(2h)**

10. NMR (^{1}H, ^{13}C) and HRMS of Aminotropone **(2i)**

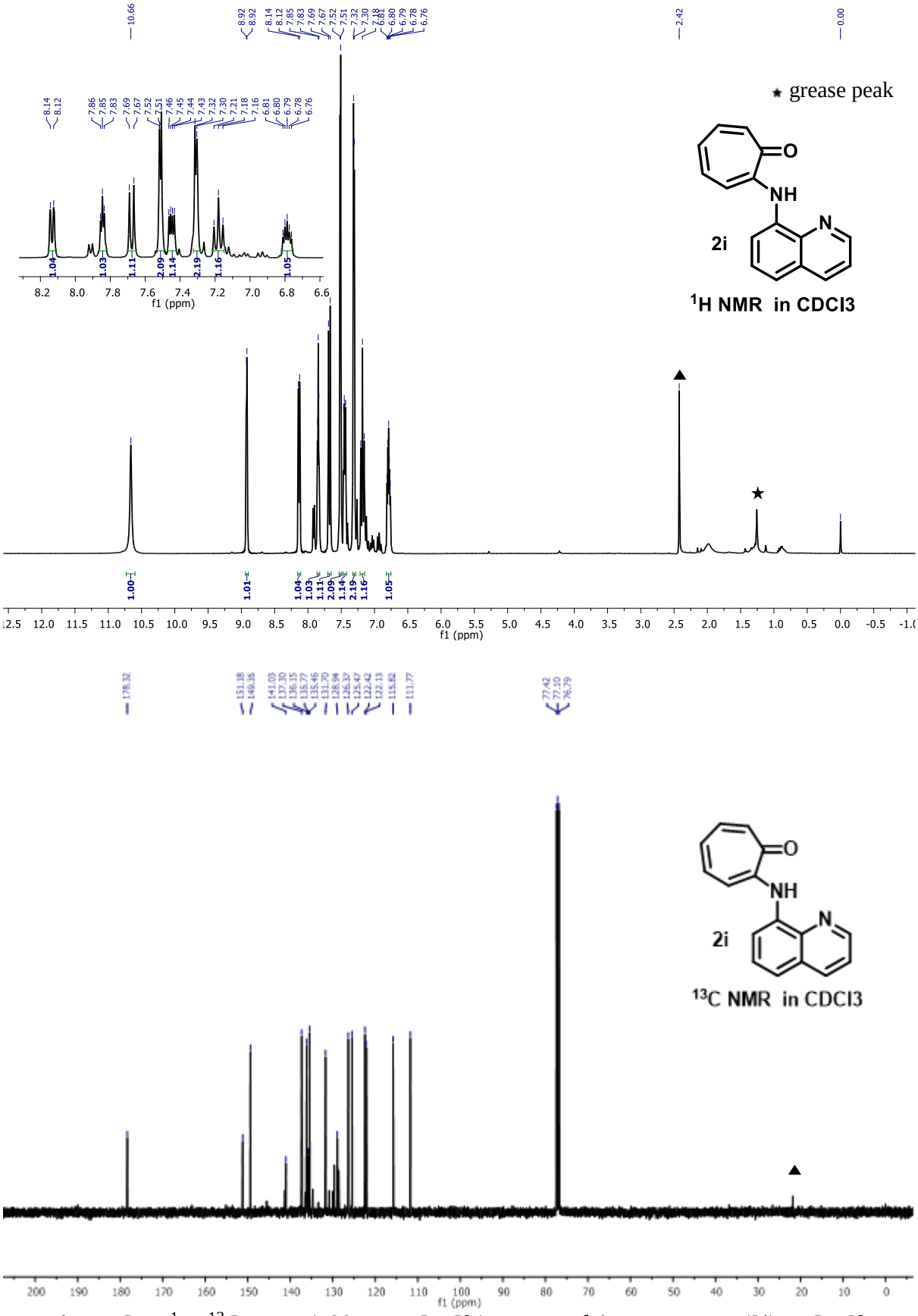

Figure S17. ^{1}H, ^{13}C NMR (400MHz, $CDCl_3$) spectra of Aminotropone **(2i)** in $CDCl_3$

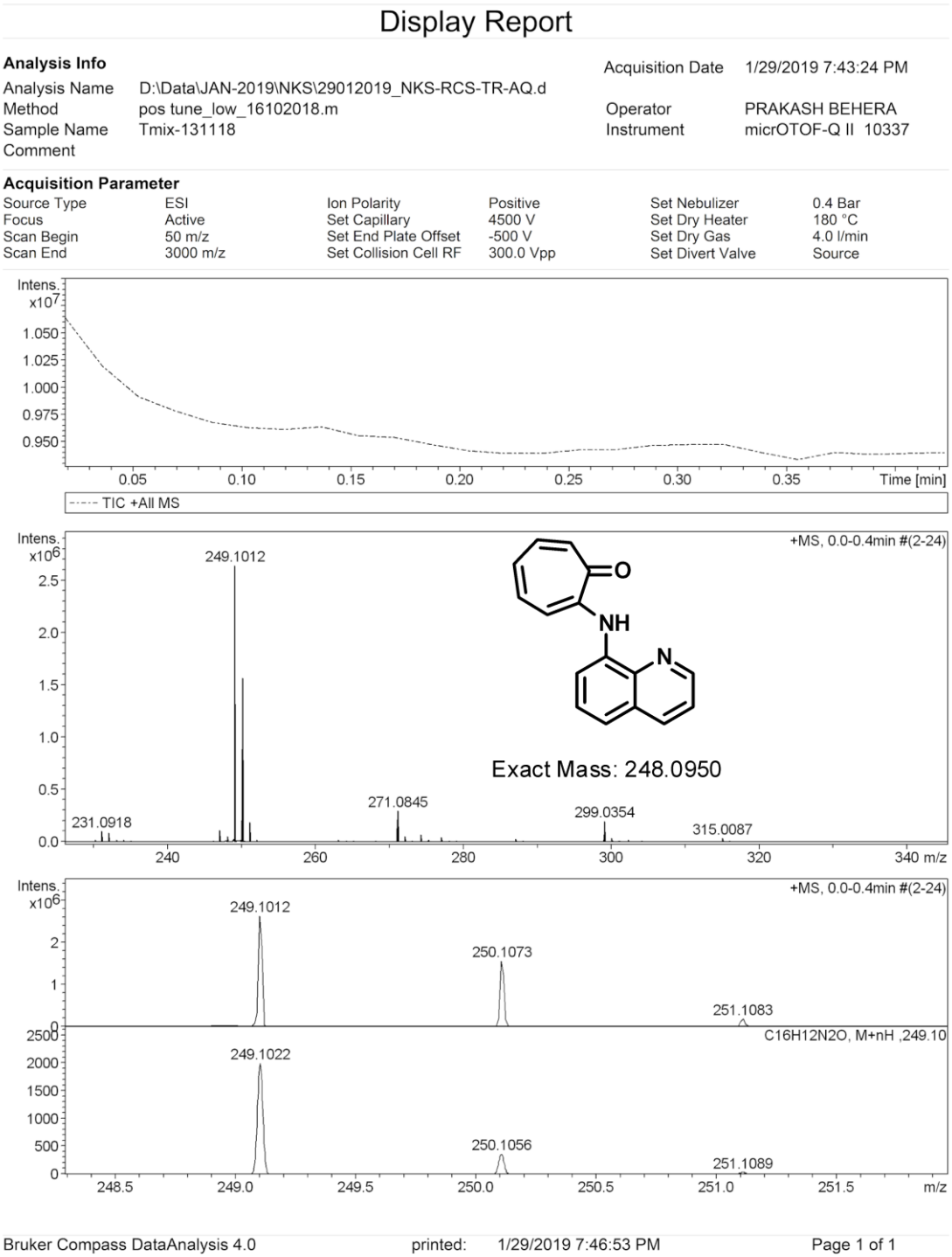

Figure S18. ESI/HRMS spectra of Aminotropone **(2i)**

11. NMR (^{1}H, ^{13}C, ^{11}B, ^{19}F) and HRMS of Boron complex *tr-gly* **(3a)**

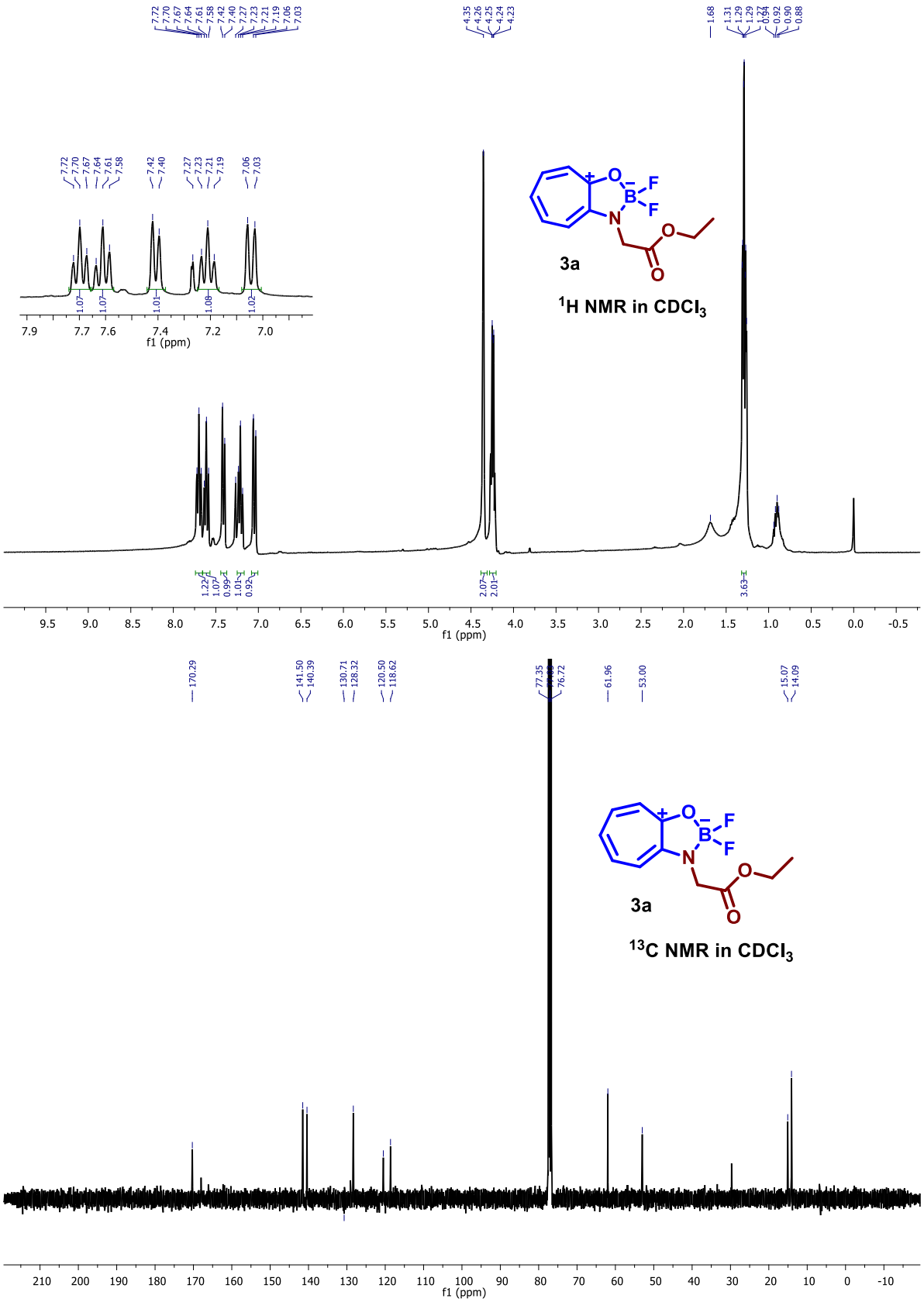

Figure S19. ^{1}H, ^{13}C NMR (400MHz, $CDCl_3$) spectra of Boron complex **(3a)** in $CDCl_3$

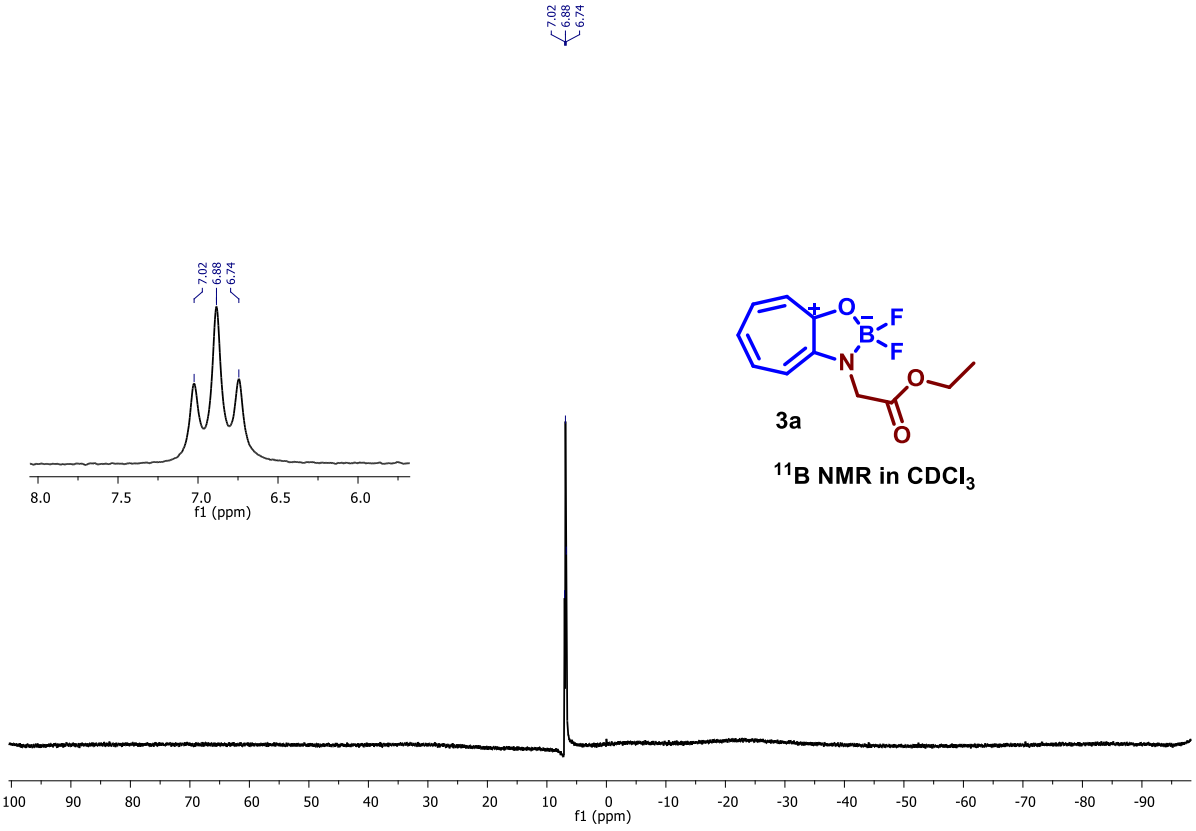

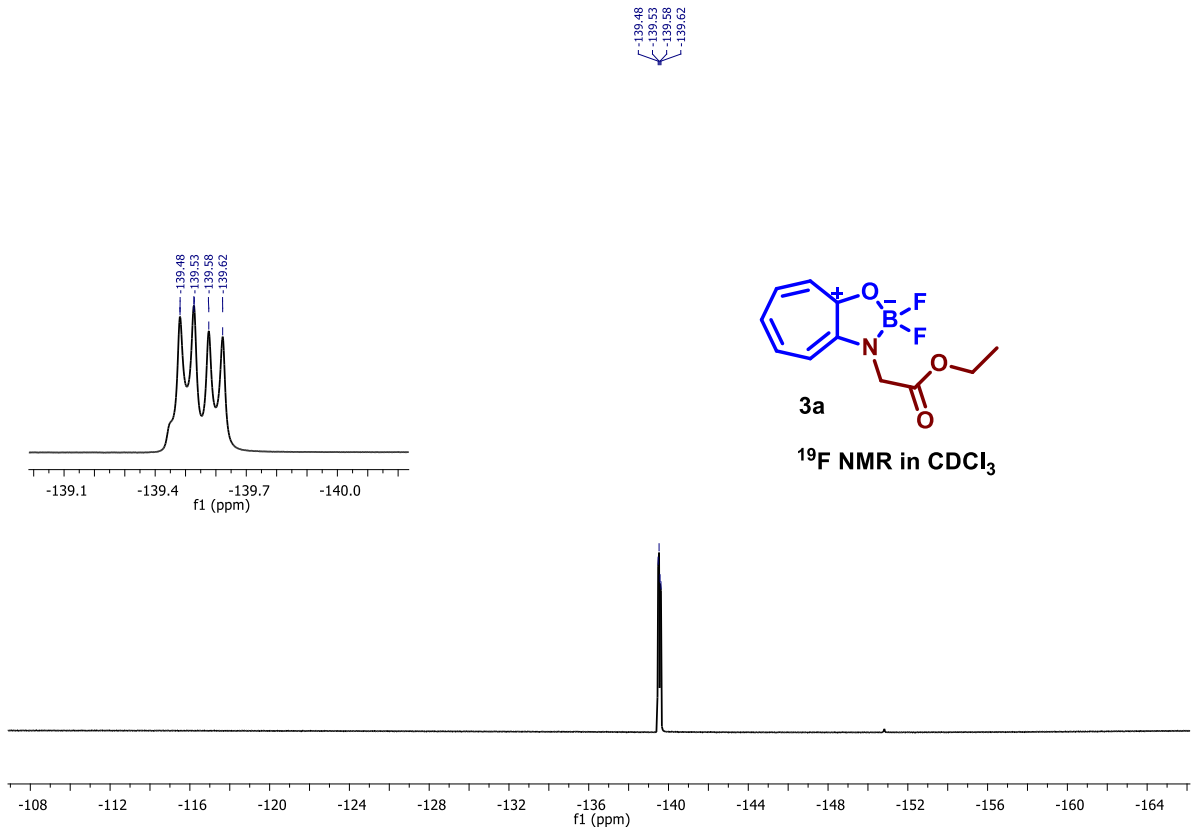

Figure S20. ^{11}B and ^{19}F NMR (400MHz, $CDCl_3$) spectra of Boron complex **(3a)** in $CDCl_3$

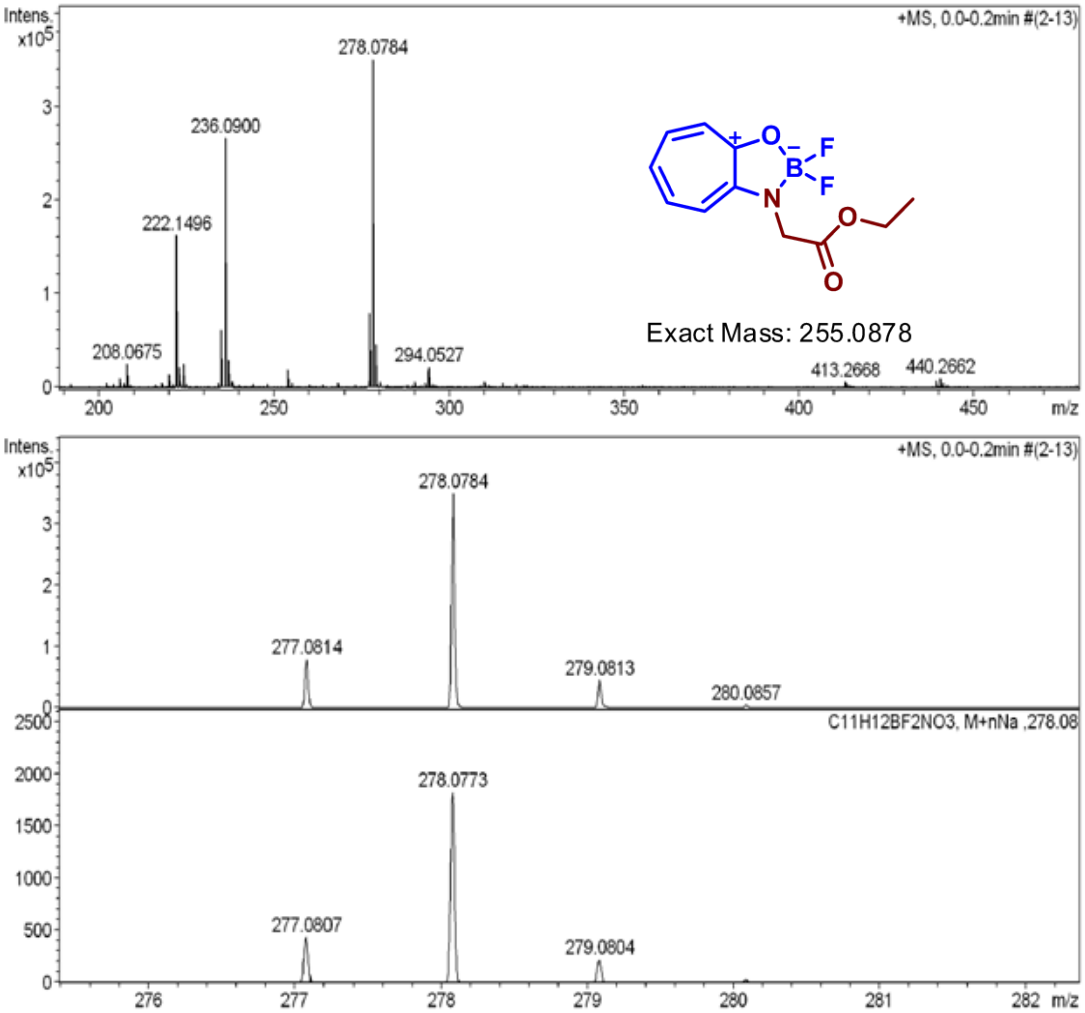

Figure S21. ESI-MS/HRMS spectra of Boron complex **(3a)**.

12. NMR (^{1}H, ^{13}C, ^{11}B, ^{19}F) and HRMS of Boron complex *tr-ala* **(3b)**

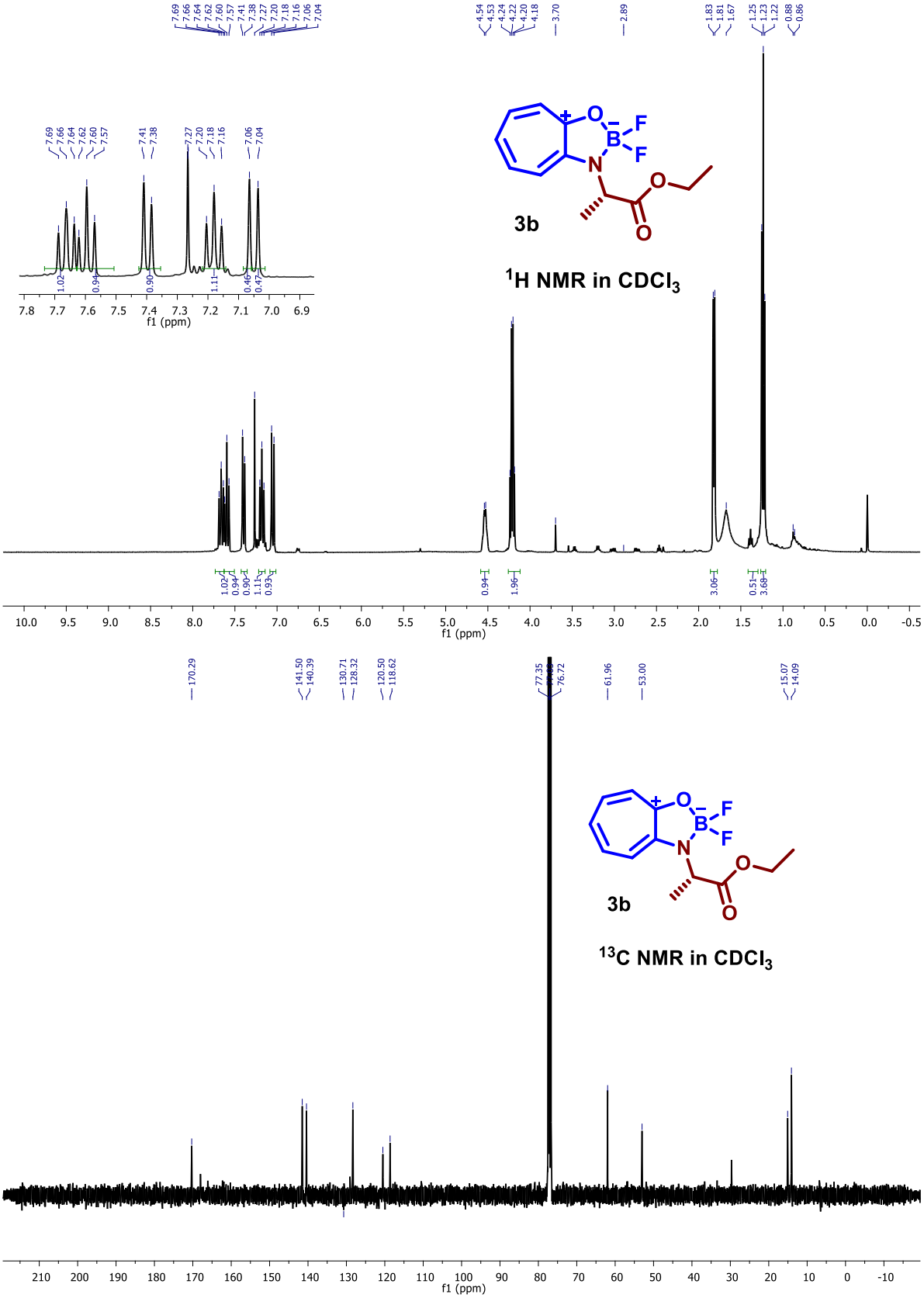

Figure S22. ^{1}H, ^{13}C NMR (400MHz, $CDCl_3$) spectra of Boron complex **(3b)** in $CDCl_3$

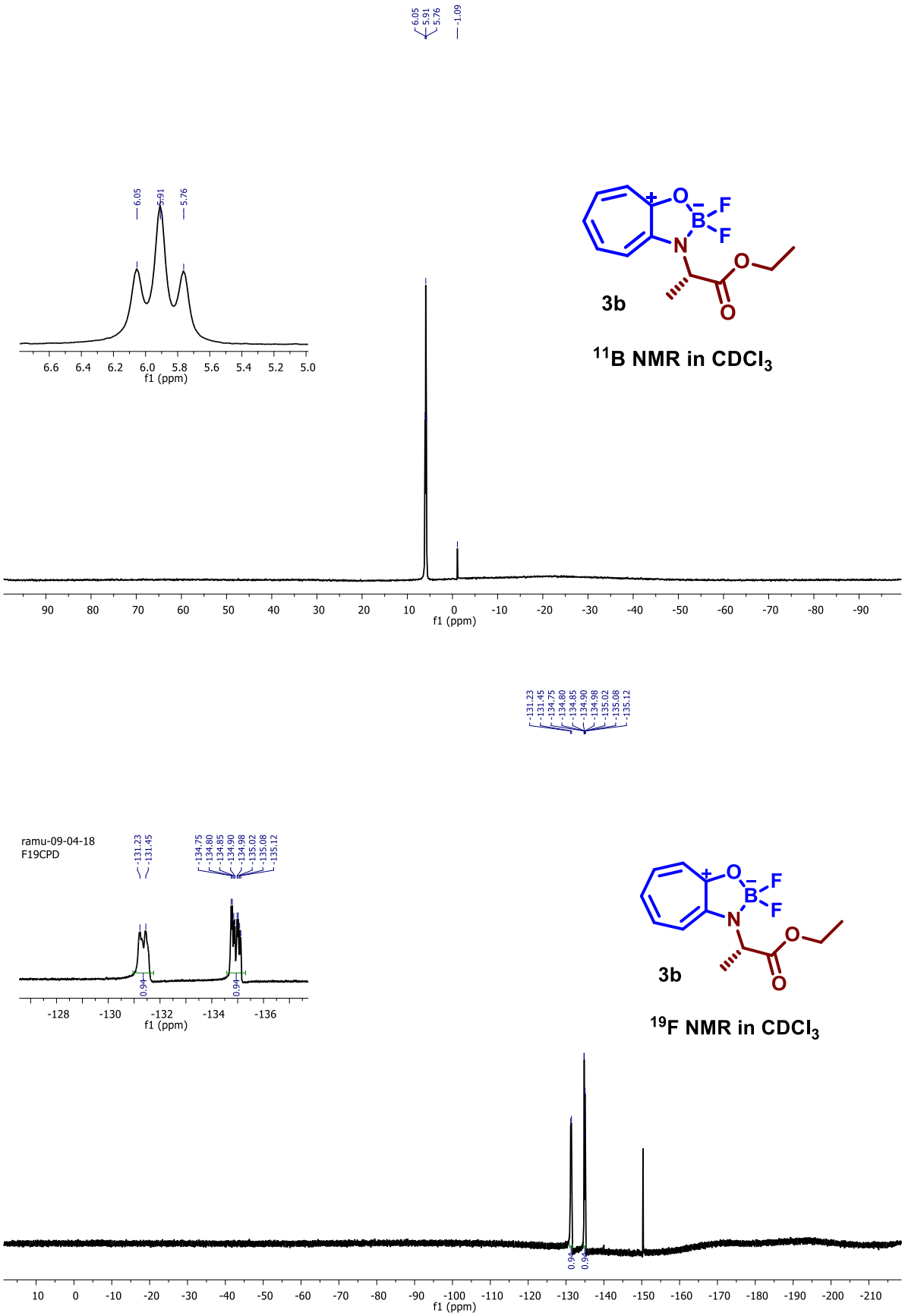

Figure S23. ^{11}B and ^{19}F NMR (400MHz, $CDCl_3$) spectra of Boron complex **(3b)** in $CDCl_3$

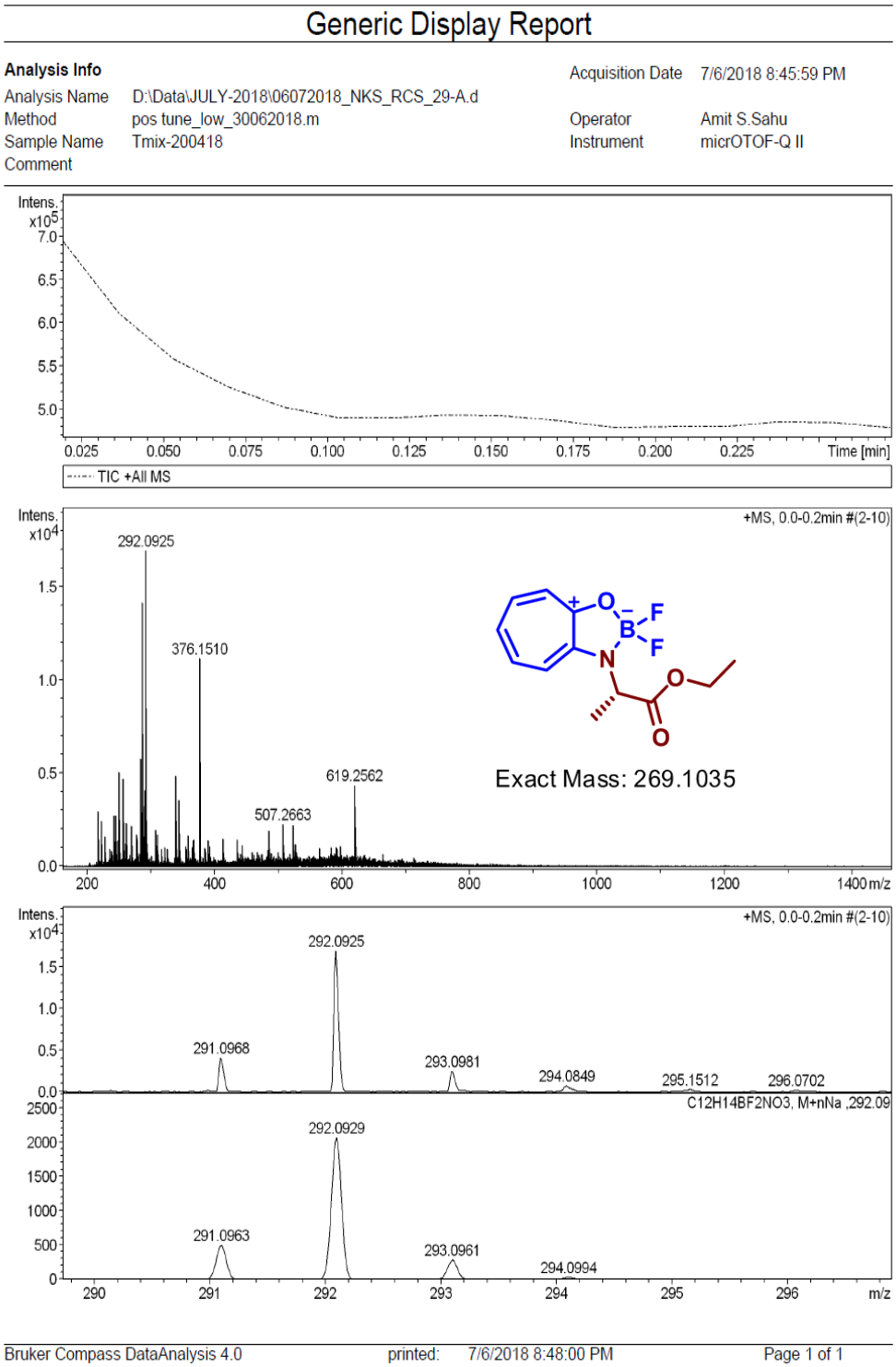

Figure S24. ESI-MS/HRMS spectra of Boron complex **(3b)**

13. NMR (^{1}H, ^{13}C, ^{11}B, ^{19}F) and HRMS of Boron complex *tr-val* **(3c)**

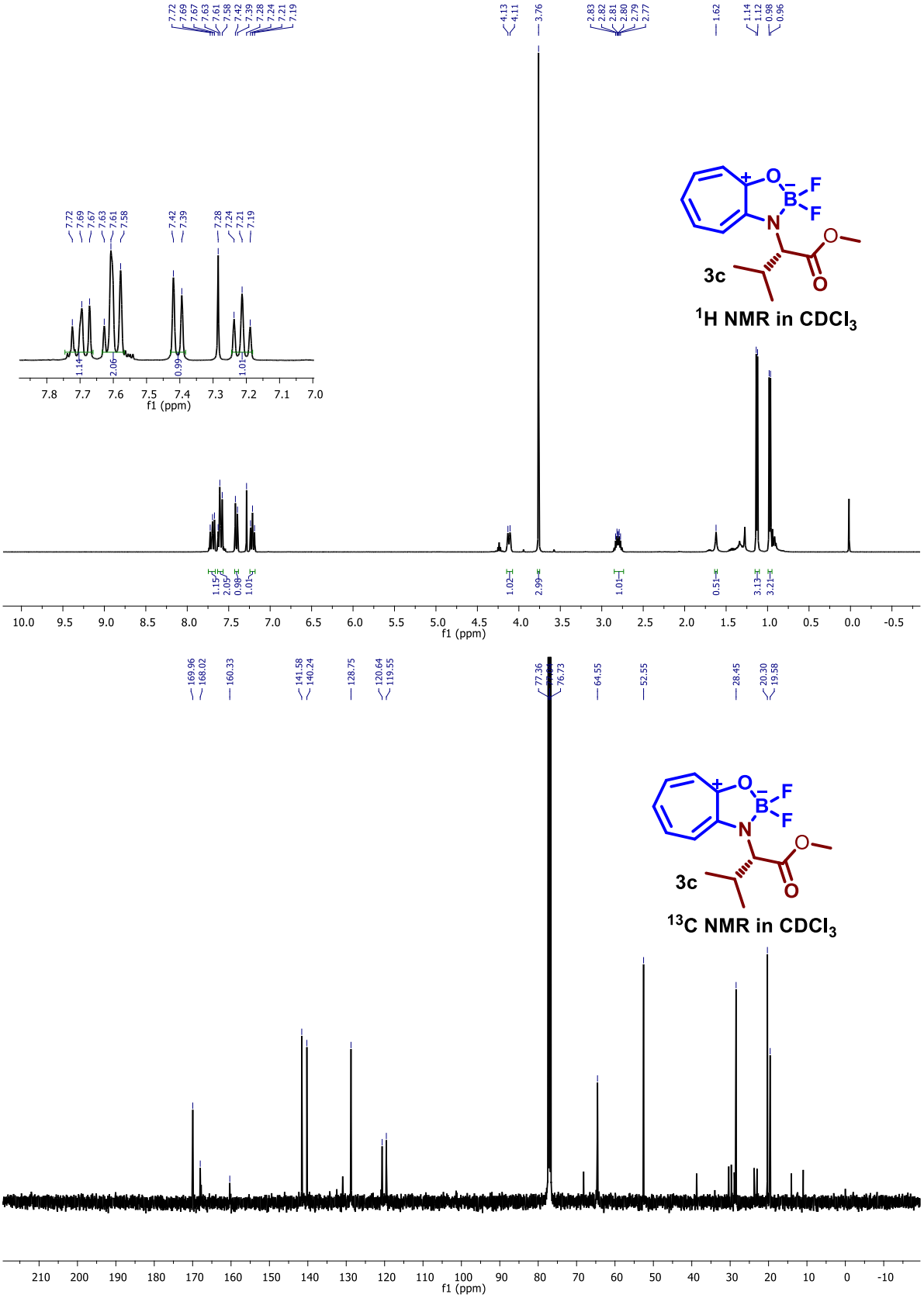

Figure S25. ^{1}H, ^{13}C NMR (400MHz, $CDCl_3$) spectra of Boron complex **(3c)** in $CDCl_3$

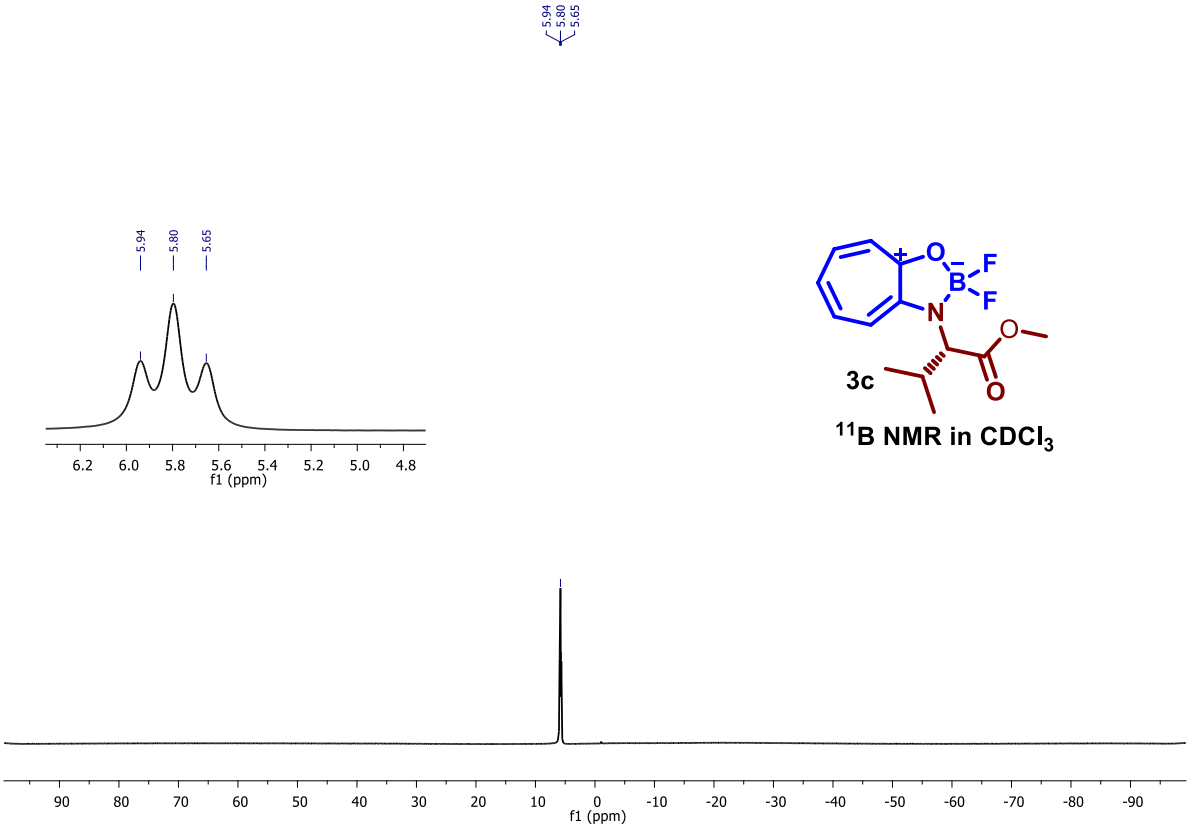

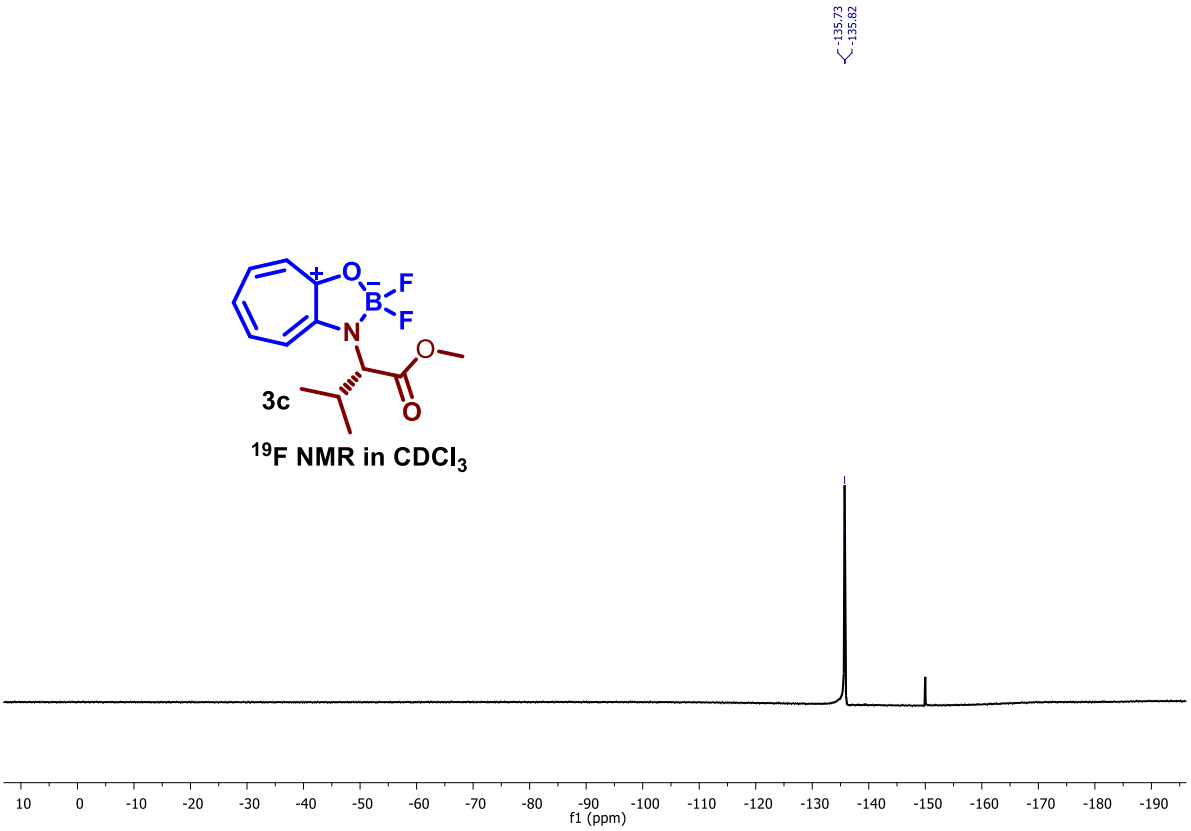

Figure S26. ^{11}B and ^{19}F NMR (400MHz, $CDCl_3$) spectra of Boron complex **(3c)** in $CDCl_3$

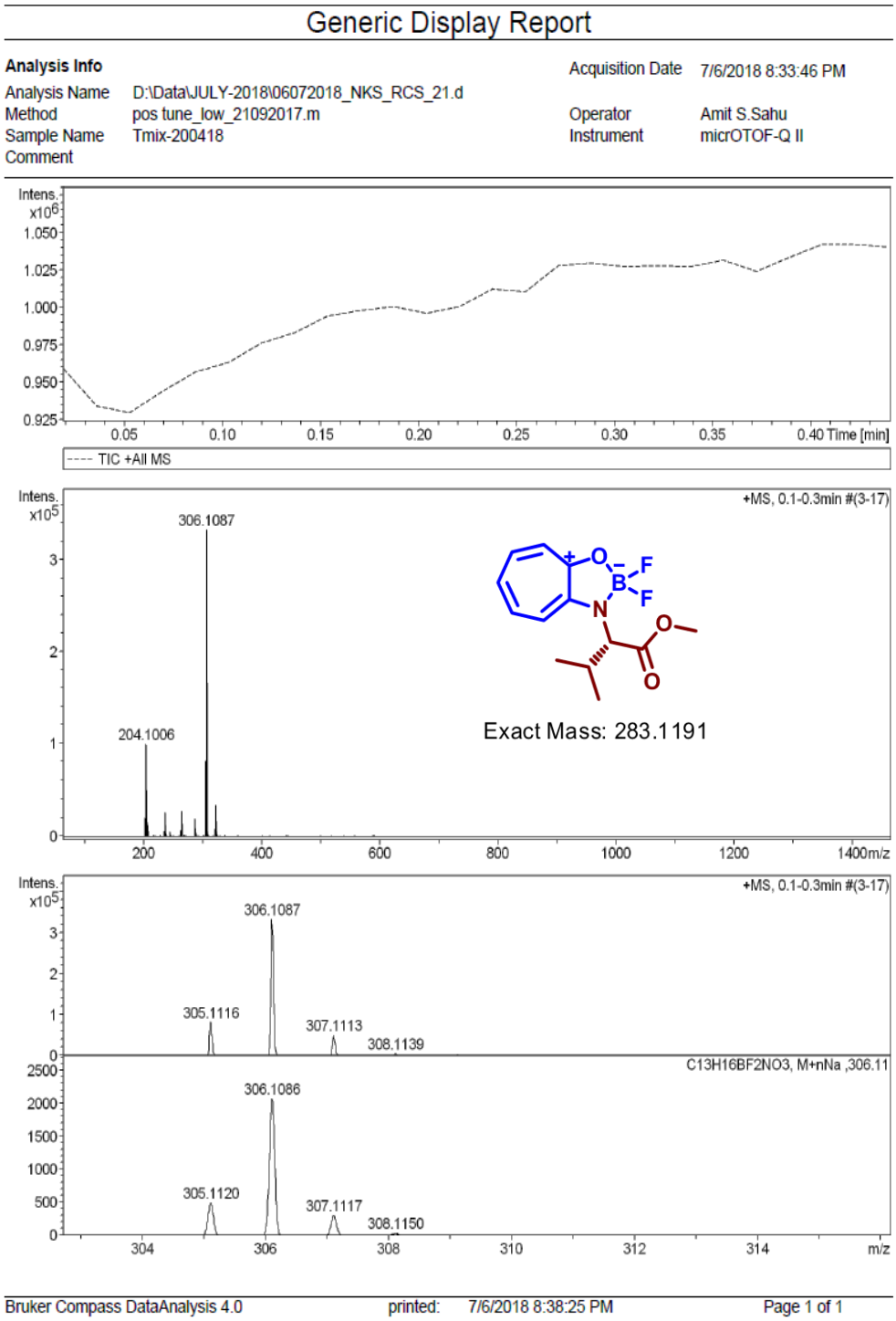

Figure S27. ESI-MS/HRMS spectra of Boron complex **(3c)**

14. NMR (^{1}H, ^{13}C, ^{11}B, ^{19}F) and HRMS of Boron complex *tr-lue* **(3d)**

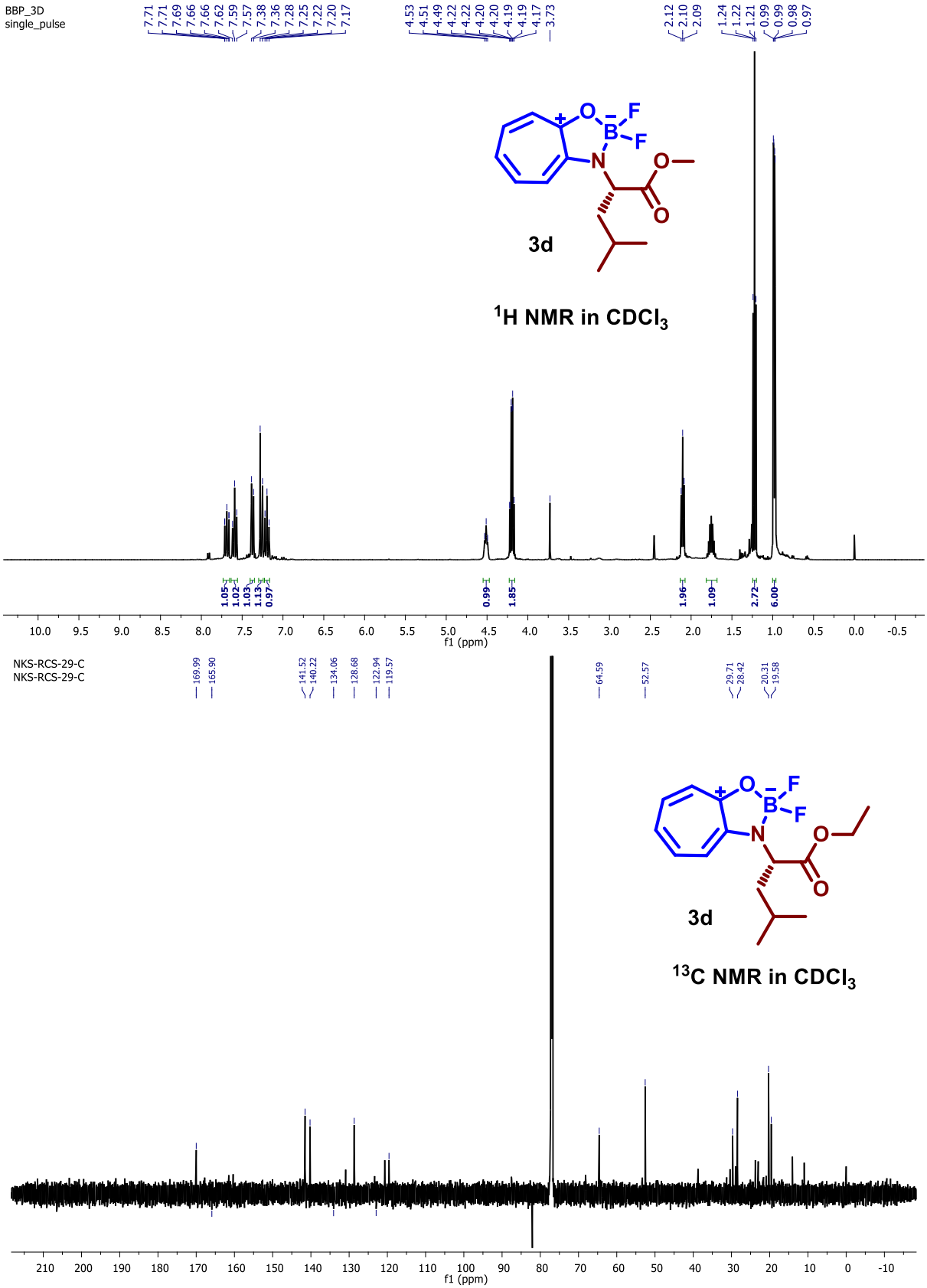

Figure S28. ^{1}H, ^{13}C NMR (400MHz, $CDCl_3$) spectra of Boron complex **(3d)** in $CDCl_3$

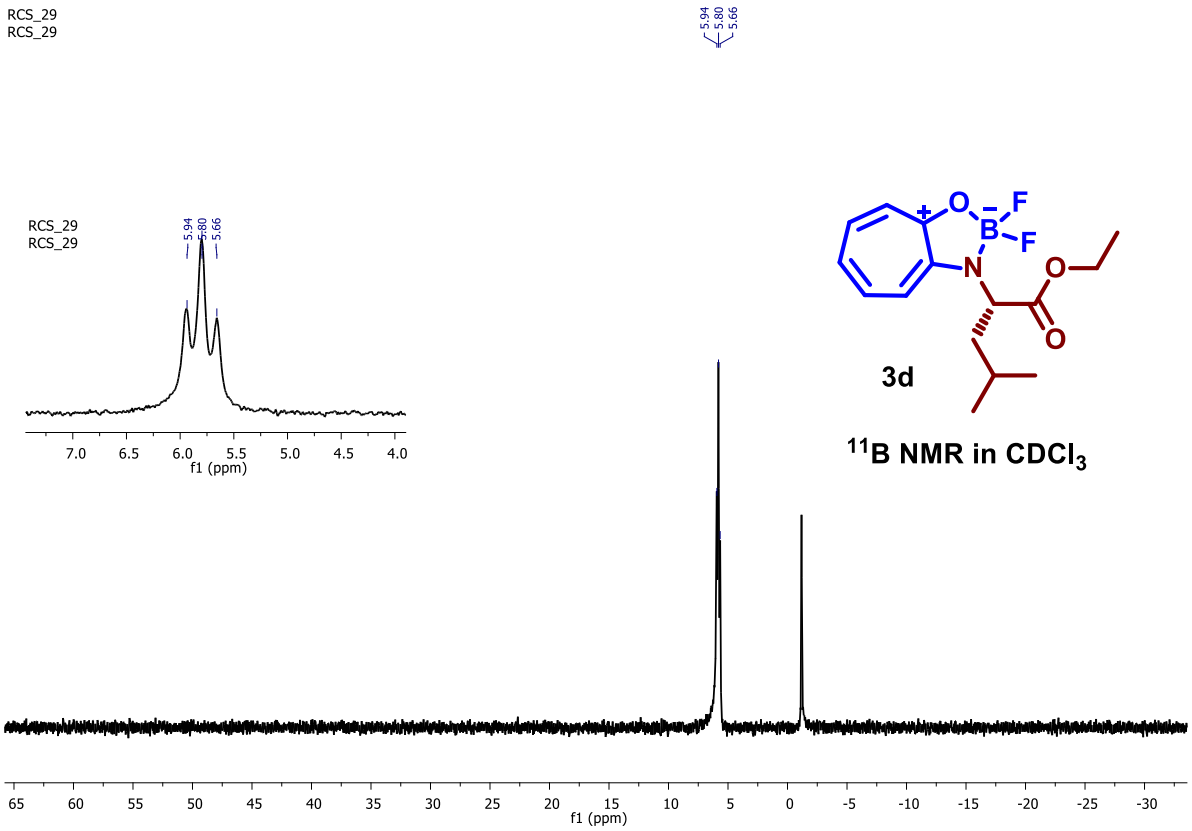

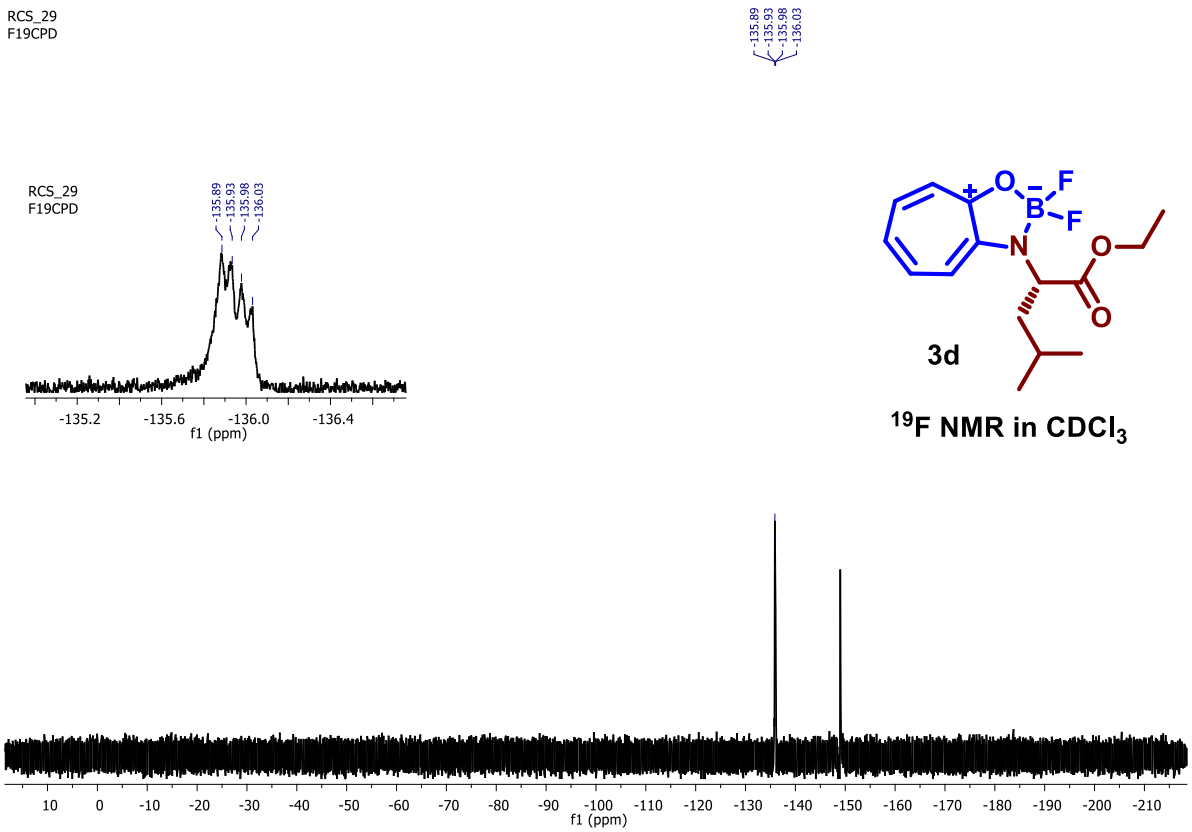

Figure S29. ^{11}B and ^{19}F NMR (400MHz, $CDCl_3$) spectra of Boron complex **(3d)** in $CDCl_3$

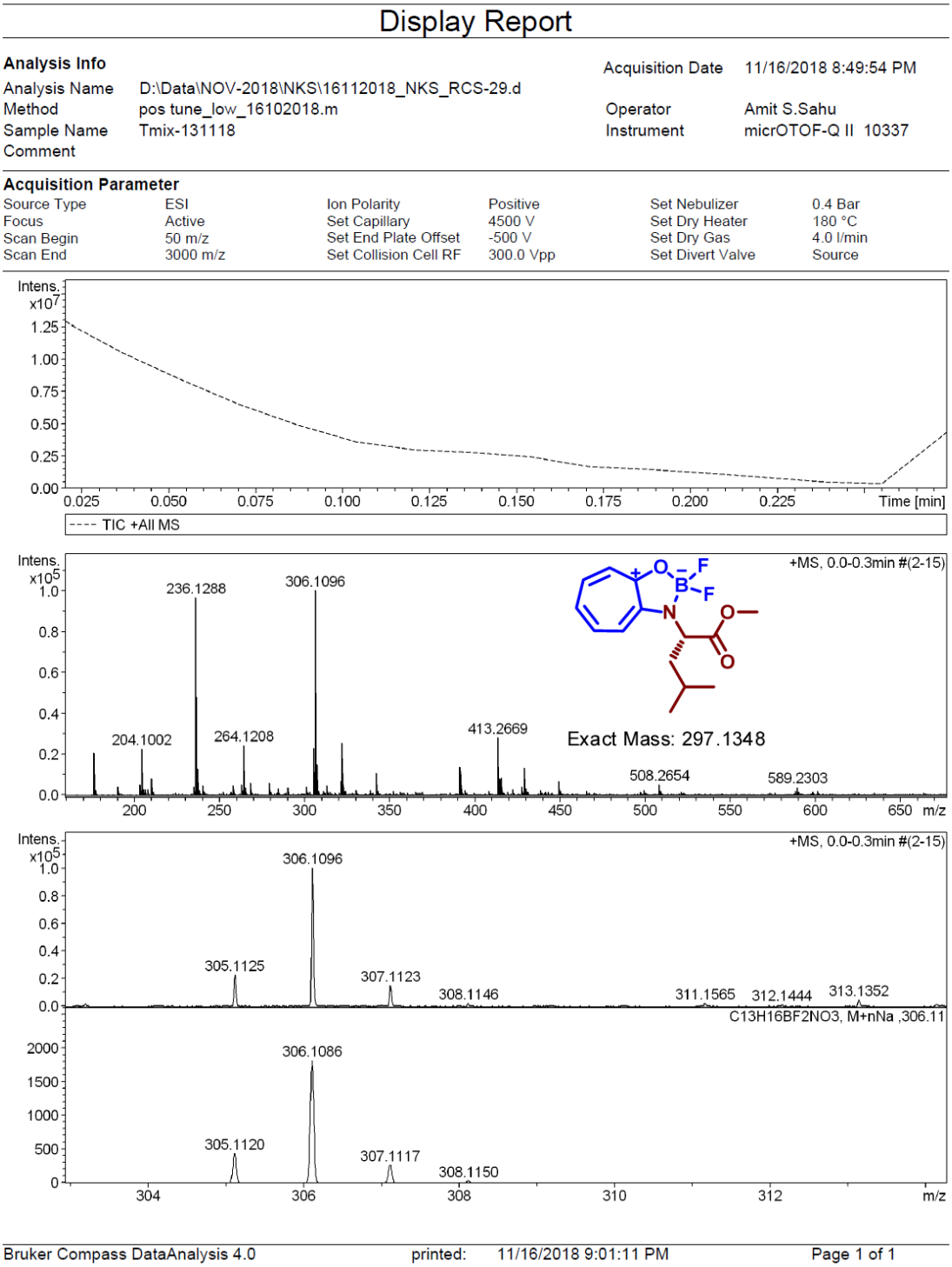

Figure S30. ESI-MS/HRMS spectra of Boron complex **(3d)**

15. NMR (^{1}H, ^{13}C, ^{11}B, ^{19}F) and HRMS of Boron complex *tr-phe* **(3e)**

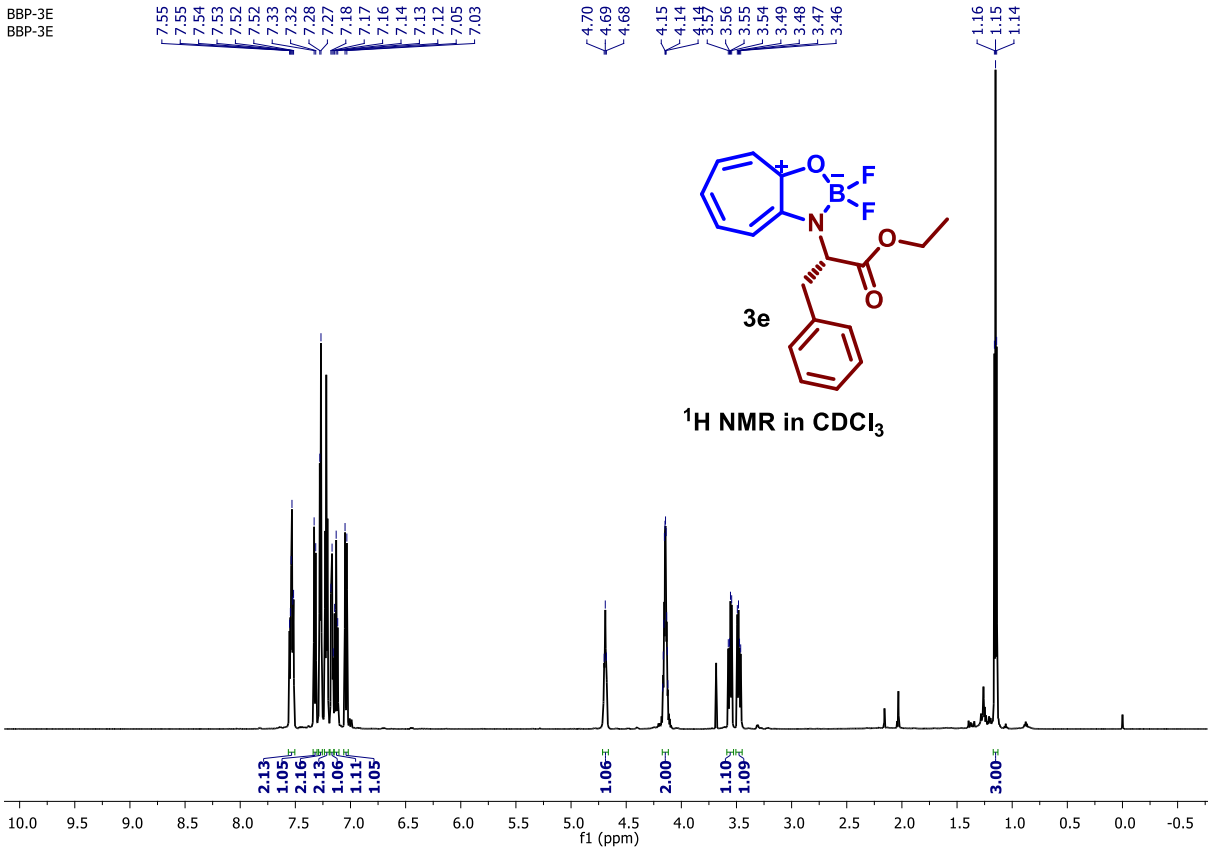

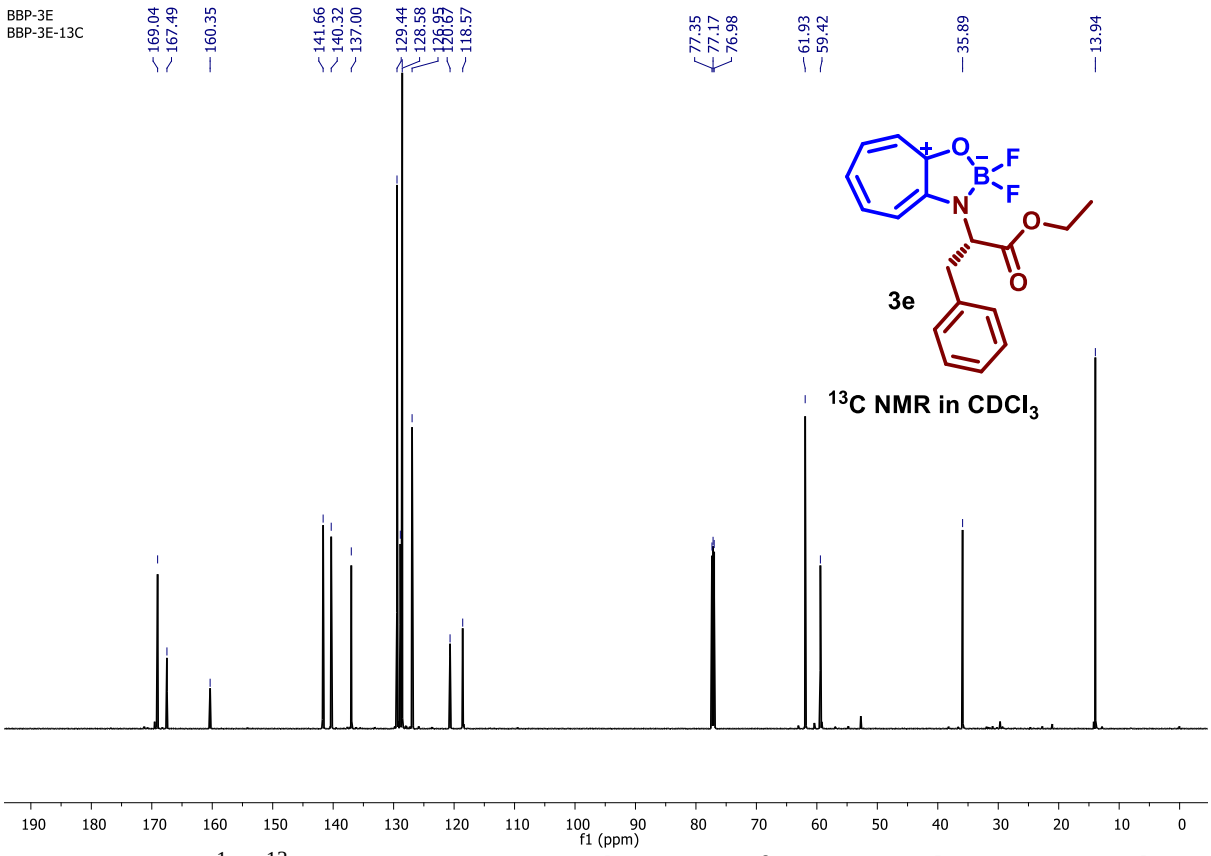

Figure S31. ^{1}H, ^{13}C NMR (700MHz, $CDCl_3$) spectra of Boron complex **(3e)** in $CDCl_3$

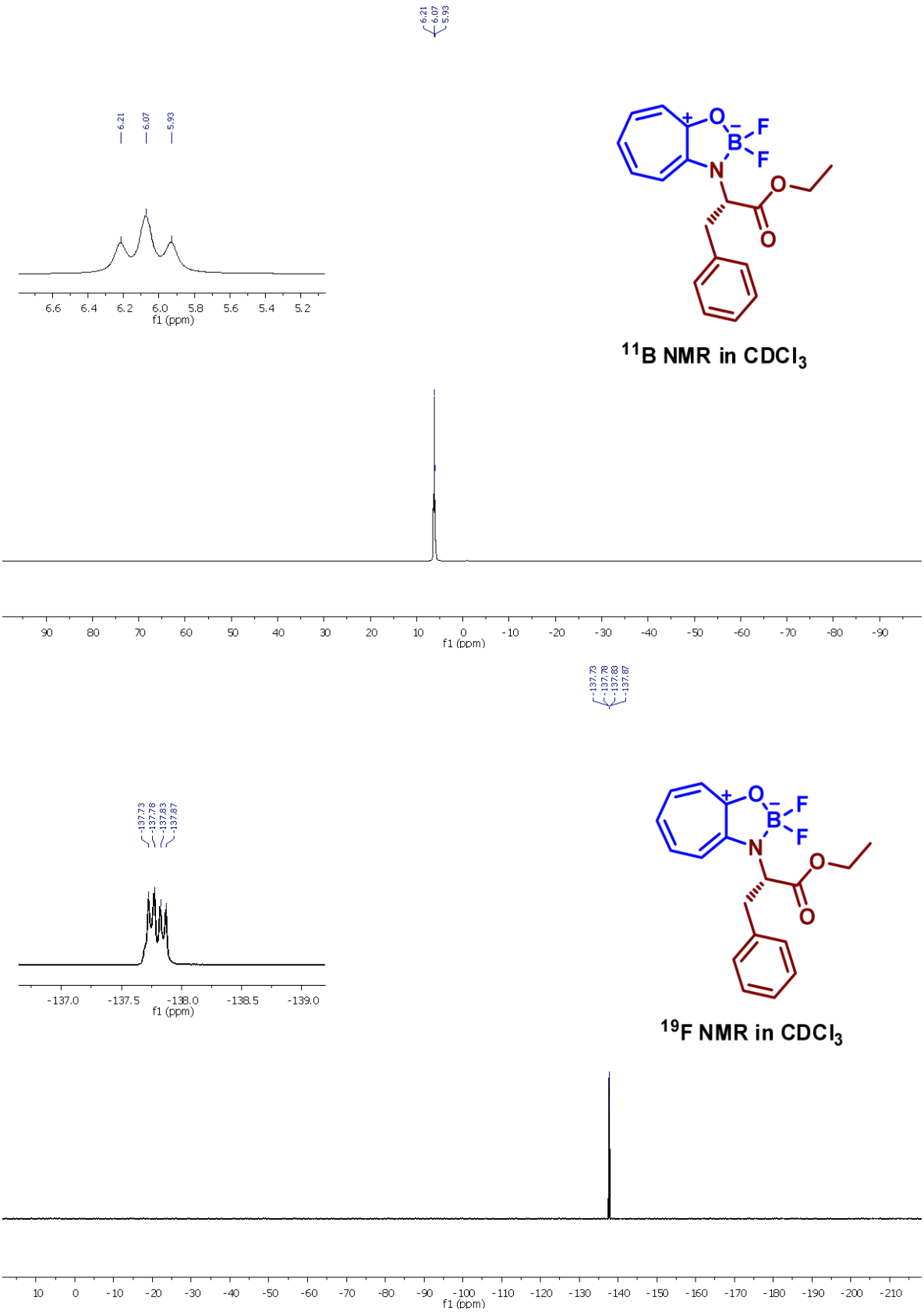

Figure S32. ^{11}B and ^{19}F NMR (400MHz, $CDCl_3$) spectra of Boron complex **(3e)** in $CDCl_3$

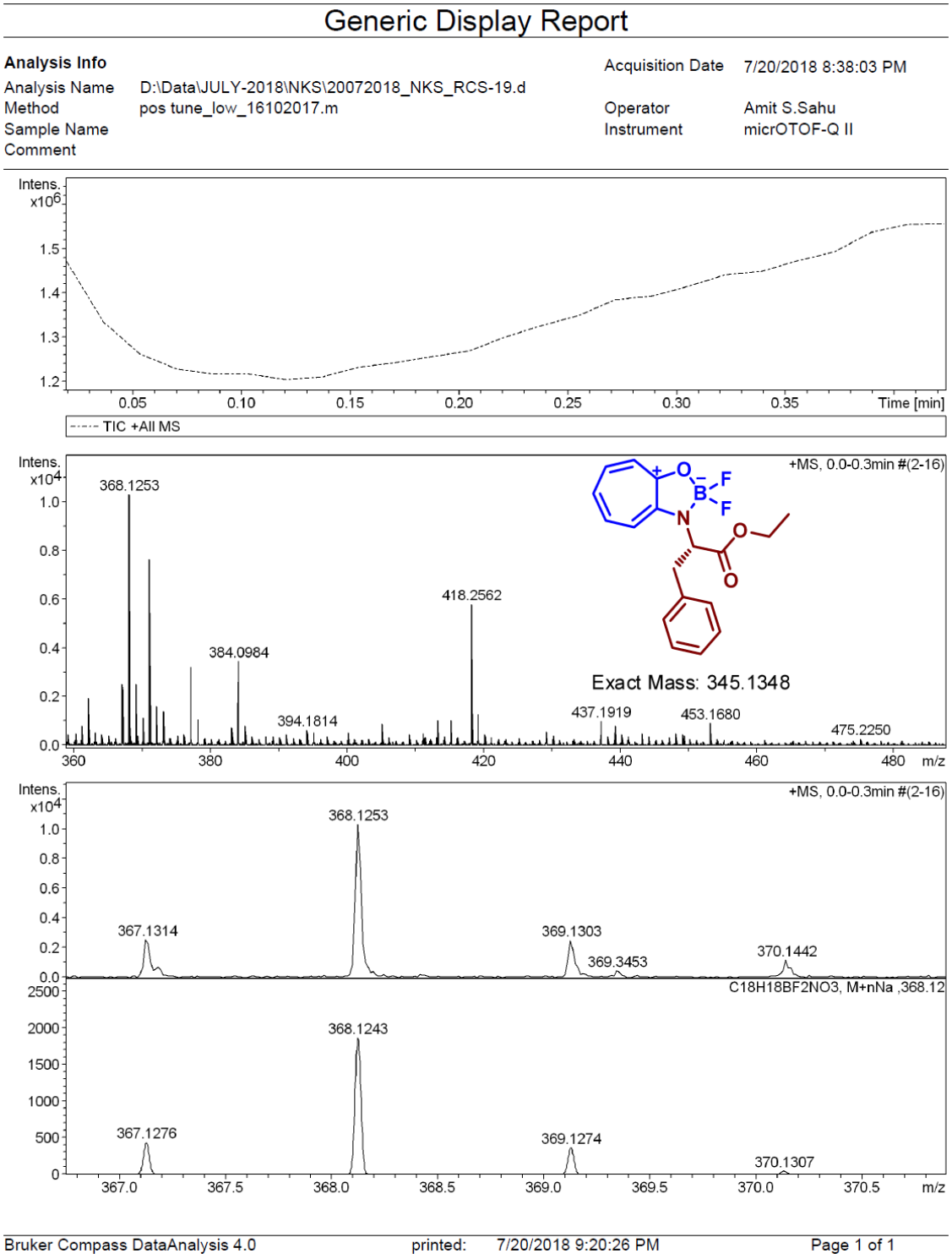

Figure S33. ESI-MS/HRMS spectra of Boron complex **(3e)**

16. NMR (^{1}H, ^{13}C, ^{11}B, ^{19}F) and HRMS of Boron complex *tr-beta ala* **(3f)**

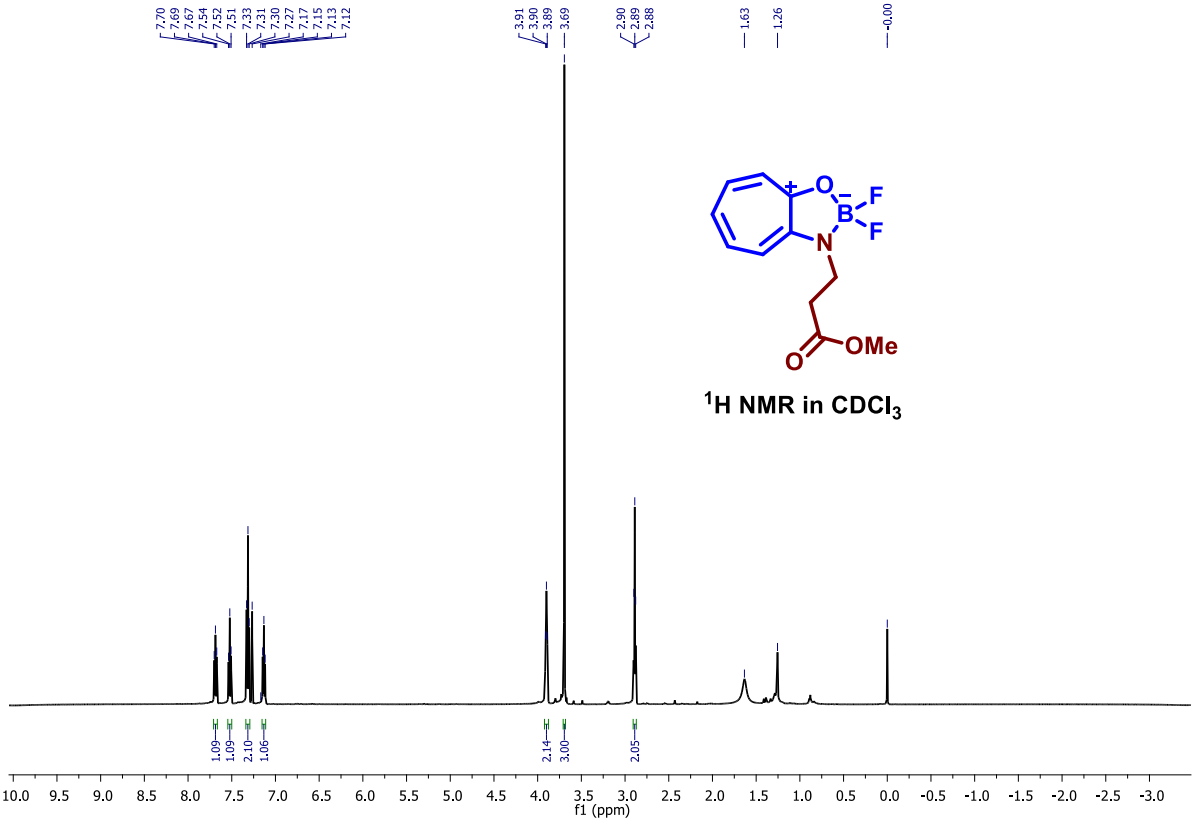

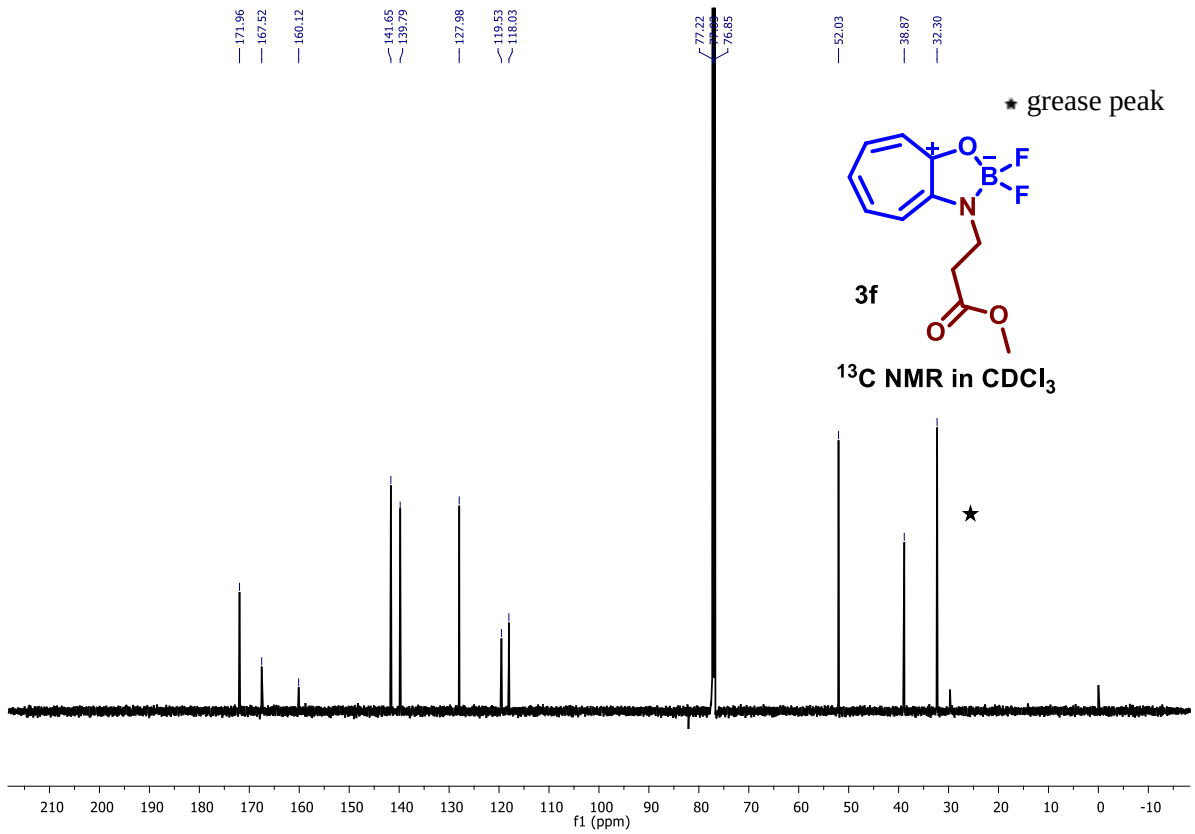

Figure S34. ^{1}H, ^{13}C NMR (700MHz, $CDCl_3$) spectra of Boron complex **(3f)** in $CDCl_3$

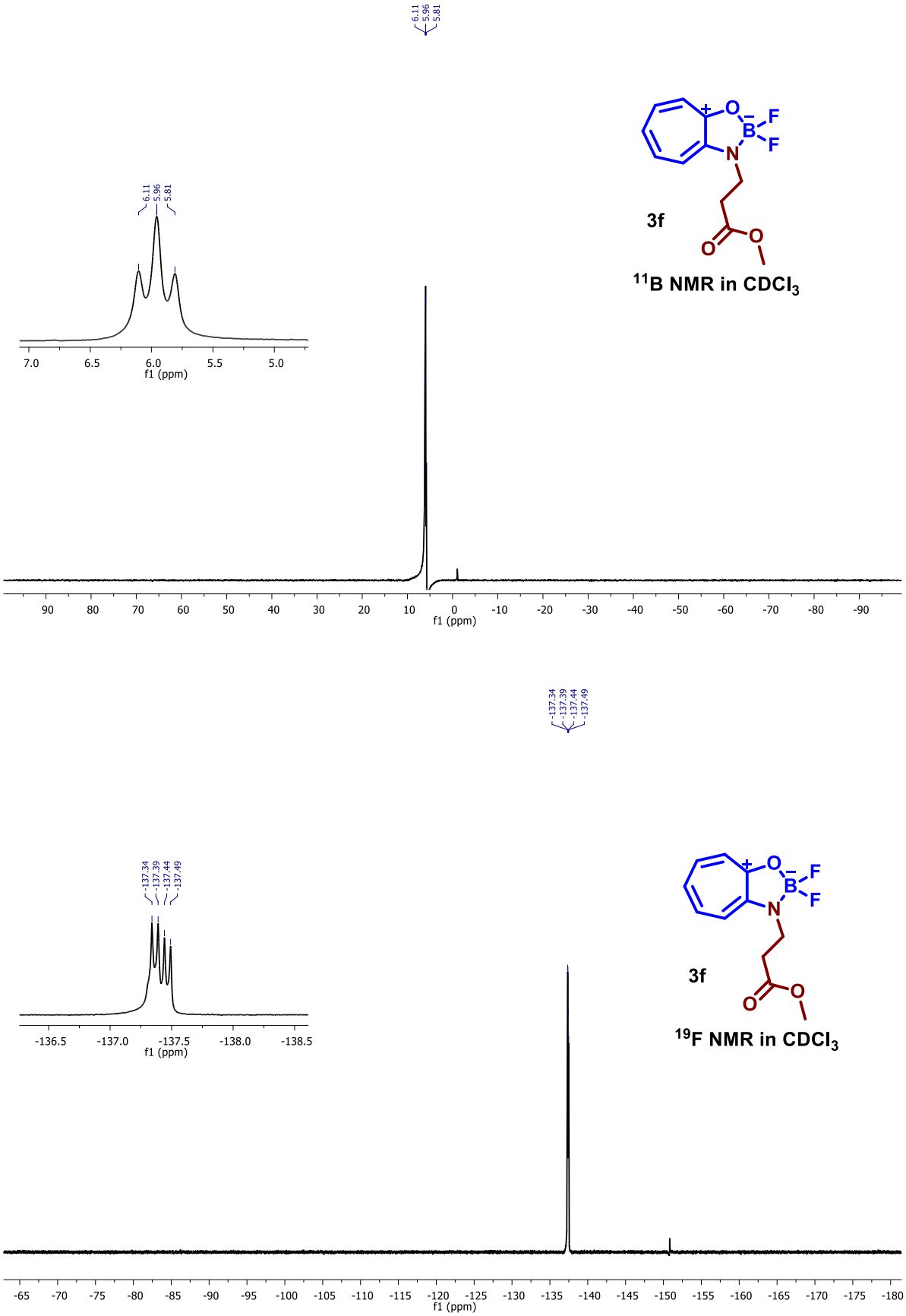

Figure S35. ^{11}B and ^{19}F NMR (400MHz, $CDCl_3$) spectra of Boron complex **(3f)** in $CDCl_3$

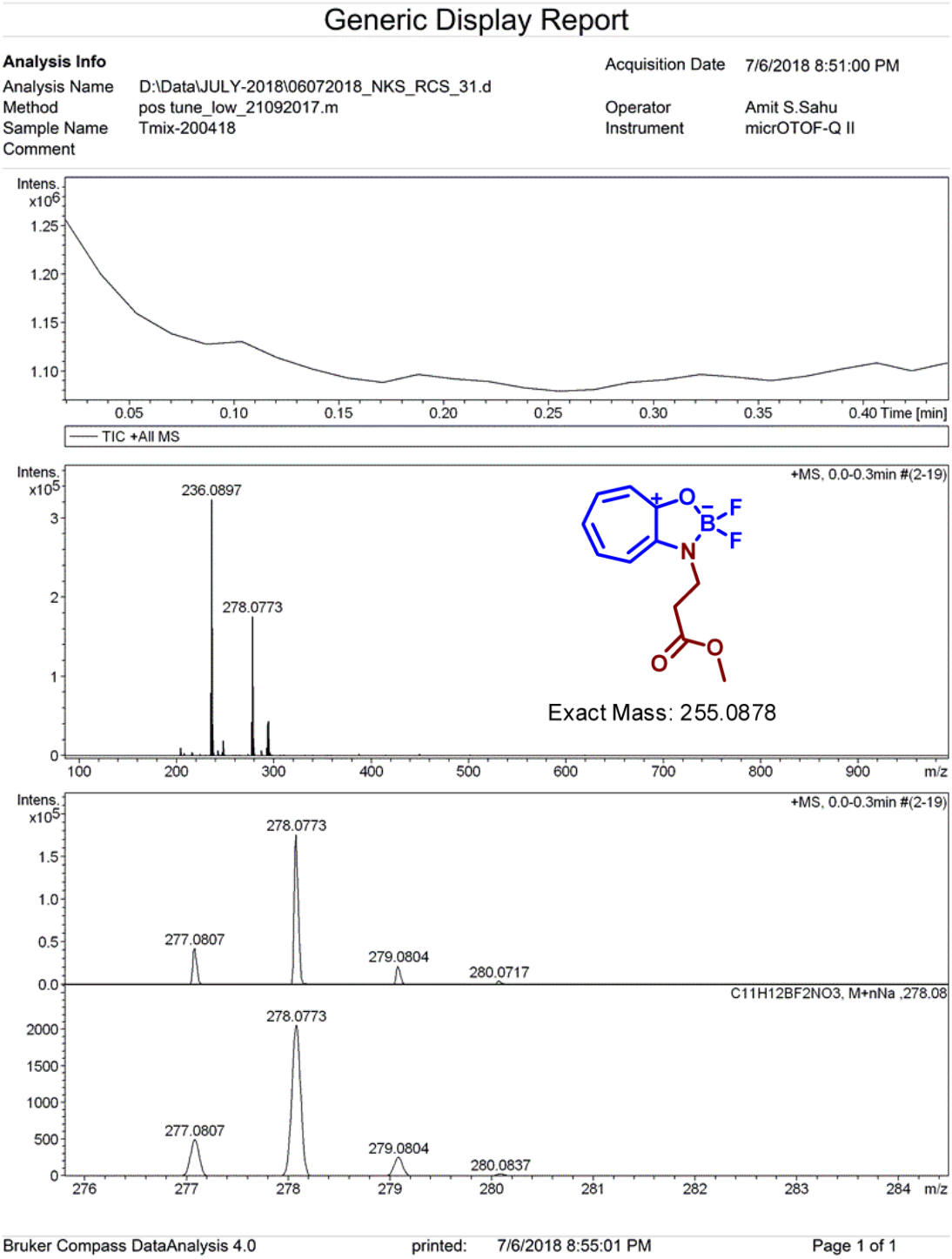

Figure S36. ESI-MS/HRMS spectra of Boron complex **(3f)**

17. NMR (^{1}H, ^{13}C, ^{11}B, ^{19}F) and HRMS of Boron complex *tr-dipep* **(3g)**

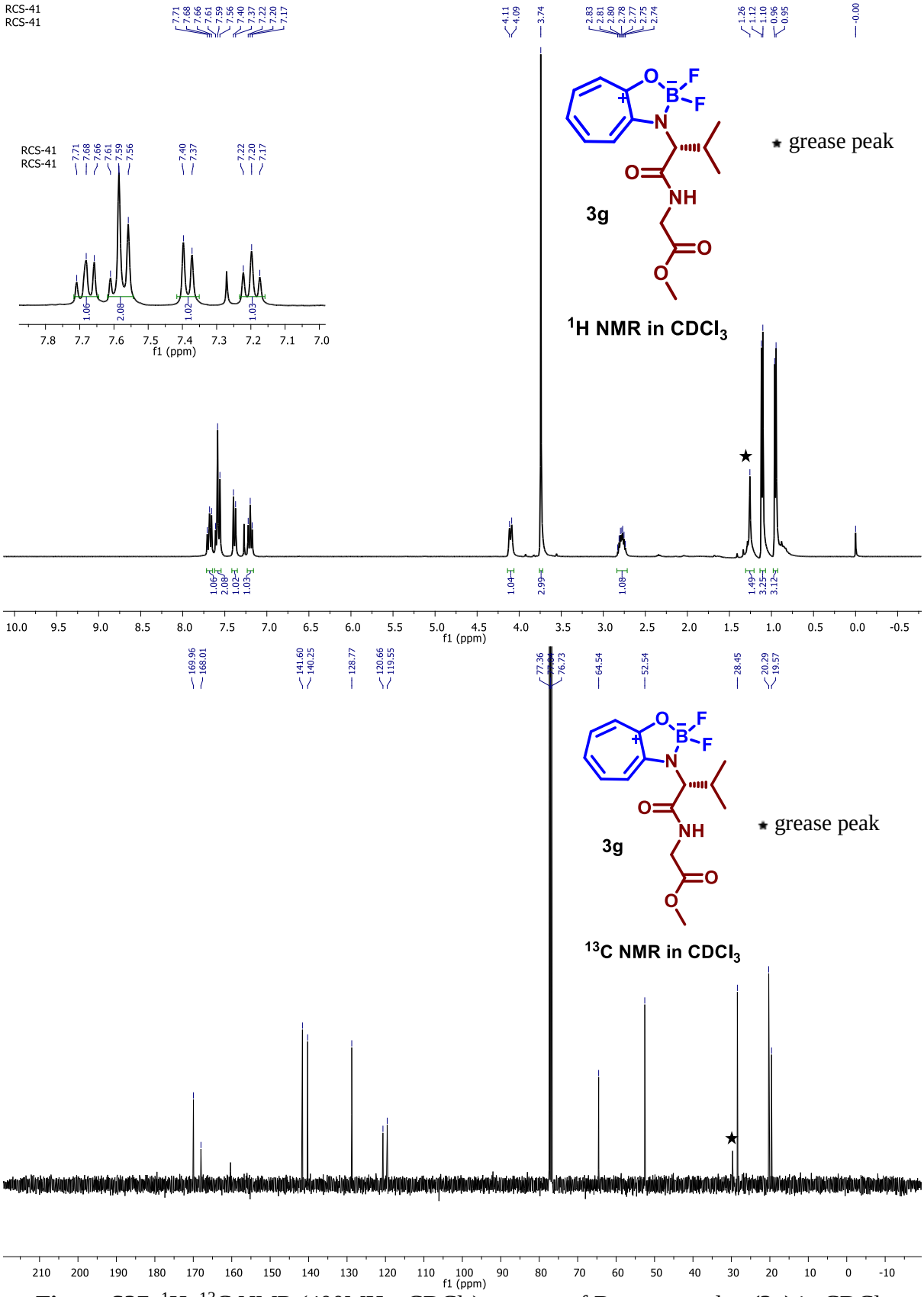

Figure S37. ^{1}H, ^{13}C NMR (400MHz, $CDCl_3$) spectra of Boron complex **(3g)** in $CDCl_3$

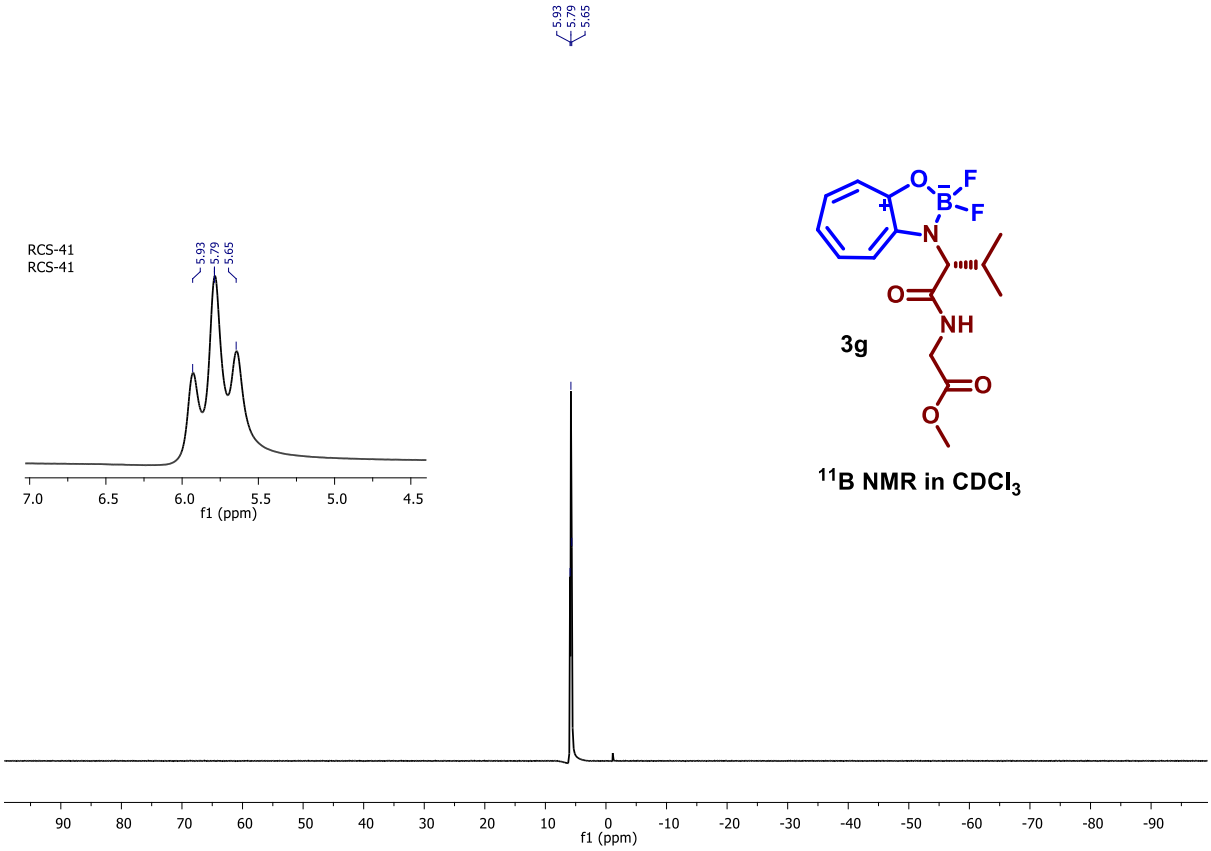

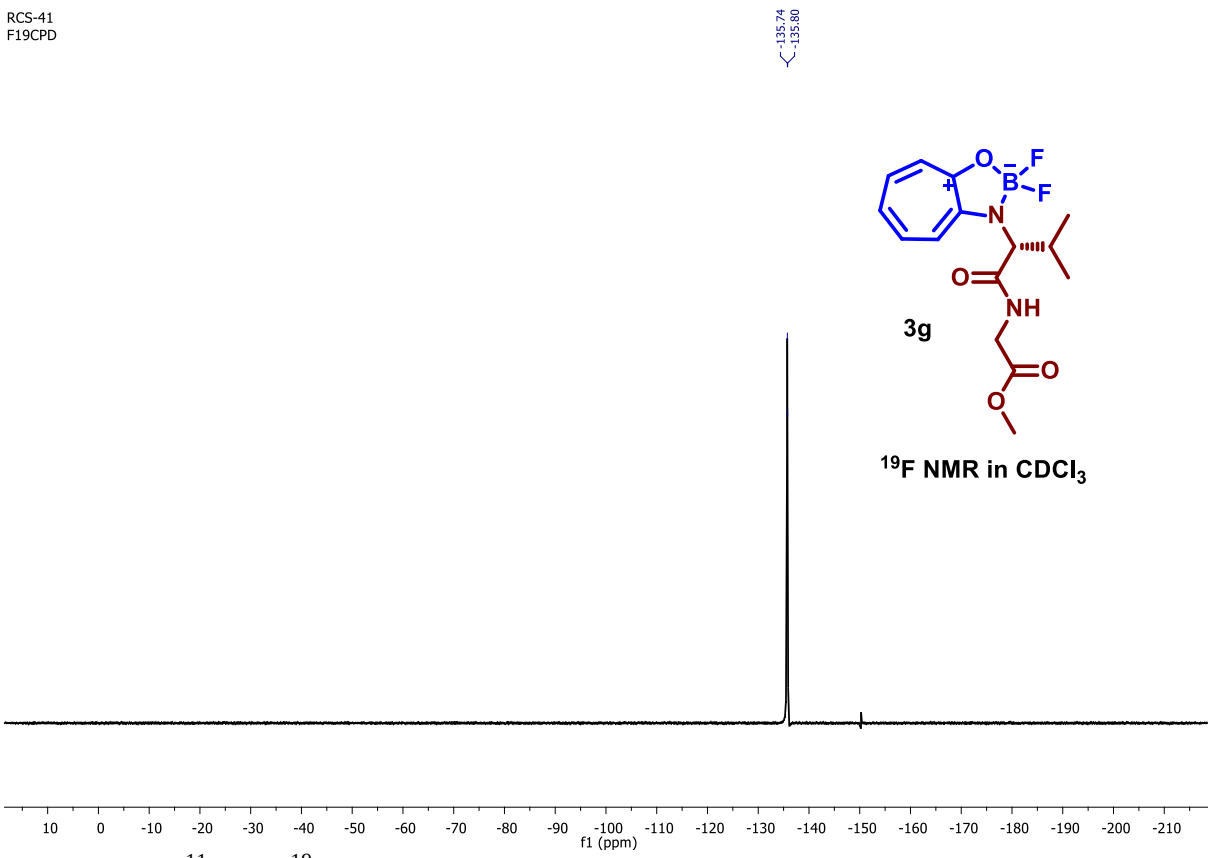

Figure S38. ^{11}B and ^{19}F NMR (400MHz, $CDCl_3$) spectra of Boron complex **(3g)** in $CDCl_3$

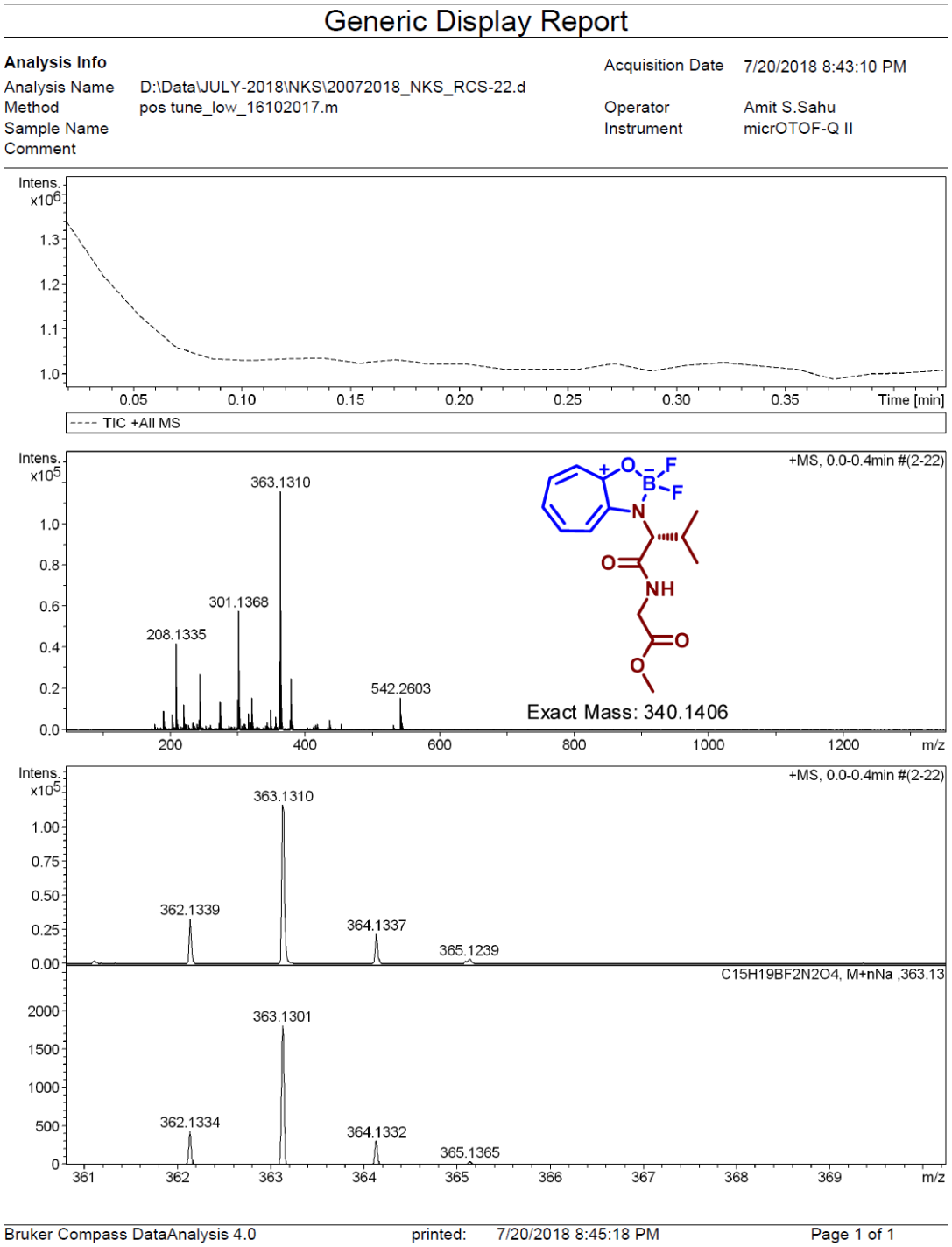

Figure S39. ESI-MS/HRMS spectra of Boron complex **(3g)**

18. NMR (^{1}H, ^{13}C, ^{11}B, ^{19}F) and HRMS of Boron complex *tr-picolylamine* **(3h)**

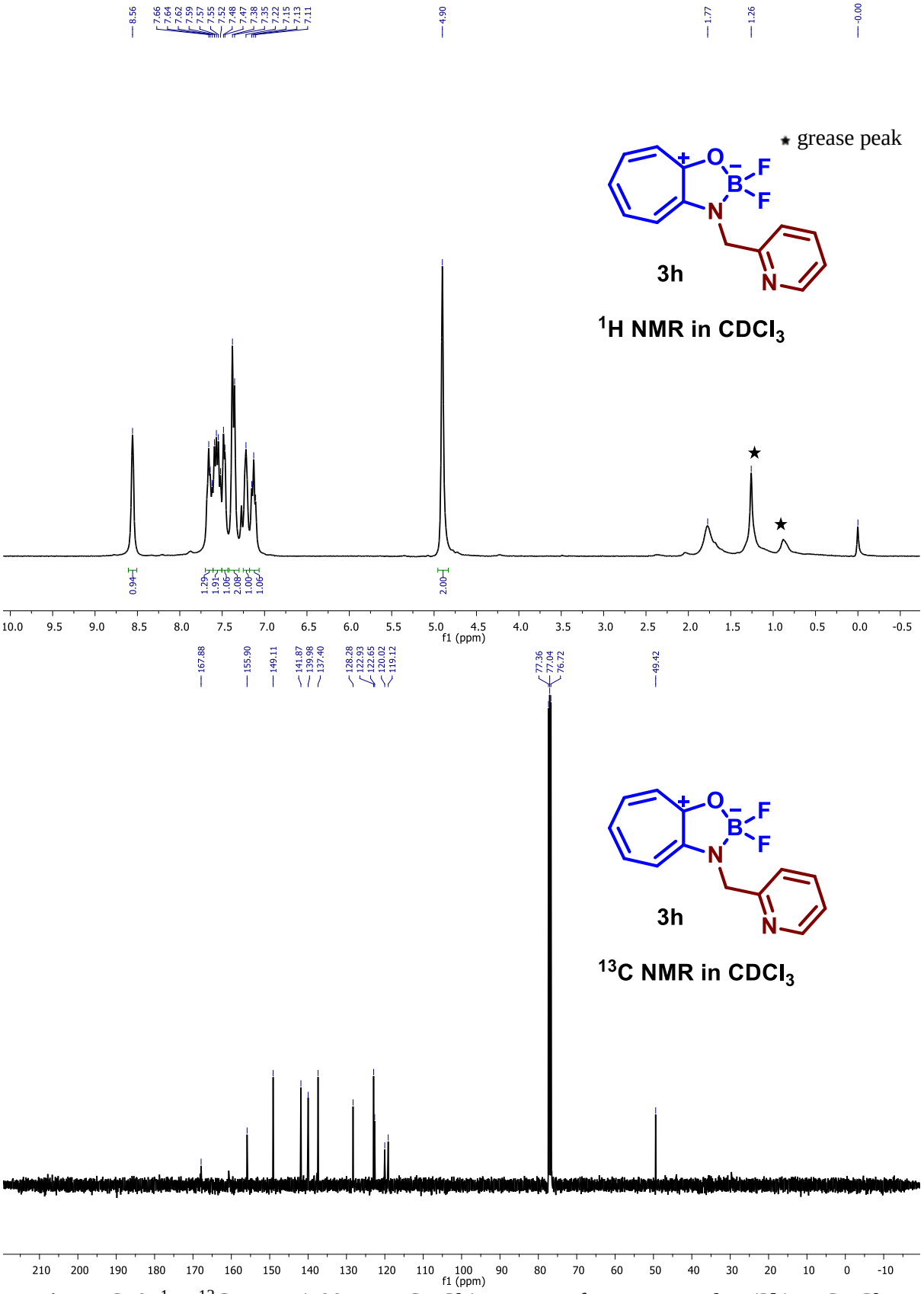

Figure S40. ^{1}H, ^{13}C NMR (400MHz, $CDCl_3$) spectra of Boron complex **(3h)** in $CDCl_3$

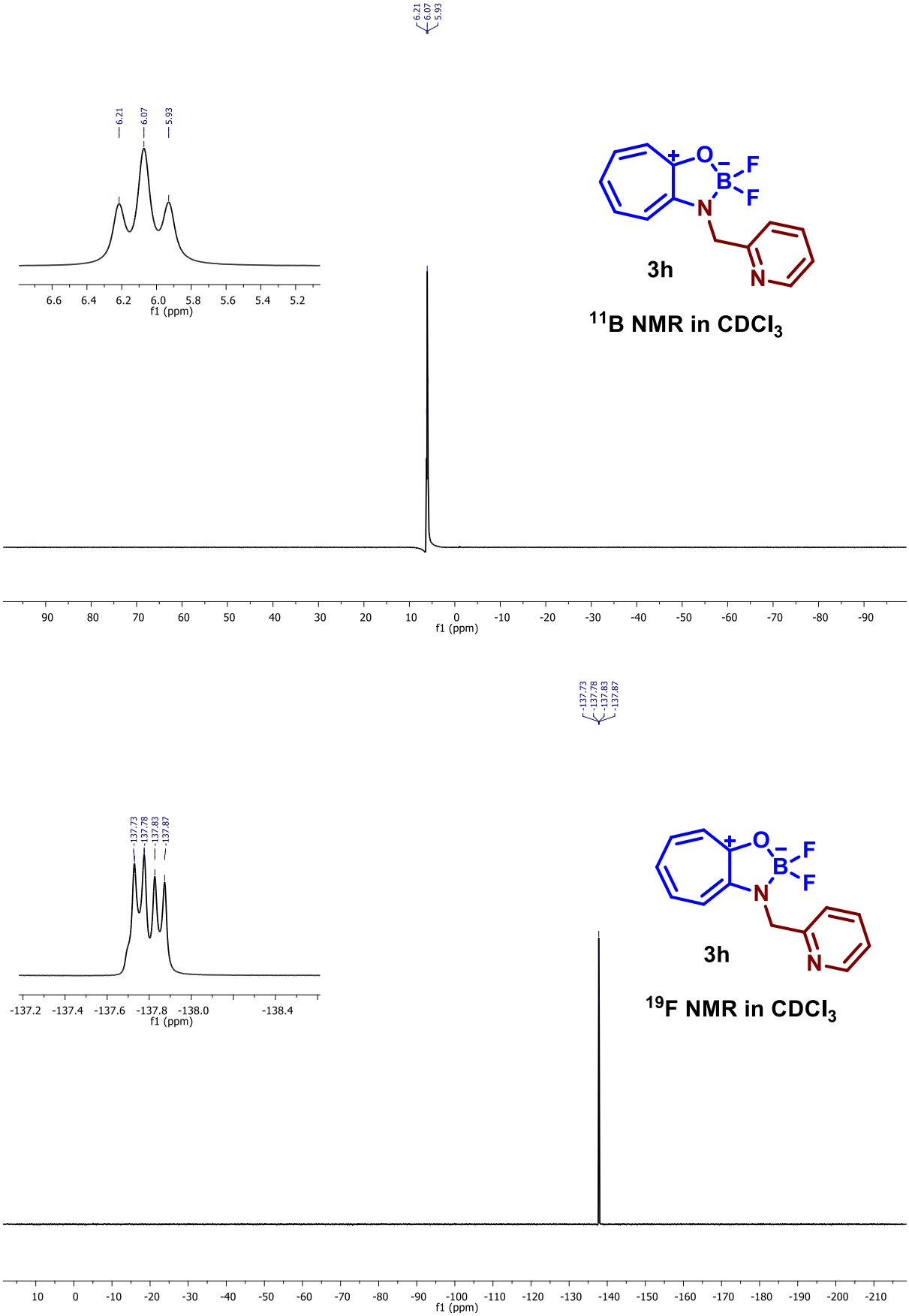

Figure S41. ^{11}B and ^{19}F NMR (400MHz, $CDCl_3$) spectra of Boron complex **(3h)** in $CDCl_3$

Display Report

Analysis Info

Analysis Name	D:\Data\NOV-2018\NKS\16112018_NKS_RCS-49.d	Acquisition Date	11/16/2018 7:57:45 PM
Method	pos tune_low_16102018.m	Operator	Amit S.Sahu
Sample Name	Tmix-131118	Instrument	micrOTOF-Q II 10337
Comment			

Acquisition Parameter

Source Type	ESI	Ion Polarity	Positive	Set Nebulizer	0.4 Bar
Focus	Active	Set Capillary	4500 V	Set Dry Heater	180 °C
Scan Begin	50 m/z	Set End Plate Offset	-500 V	Set Dry Gas	4.0 l/min
Scan End	3000 m/z	Set Collision Cell RF	300.0 Vpp	Set Divert Valve	Source

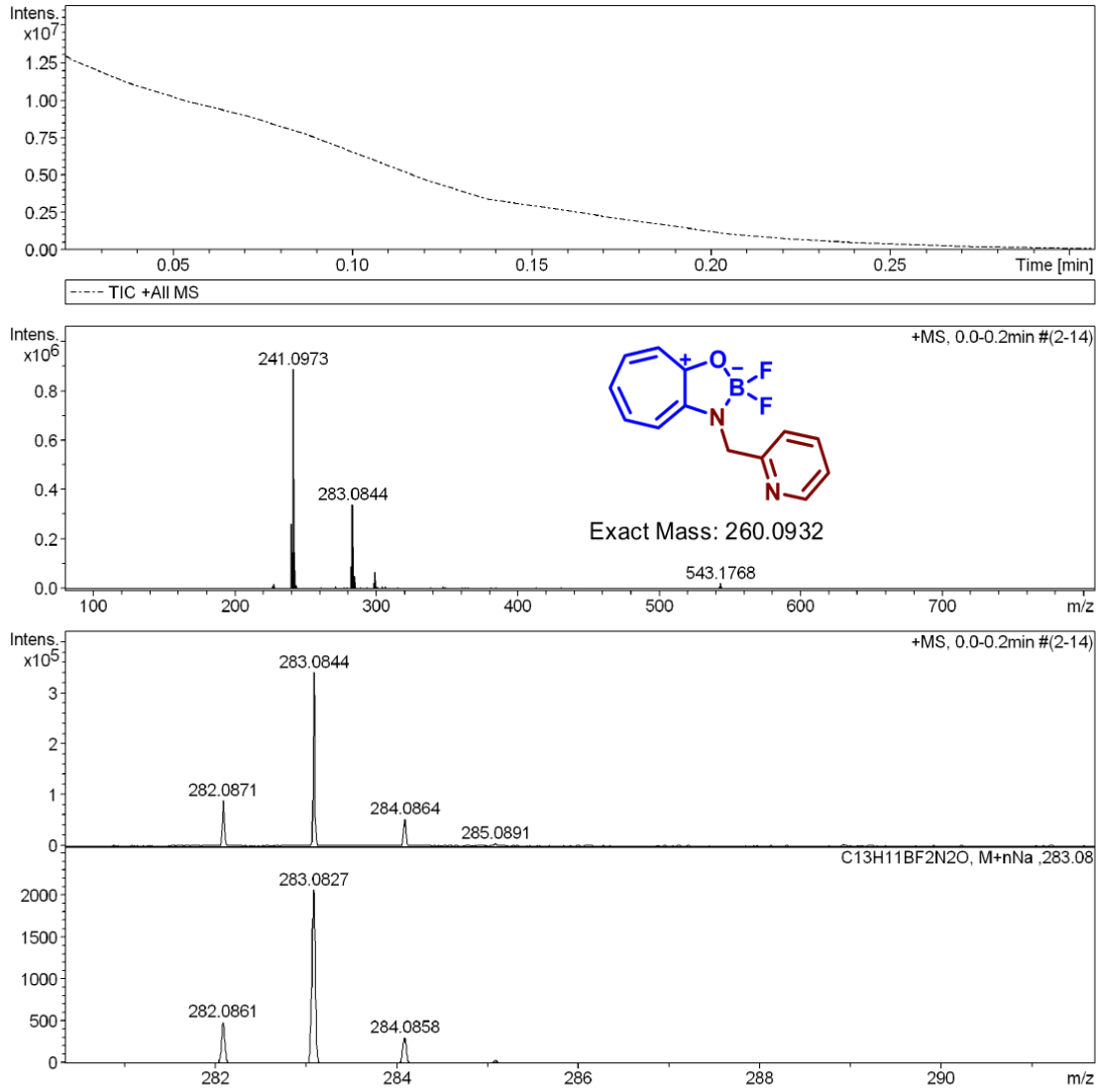

Bruker Compass DataAnalysis 4.0 printed: 11/16/2018 8:00:40 PM Page 1 of 1

Figure S42. ESI-MS/HRMS spectra of Boron complex **(3h)**

19. NMR (^{1}H, ^{13}C, ^{11}B, ^{19}F) and HRMS of boron complex *tr-aminoquinoline* **(3i)**

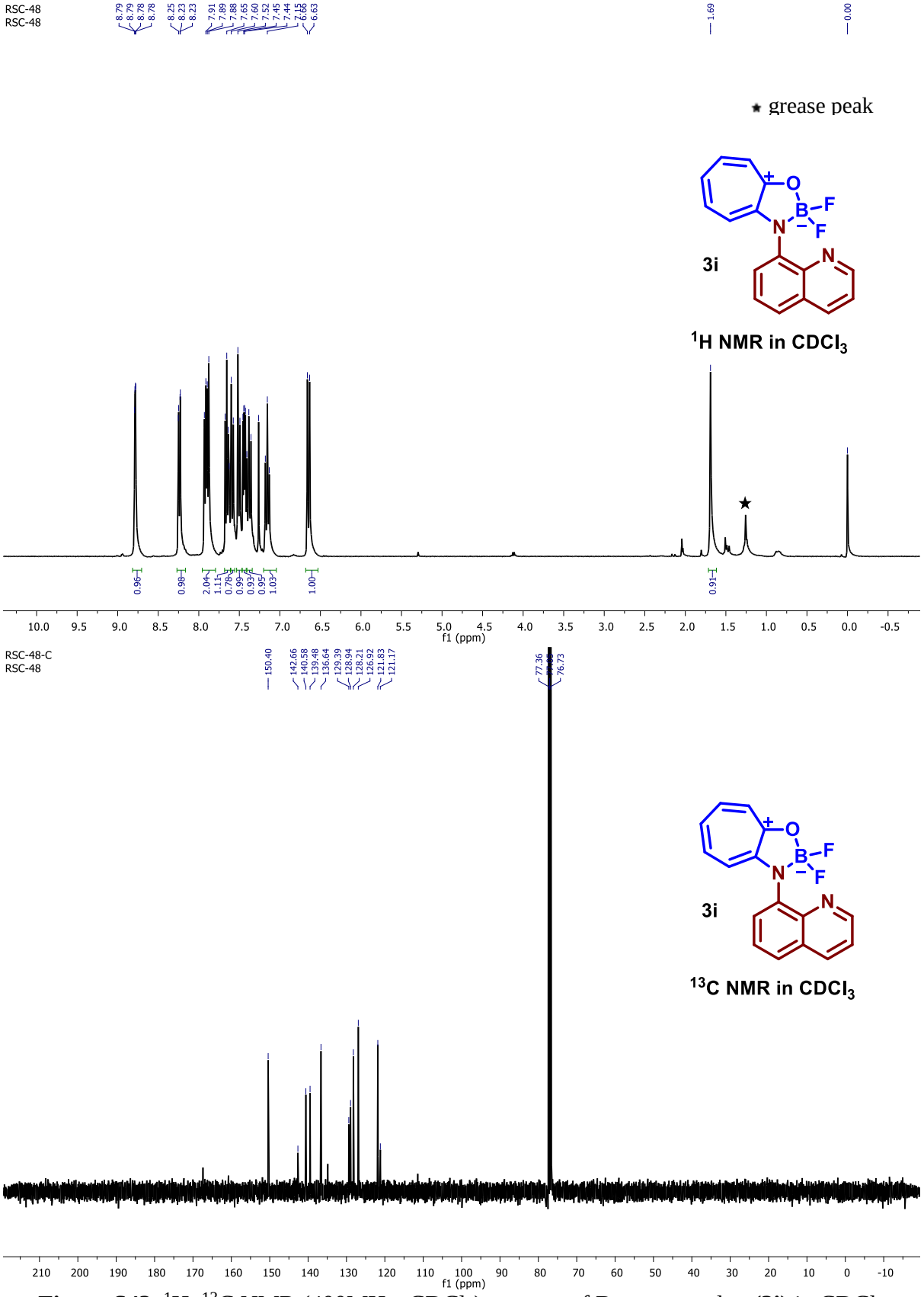

Figure S43. ^{1}H, ^{13}C NMR (400MHz, $CDCl_3$) spectra of Boron complex **(3i)** in $CDCl_3$

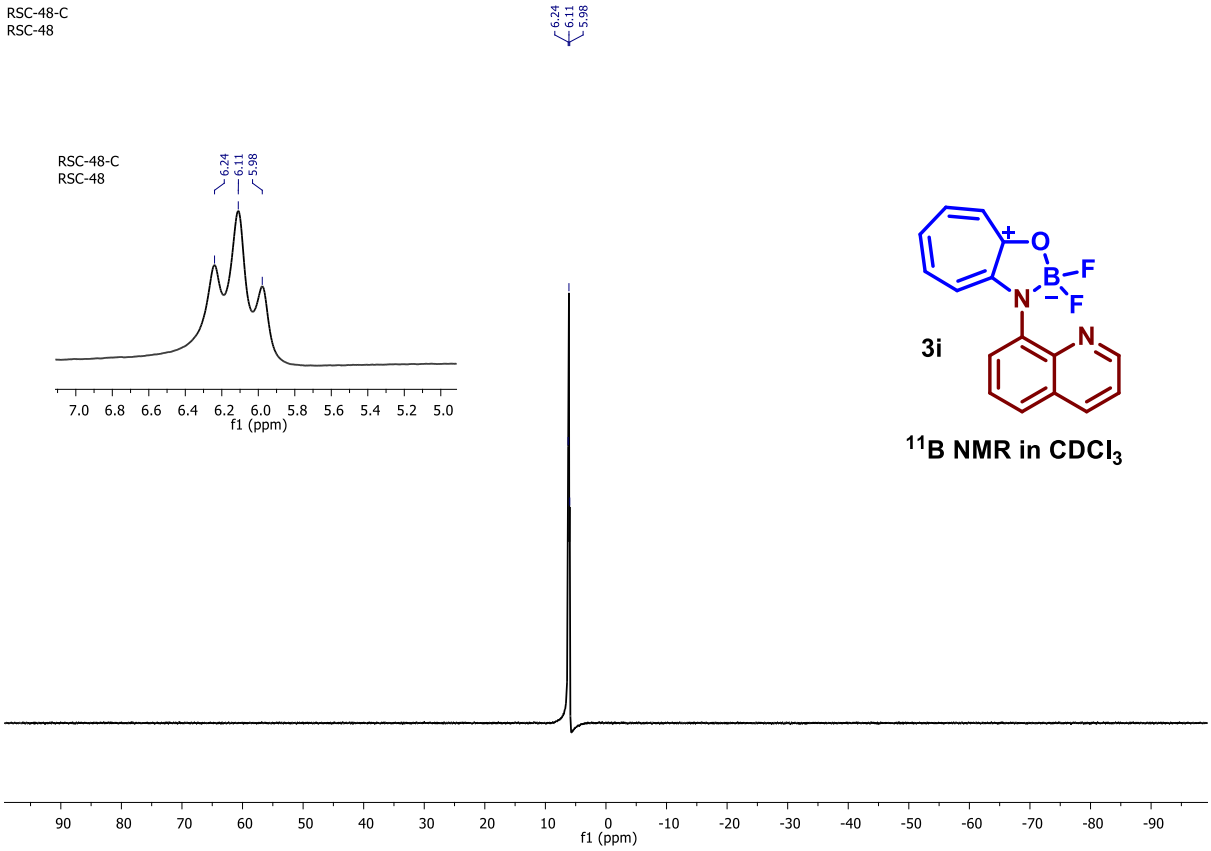

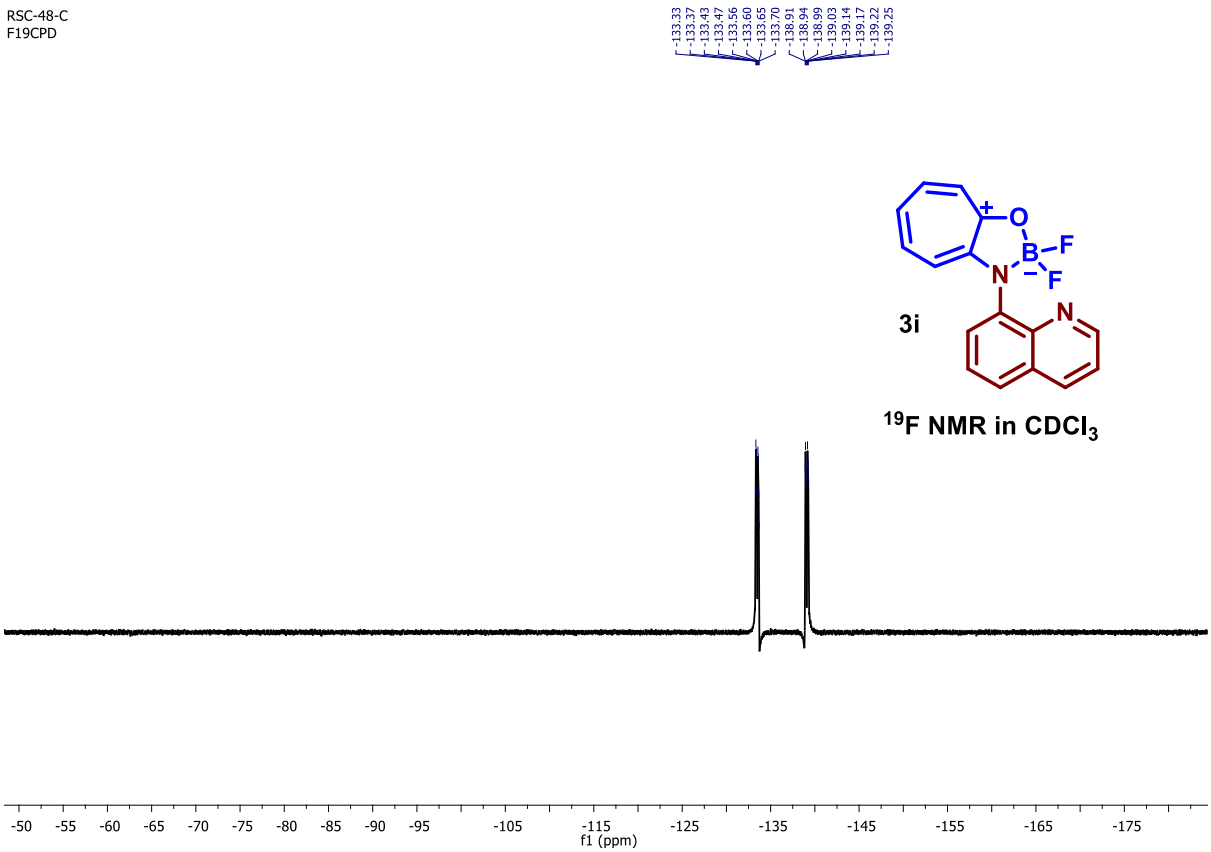

Figure 44. ^{11}B and ^{19}F NMR (400MHz, $CDCl_3$) spectra of Boron complex **(3i)** in $CDCl_3$

Display Report

Analysis Info

Analysis Name	D:\Data\NOV-2018\NKS\16112018_NKS_RCS-48.d	Acquisition Date	11/16/2018 7:50:18 PM
Method	pos tune_low_16102018.m	Operator	Amit S.Sahu
Sample Name	Tmix-131118	Instrument	micrOTOF-Q II 10337
Comment			

Acquisition Parameter

Source Type	ESI	Ion Polarity	Positive	Set Nebulizer	0.4 Bar
Focus	Active	Set Capillary	4500 V	Set Dry Heater	180 °C
Scan Begin	50 m/z	Set End Plate Offset	-500 V	Set Dry Gas	4.0 l/min
Scan End	3000 m/z	Set Collision Cell RF	300.0 Vpp	Set Divert Valve	Source

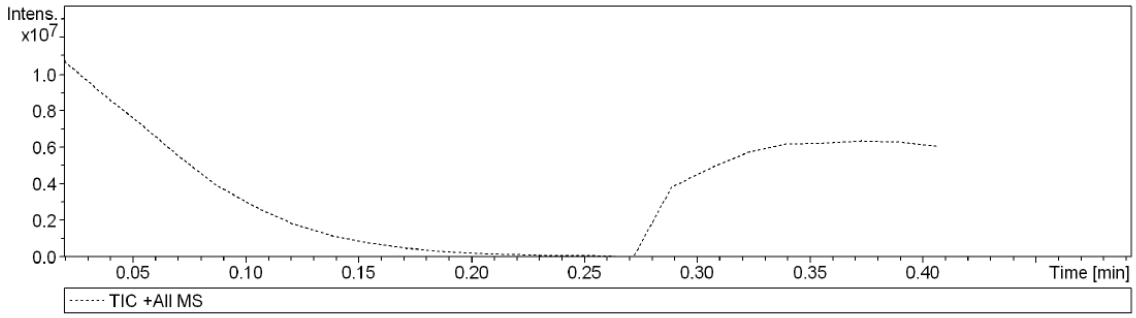

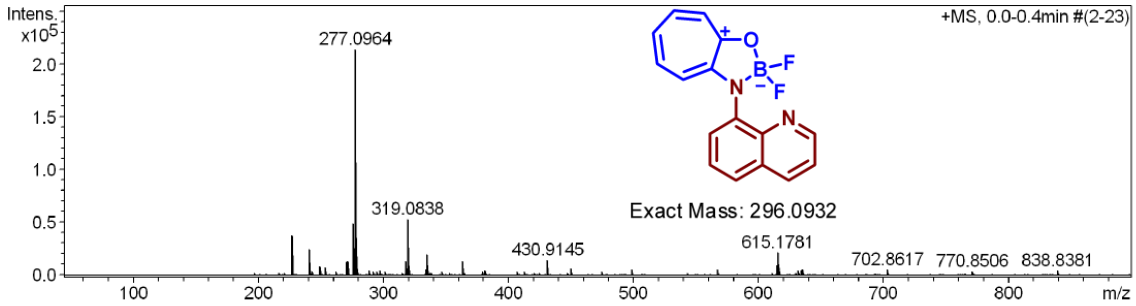

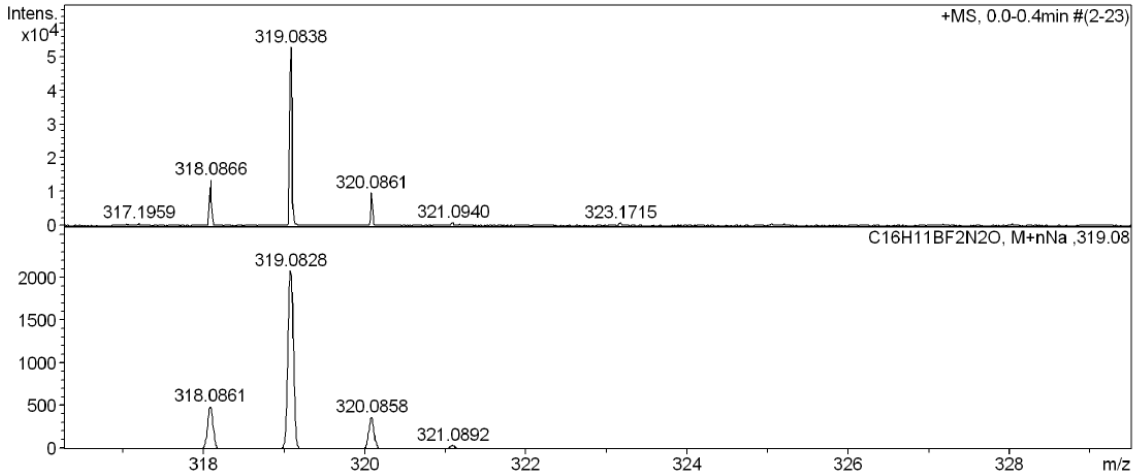

Bruker Compass DataAnalysis 4.0 printed: 11/16/2018 7:53:12 PM Page 1 of 1

Figure S45. ESI-MS/HRMS spectra of Boron complex **(3i)**

20. Crystal structures and data

Good quality crystals of compounds were obtained in solvent mixture dichloromethane and hexane by slow evaporation method. The crystals data of all boron complexes were collected on a Rigaku Oxford diffractometer at 293 K respectively. Selected data collection parameters and other crystallographic results are summarized below. The program package SHELXTL[1] and Olex2 was used for structure solution and packing diagram carried out by DIAMOND-3.2 software.

CCDC 1888894-1888899 contain the supplementary crystallographic data for **3a,3a-OH,3b,3h** and **3i**. These data can be obtained free of charge via https://www.ccdc.cam.ac.uk/data

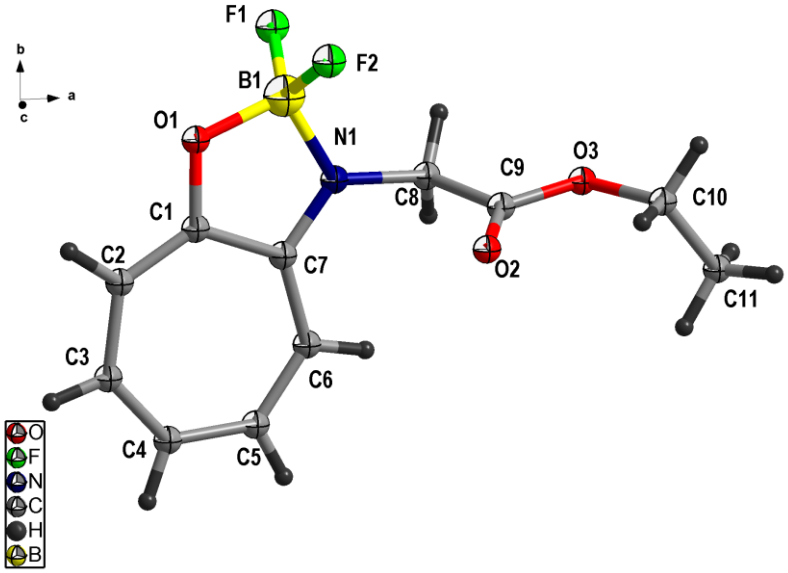

Figure S46. ORTEP Diagram of boron complex **(3a)** [ellipsoid contour probability: 50%].

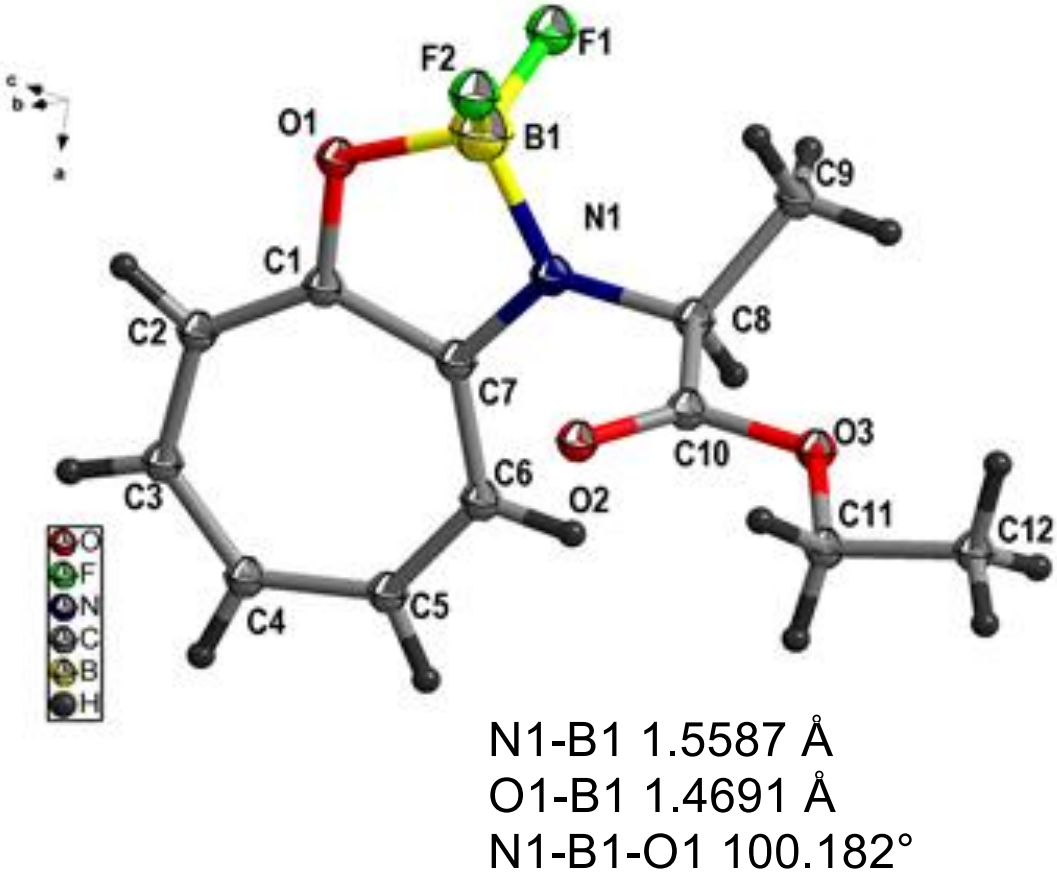

Figure S47. ORTEP Diagram of boron complex **(3b)** [ellipsoid contour probability: 50%].

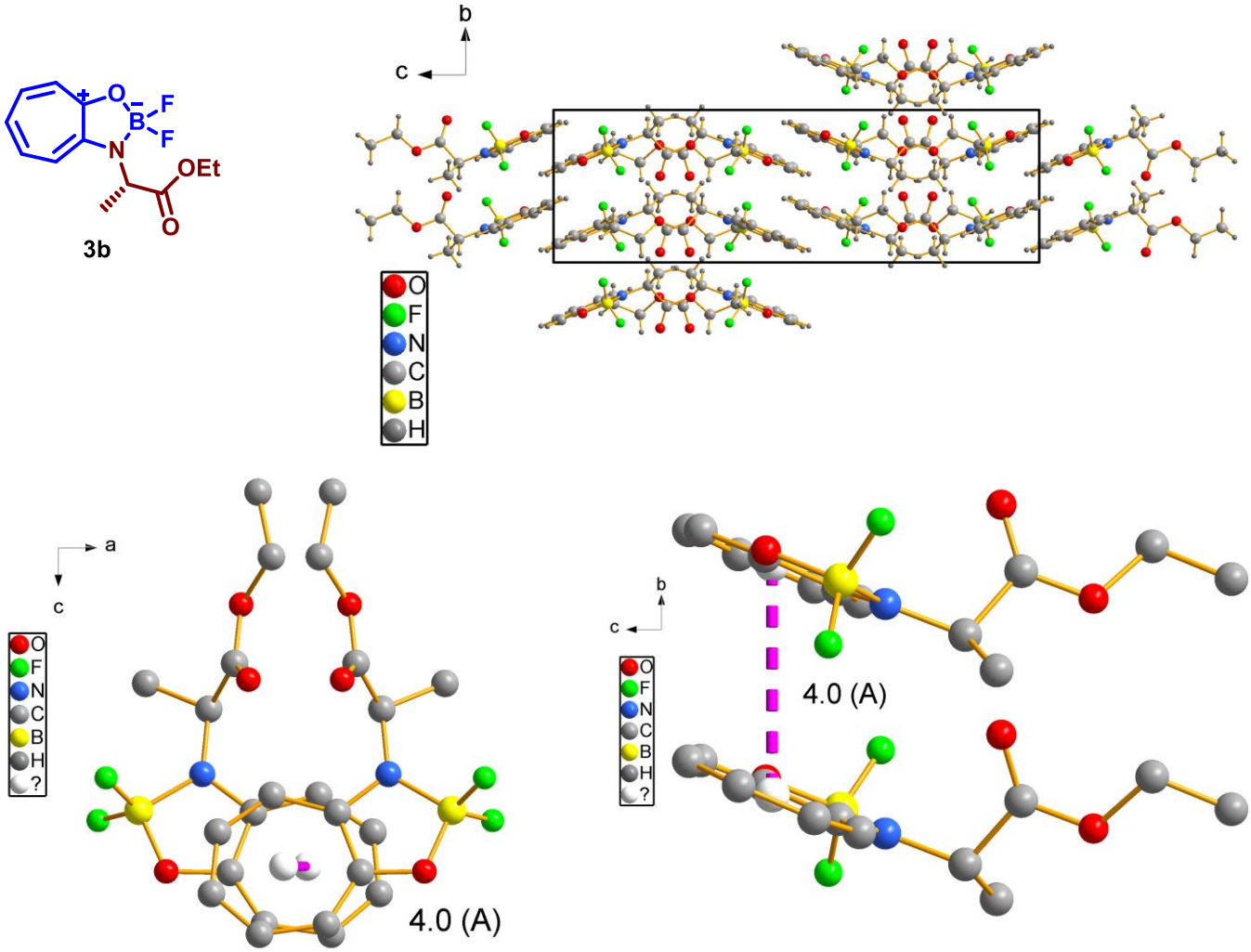

Figure S48. Crystal packing-diagram and intermolecular interactions of compound **3b**.

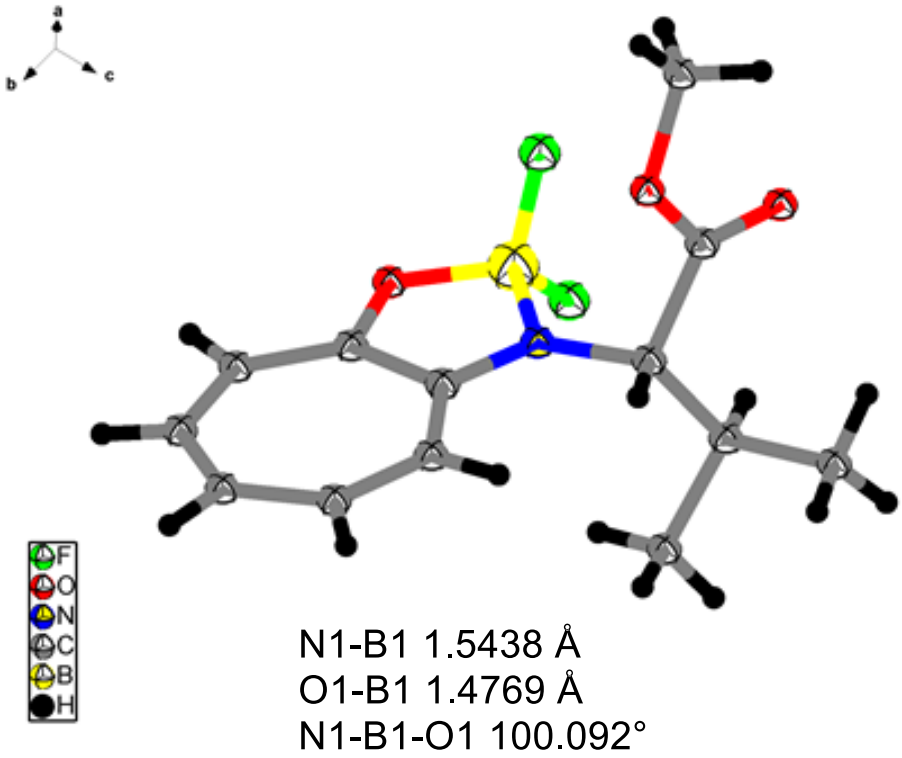

Figure S49. ORTEP Diagram of boron complex **(3c) [**ellipsoid contour probability: 50%].

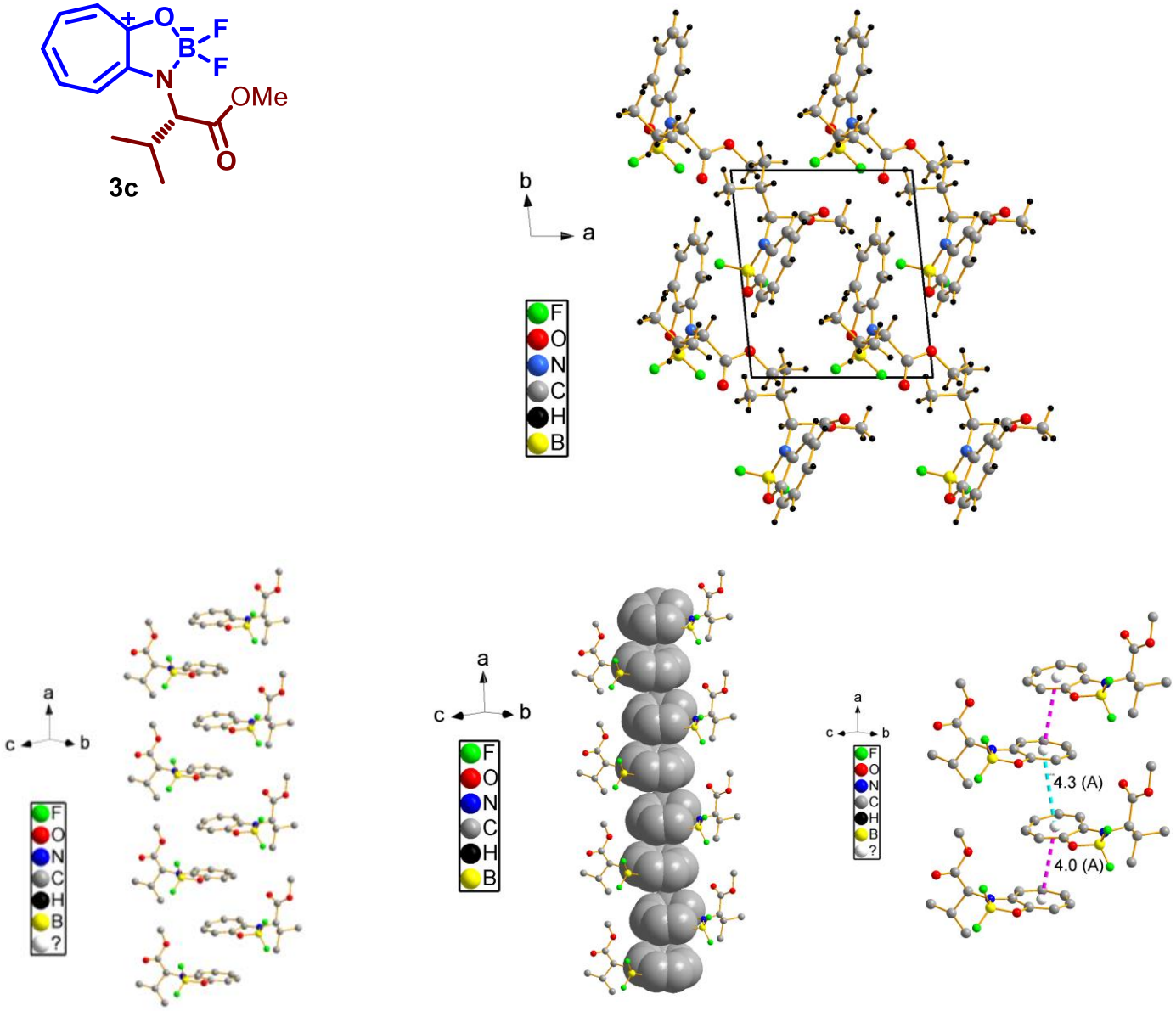

Figure S50. Crystal packing-diagram and intermolecular interactions of compound **3c**.

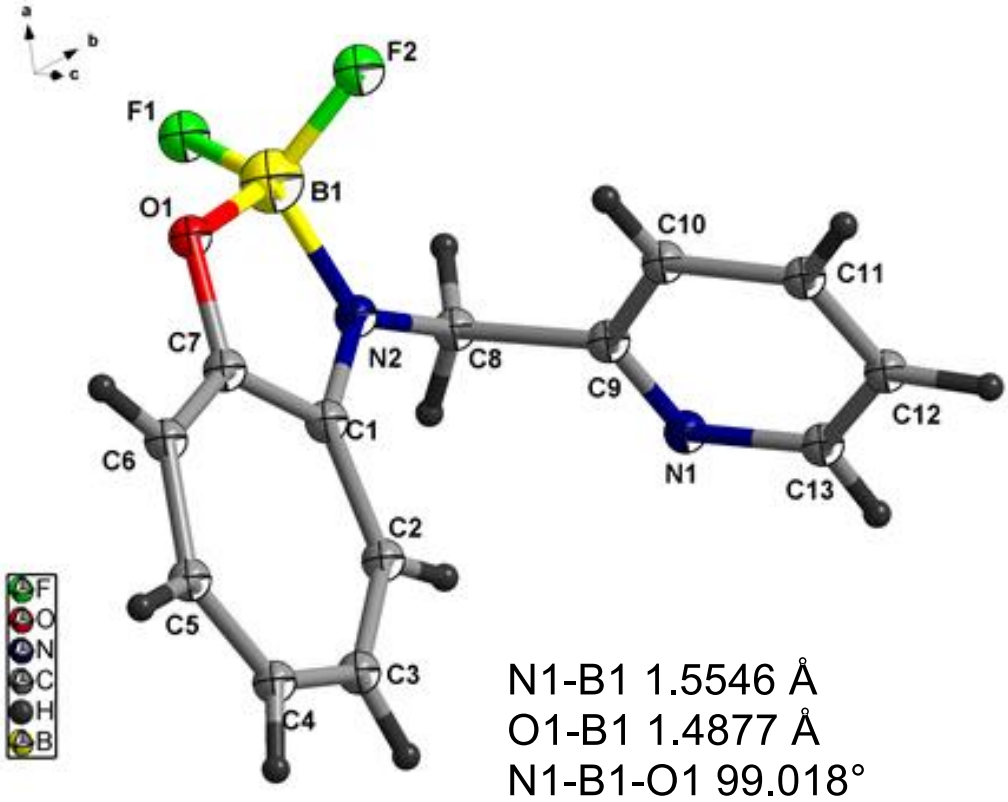

Figure S51. ORTEP Diagram of boron complex **(3h)** [ellipsoid contour probability: 50%].

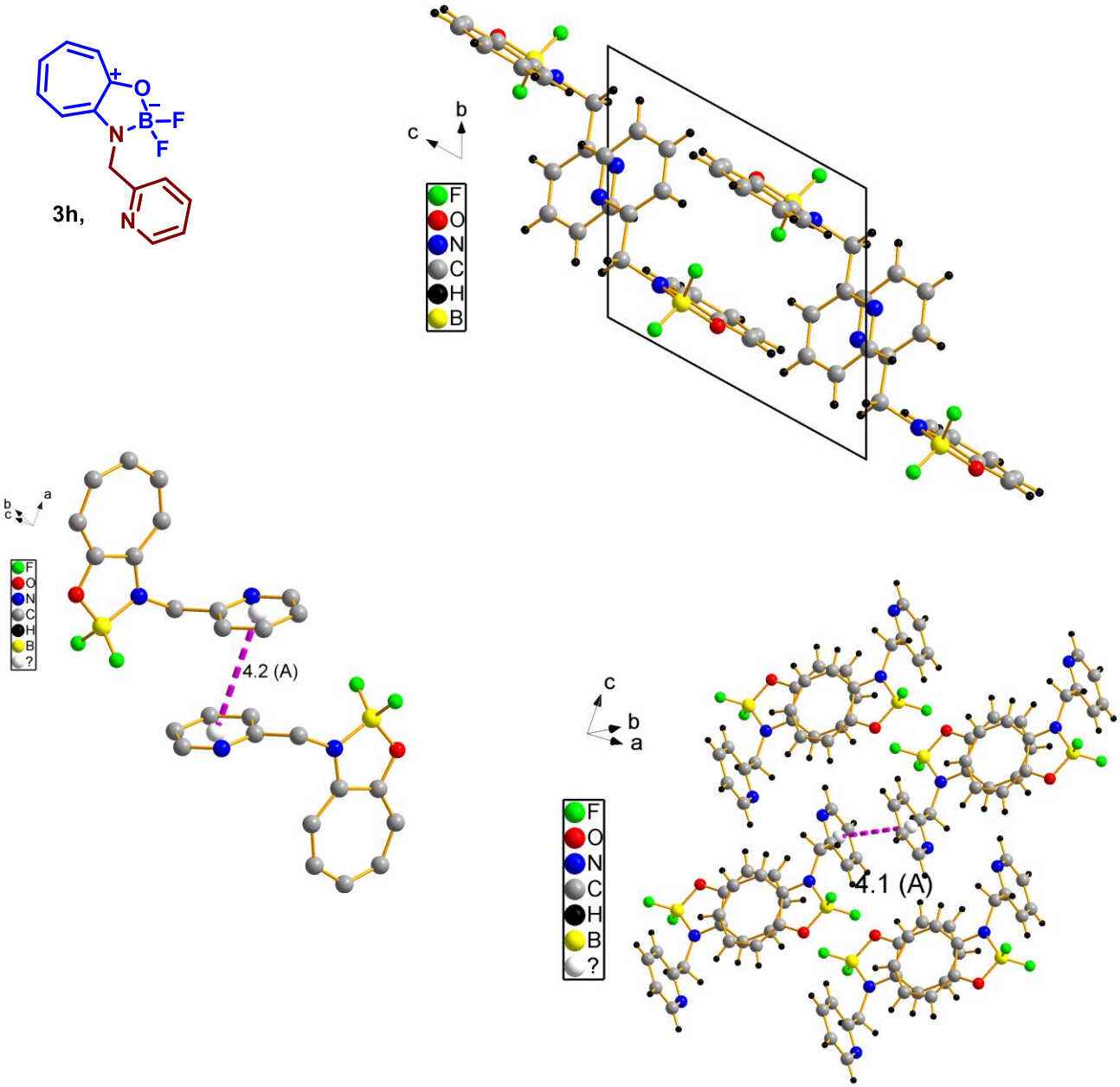

Figure 52. Crystal packing-diagram and intermolecular interactions of compound **3h**.

.

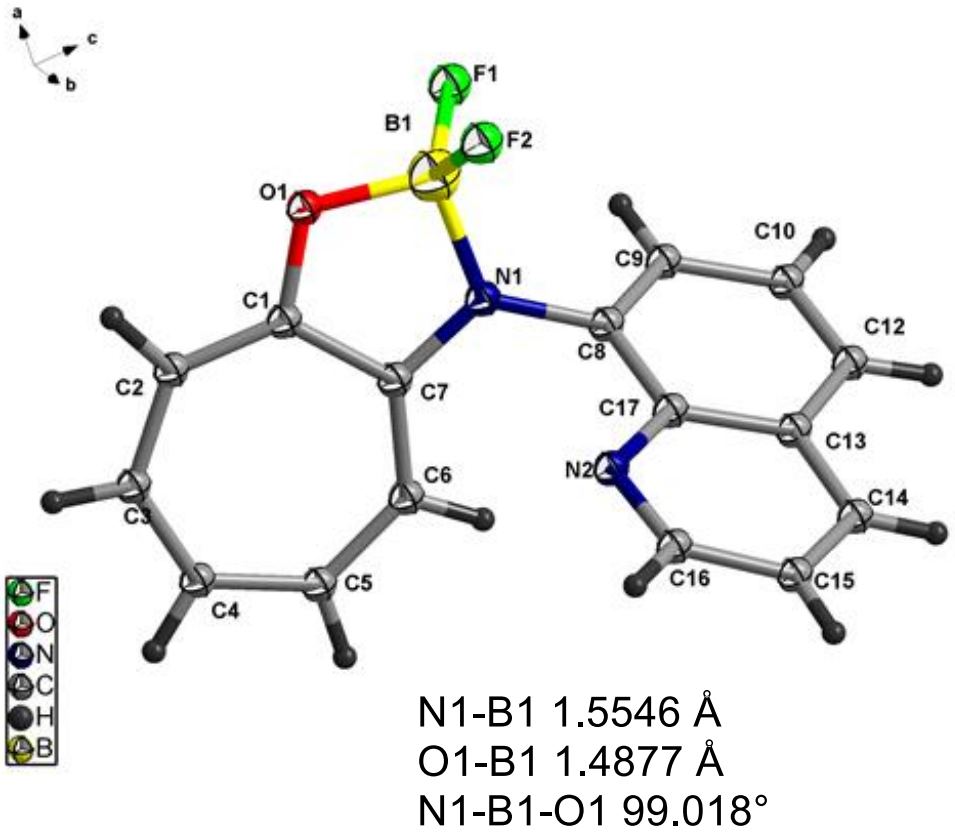

Figure S53. ORTEP Diagram of boron complex **(3i)** [ellipsoid contour probability: 50%].

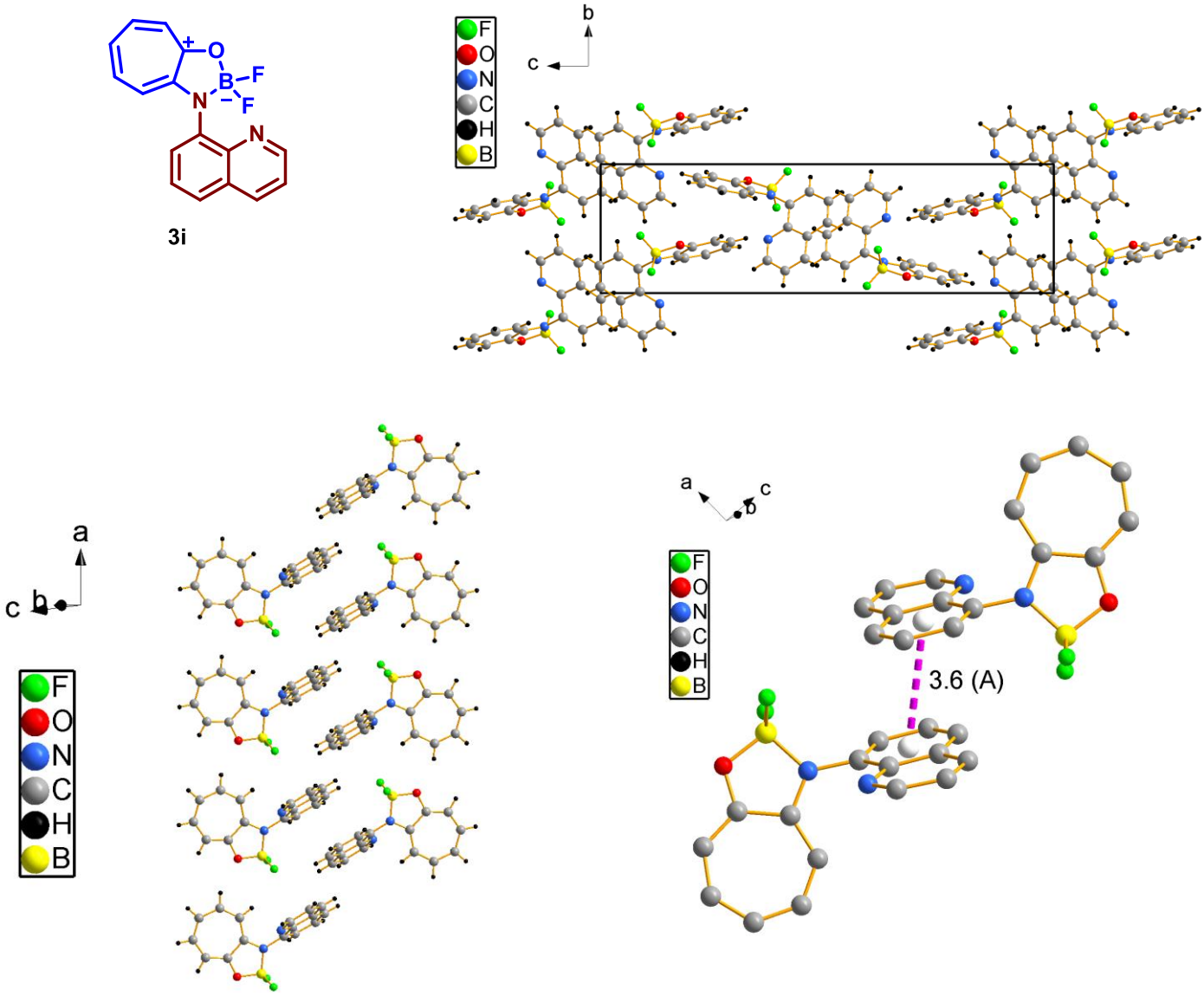

Figure 54. Crystal packing-diagram and intermolecular interactions of compound **3h**.

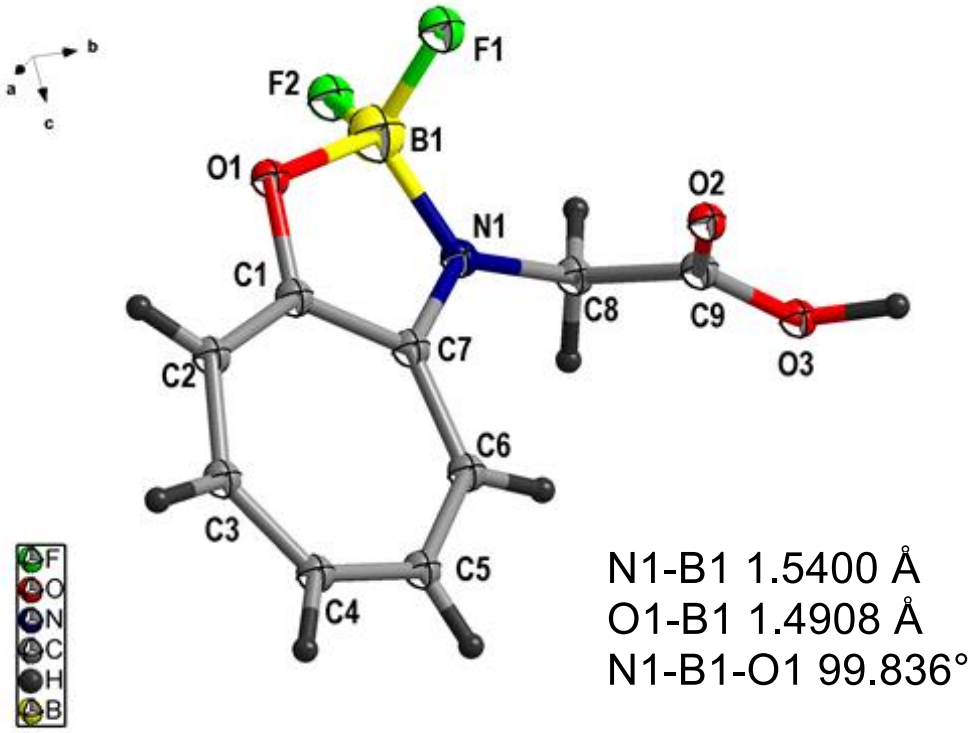

Figure S55. ORTEP Diagram of boron complex **(3a-OH)** [ellipsoid contour probability:50%].

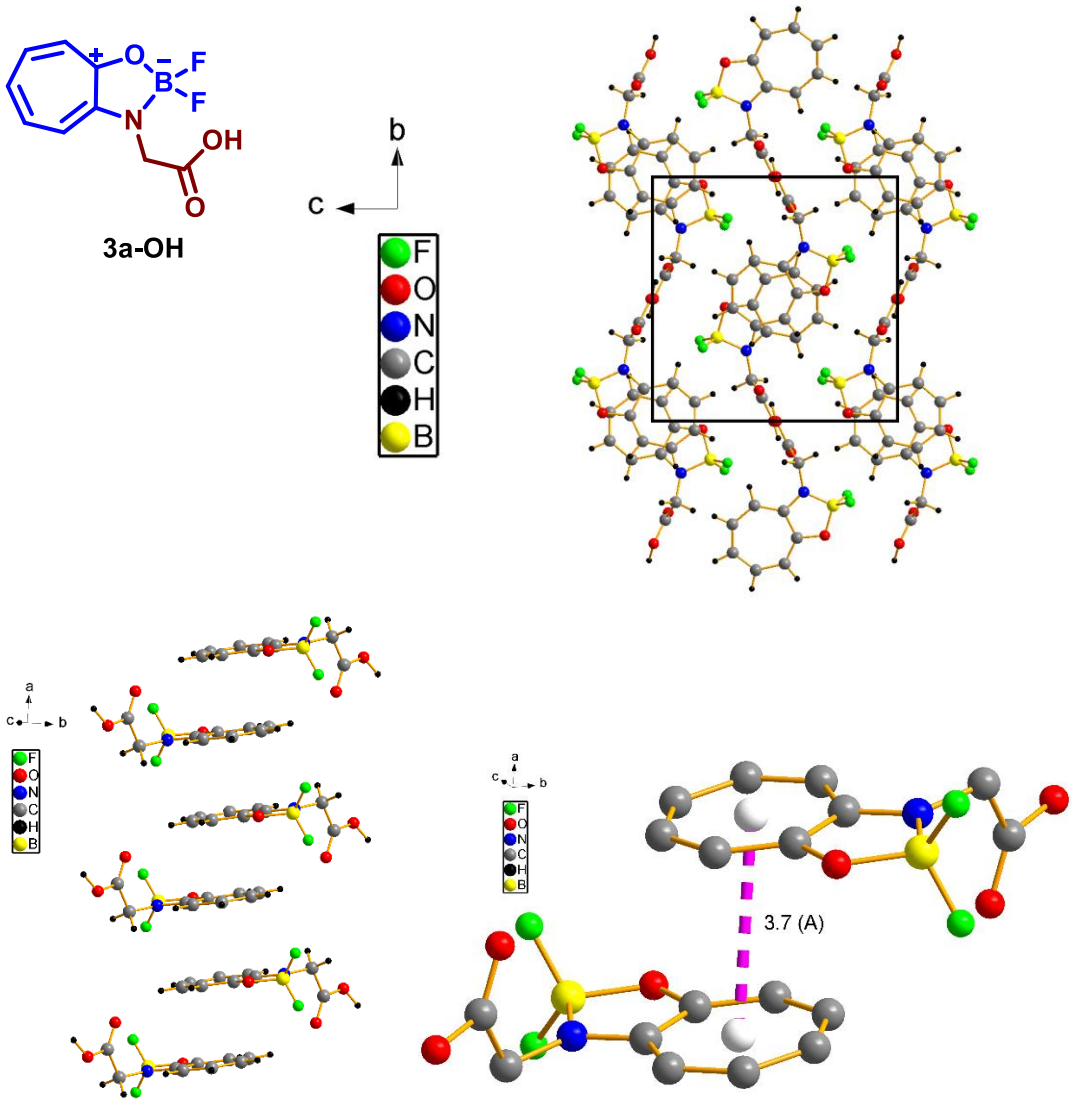

Figure 56. Crystal packing-diagram and intermolecular interactions of compound **3h**.

Table S1: Crystallographic table

compounds	(3a)	(3b)	(3c)	(3h)	(3i)	(3a-OH)
Identification code	**CCDC 1888899**	**CCDC 1888896**	**CCDC 1888897**	**CCDC 1888895**	**CCDC 1888898**	**CCDC1888894**
Empirical formula	$C_{11}H_{12}BF_2NO_3$	$C_{12}H_{14}BF_2NO_3$	$C_{26}H_{32}B_2F_4N_2O_6$	$C_{13}H_{11}BF_2N_2O$	$C_{16}H_{11}BF_2N_2O$	$C_9H_8BF_2NO_3$
Formula weight	255.04	269.07	566.20	260.07	296.10	226.97
Temperature/k	298.0	296(2)	293(2)	296.0	298	293(2)
Crystal system	monoclinic	Orthorhombic	triclinic	triclinic	monoclinic	monoclinic
Space group	$P2_1/c$	Pbca	P1	P-1	$P2_1/c$	$P2_1/n$
A/å	13.1705(7)	13.5273(5)	8.1582(2)	8.8495(2)	7.0792(4)	7.0433(4)
B/å	12.9185(4)	7.7581(4)	9.4094(2)	9.1023(2)	7.4313(4)	11.5620(8)
C/å	7.3648(2)	24.7812(15)	9.4305(2)	9.2653(2)	26.3653(14)	11.6118(8)
α/°	90	90	98.033(1)	62.940(2)	90	90
β/°	97.809(3)	90	94.918(2)	89.372(2)	96.772(5)	90.857(5)
γ/°	90	90	94.971(1)	69.175(2)	90	90
Volume/$å^3$	1241.45(8)	2600.7(2)	710.60(3)	610.93(3)	1377.34(13)	945.50(11)
Z	4	8	1	2	4	4
$\rho_{calc}g/cm^3$	1.3644	1.3742	1.3229	1.4136	1.4277	1.594
M/mm^{-1}	1.005	0.987	0.929	0.937	0.108	1.242
F(000)	530.2	1124.5	297.2	269.0	608.4	464.0
Crystal size/mm^3	0.001 × 0.0001 × 0.0001	0.001 × 0.0001 × 0.0001	0.21 × 0.21 × 0.2	0.001 × 0.0001 × 0.0001	0.001 × 0.0002 × 0.0001	0.01 × 0.01 × 0.01
Radiation	Cu Kα (λ = 1.54184)	Cu Kα (λ = 1.54184)	Cu Kα (λ = 1.54184)	Cu Kα (λ = 1.54184)	Mo Kα (λ = 0.71073)	CuKα (λ = 1.54184)
2θ range for data collection/°	6.78 to 148.96	7.14 to 148.92	9.52 to 148.94	10.88 to 150.68	6.9 to 52.74	10.798 to 148.932
Index ranges	$-15 \le h \le 16$, $-16 \le k \le 16$, $-9 \le l \le 6$	$-17 \le h \le 16$, $-5 \le k \le 9$, $-30 \le l \le 29$	$-8 \le h \le 10$, $-11 \le k \le 11$, $-12 \le l \le 12$	$-8 \le h \le 11$, $-10 \le k \le 11$, $-11 \le l \le 11$	$-9 \le h \le 9$, $-9 \le k \le 9$, $-34 \le l \le 33$	$-8 \le h \le 8$, $-11 \le k \le 14$, $-14 \le l \le 14$
Reflections collected	8441	10196	23106	9421	13111	6207
Independent reflections	2449 [R_{int} = 0.0828, R_{sigma} = 0.0590]	2546 [R_{int} = 0.0731, R_{sigma} = 0.0497]	5386 [R_{int} = 0.0504, R_{sigma} = 0.0278]	2469 [R_{int} = 0.0382, R_{sigma} = 0.0262]	2802 [R_{int} = 0.0177, R_{sigma} = 0.0158]	1880 [R_{int} = 0.0962, R_{sigma} = 0.0460]
Data/restraints/parameters	2449/0/164	2546/0/174	5386/3/367	2469/0/179	2802/0/199	1880/0/149
Goodness-of-fit on f^2	1.211	1.126	1.062	1.143	0.842	1.567
Final r indexes [i>=2σ (i)]	R_1 = 0.0974, wR_2 = 0.2898	R_1 = 0.0922, wR_2 = 0.2806	R_1 = 0.0594, wR_2 = 0.1735	R_1 = 0.0390, wR_2 = 0.1006	R_1 = 0.0391, wR_2 = 0.1750	R_1 = 0.1201, wR_2 = 0.3423
Final r indexes [all data]	R_1 = 0.1180, wR_2 = 0.3107	R_1 = 0.1296, wR_2 = 0.3336	R_1 = 0.0609, wR_2 = 0.1767	R_1 = 0.0423, wR_2 = 0.1034	R_1 = 0.0443, wR_2 = 0.1867	R_1 = 0.1295, wR_2 = 0.3485
Largest diff. Peak/hole / e $å^{-3}$	0.41/-0.36	0.29/-0.43	0.44/-0.25	0.12/-0.22	0.20/-0.22	0.64/-0.46

Table S2: Selected bond lengths and bond angles of boron complexes in solid state

compounds		3a	3b	3c	3h	3i	3a-OH
Selected bond lengths	C_1—C_7	1.4503 Å	1.4425 Å	1.4532 Å	1.4440 Å	1.4578 Å	1.4359 Å
	C_7—N_1	1.3252 Å	1.3394 Å	1.3317 Å	1.3250 Å	1.3273 Å	1.3257 Å
	C_1—O_1	1.3116 Å	1.3201 Å	1.3191 Å	1.3224 Å	1.3162 Å	1.3237 Å
	N_1—B_1	1.5331 Å	1.5587 Å	1.5438 Å	1.5453 Å	1.5546 Å	1.5400 Å
	O_1—B_1	1.4754 Å	1.4691 Å	1.4769 Å	1.4799 Å	1.4877 Å	1.4908 Å
	B_1—F_1	1.3800Å	1.3730 Å	1.3678 Å	1.3752 Å	1.3642 Å	1.3794 Å
	B_1—F_2	1.3790 Å	1.3783 Å	1.3700 Å	1.3821 Å	1.3754 Å	1.3878 Å
Selected bond angles	N_1—B_1—O_1	99.887°	100.182°	100.092°	99.688°	99.018°	99.836°
	O_1—B_1—F_1	111.216°	111.952°	110.796°	111.746°	111.616°	112.599°
	O_1—B_1—F_2	111.112°	110.886°	111.453°	111.092°	110.190°	112.566°
	N_1—B_1—F_1	111.417°	112.846°	113.098°	112.124°	112.744°	110.284°
	N_1—B_1—F_2	112.601°	111.091°	112.638°	112.609°	112.539°	112.401°
	F_1—B_1—F_2	109.349°	109.623°	108.610°	109.342°	110.291°	108.960°
	B_1—N_1—C_7	110.825°	109.191°	110.680°	110.607°	111.312°	110.641°
	B_1—O_1—C_1	111.621°	111.926°	111.200°	111.322°	111.839°	110.412°
	O_1—C_1—C_7	110.080°	110.144°	110.738°	110.323°	110.605°	108.537°
	N_1—C_7—C_1	107.553°	107.537°	107.242°	107.976°	107.209°	110.144°

21. FT-IR spectra

.FT-IRspectra were recorded by dissolving respective compounds in degassed CH_2Cl_2, drop casted on KBr plate and dried thoroughly. The samples were scanned from 500-4000 ($\tilde{\nu}$,cm^{-1}), the spectra are obtained from average of 64 scans

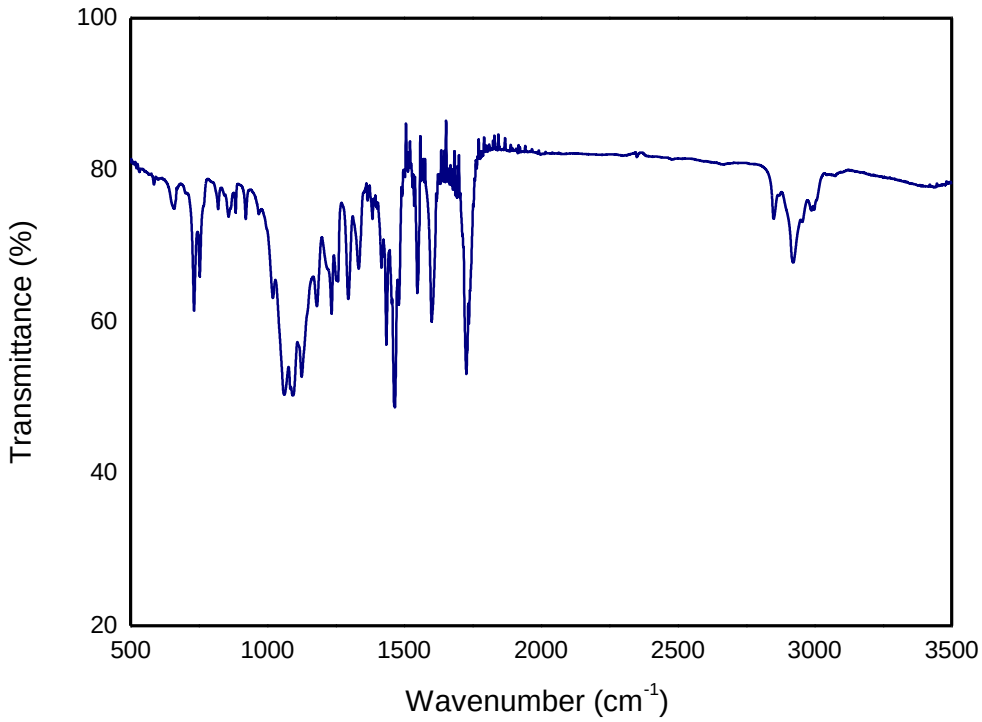

Figure S57. FT-IR Spectra of **(3a).**

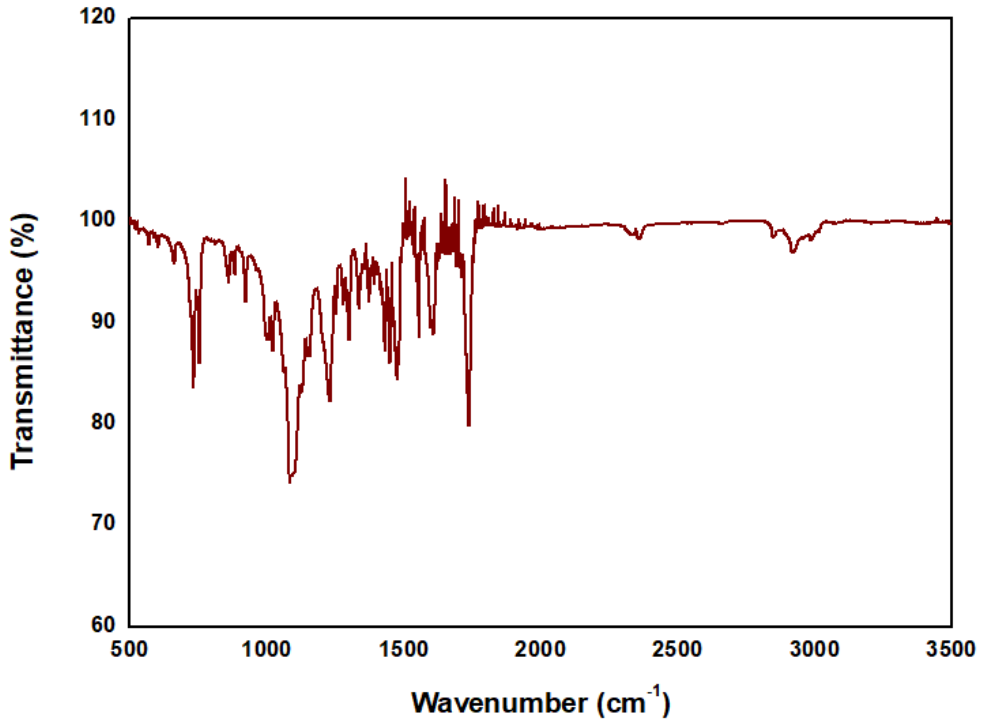

Figure S58. FT-IR Spectra of **(3b)**

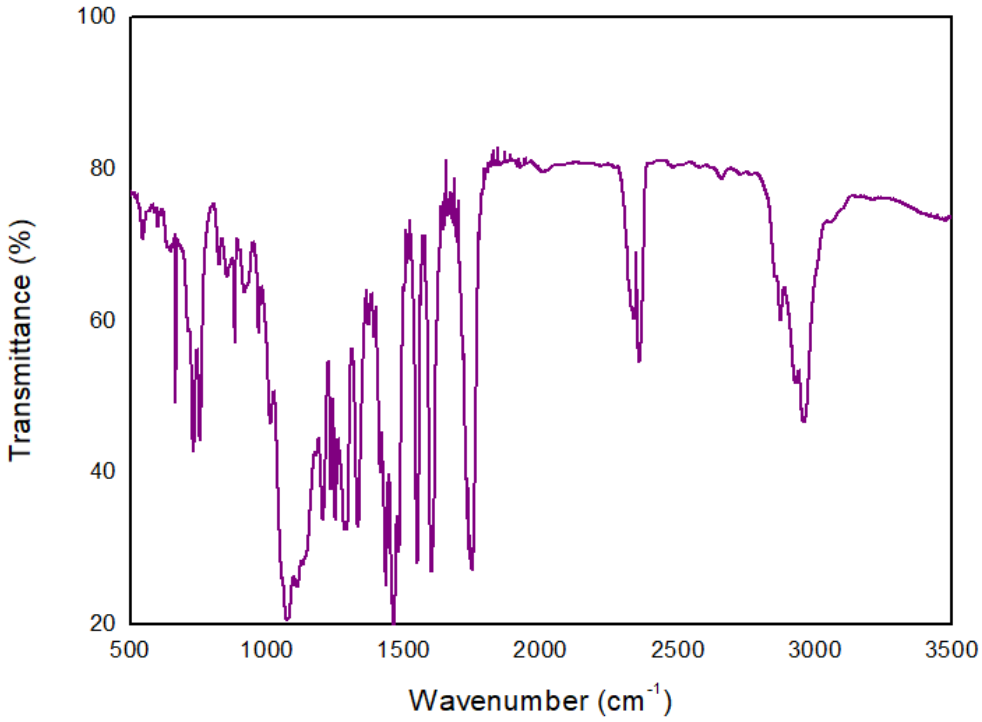

Figure S59. FT-IR Spectra of **(3c)**

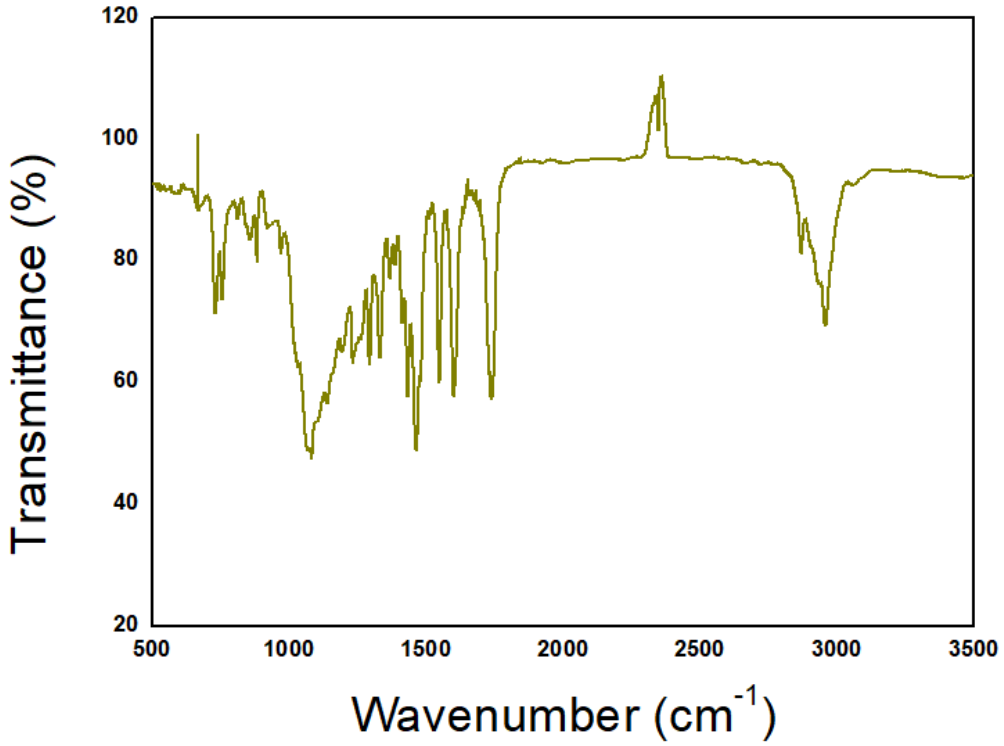

Figure S60. FT-IR Spectra of **(3d)**

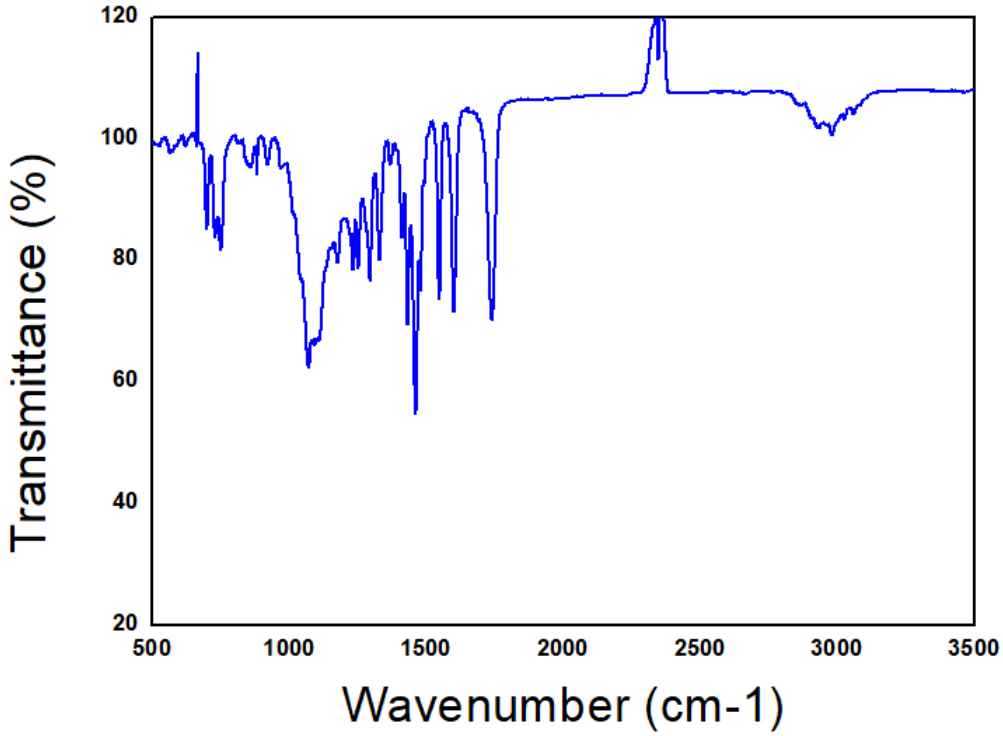

Figure S61. FT-IR Spectra of **(3e)**

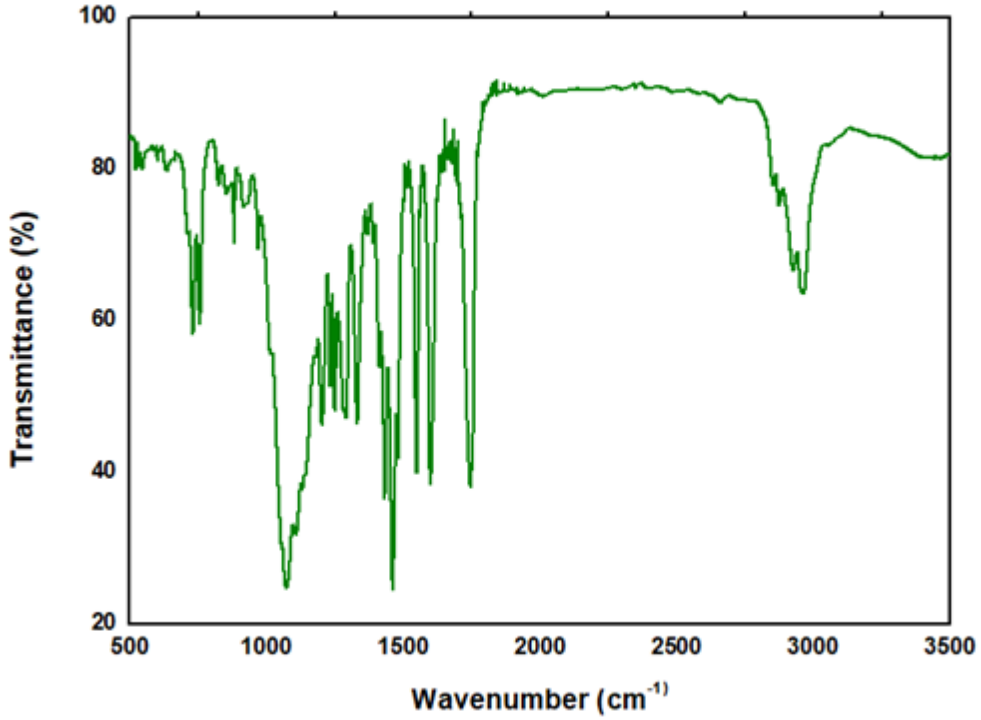

Figure S62. FT-IR Spectra of **(3f)**

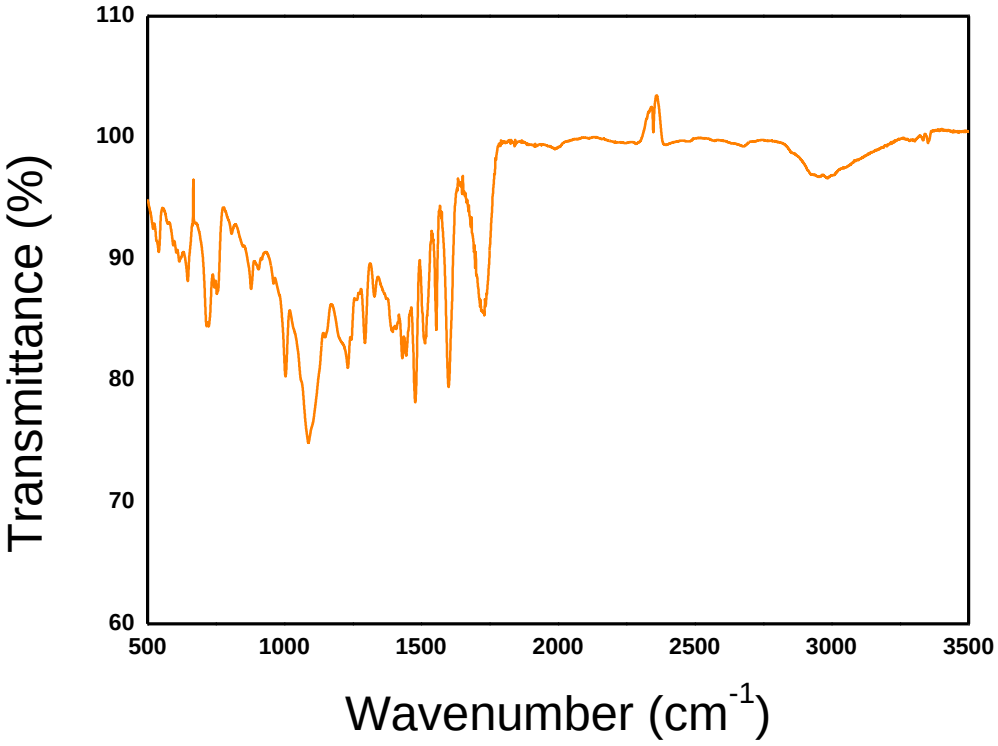

Figure S63. FT-IR Spectra of **(3g)**

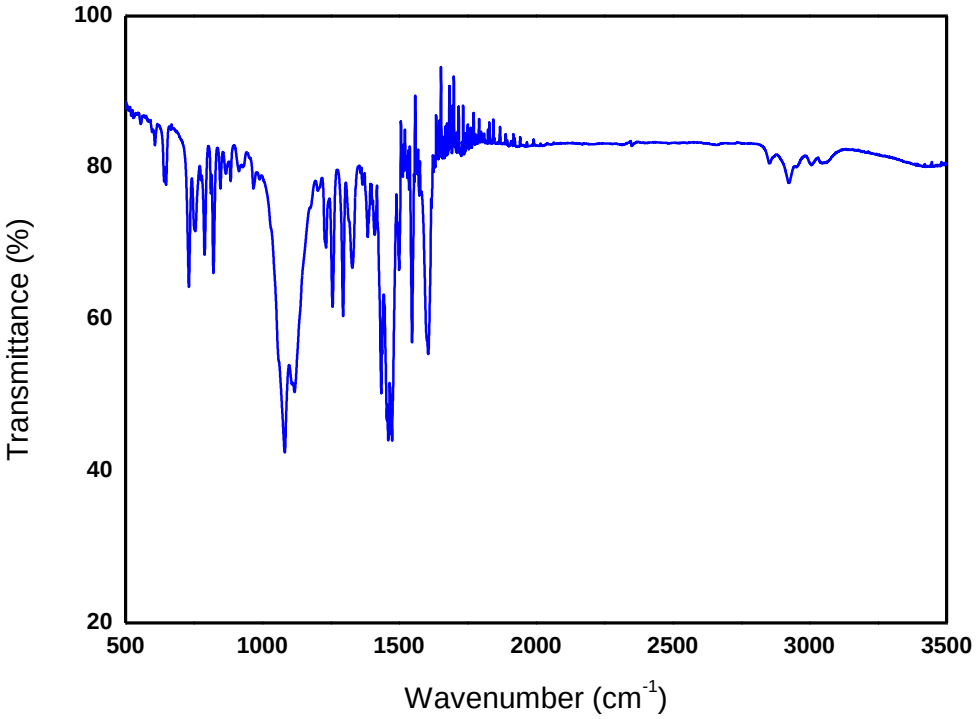

Figure S64. FT-IR Spectra of **(3h)**

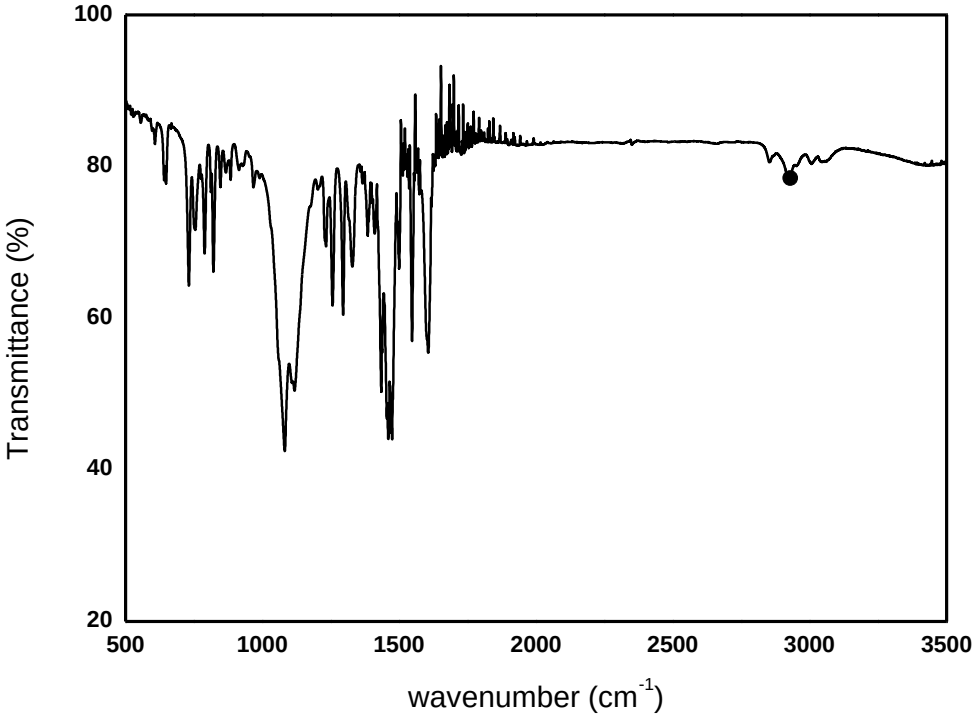

Figure S65. FT-IR Spectra of **(3i)**

22. Photophysical studies

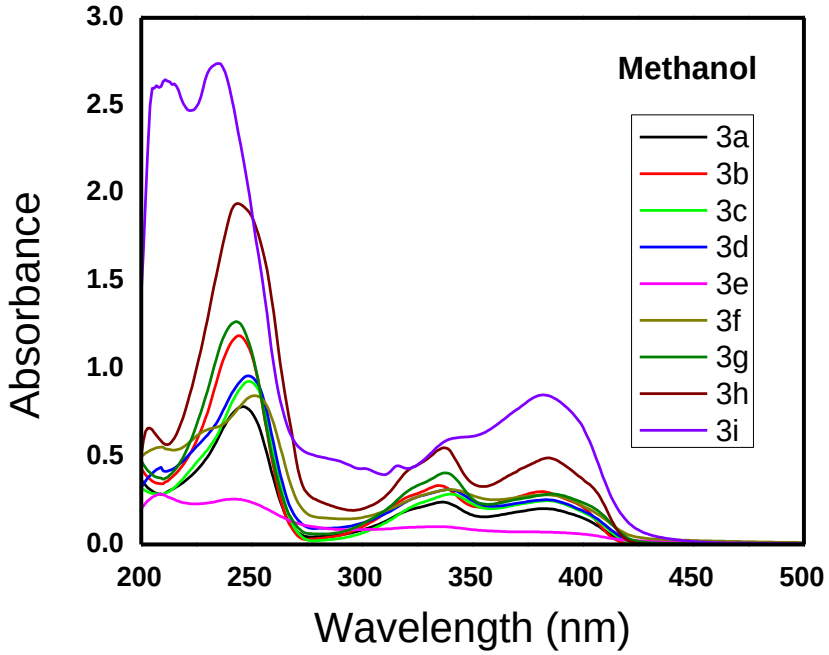

Figure S66: Absorption spectra of boron-aminotropone complexes (**3a-i**) in methanol at $50x10^{-5}$M concentration.

Table-S3: Photophysical parameters of Boron-aminotropone complexes.

Entry	λ_{abs} [a] (nm)	Abs [a]	λ_{em} [a,c] (nm)	Σmax [a] ($M^{-1}cm^{-1}$)	Stoke's Shift (nm)	OD/Abs (nm)	Φ_f [b]
3a	333, 381	0.3383	417,438	6766	105	338	0.15
3b	336,382	0.2421	414,445	4842	109	339	0.13
3c	339,384	0.28905	418,446	5781	107	347	0.14
3d	339,384	0.3148	419,445	6296	106	343	0.12
3e	333,383	0.10306	418,446	2061	109	332	0.06
3f	339,384	0.4114	423,448	8228	109	341	0.09
3g	339,384	0.3144	424,448	6288	109	339	0.09
3h	337,384	0.5501	420,445	11002	108	357	0.14
3i	316,382	0.8510		17020		351	0.0

a. All measurements were carried out in methanol, b. Quantum yields were determined by considering quinine sulfate in 0.1 M H_2SO_4 as standard reference, c. λ_{ex} = 380 nm, d. boron complex **3i** has shown negligible fluorescence in methanol.

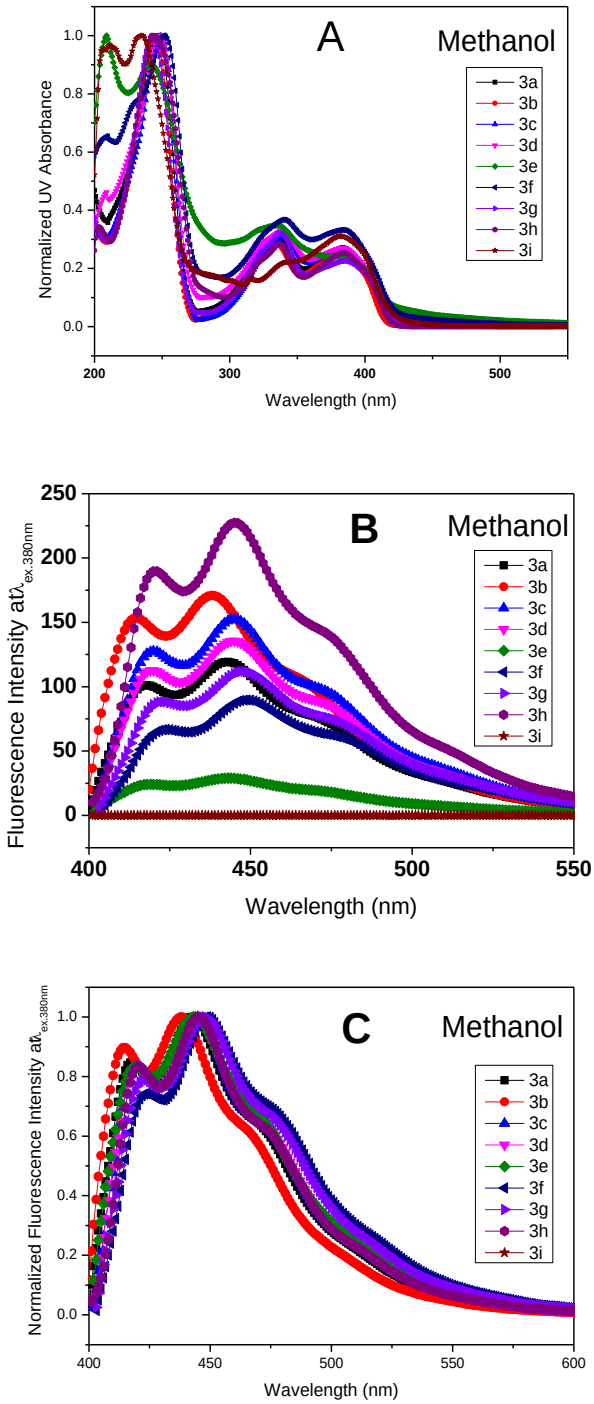

Figure S67: A) Normalized absorption B) Emission C) Normalized emission spectra of boron-aminotropone complexes (**3a-i**) in methanol at $50x10^{-5}$M concentration.

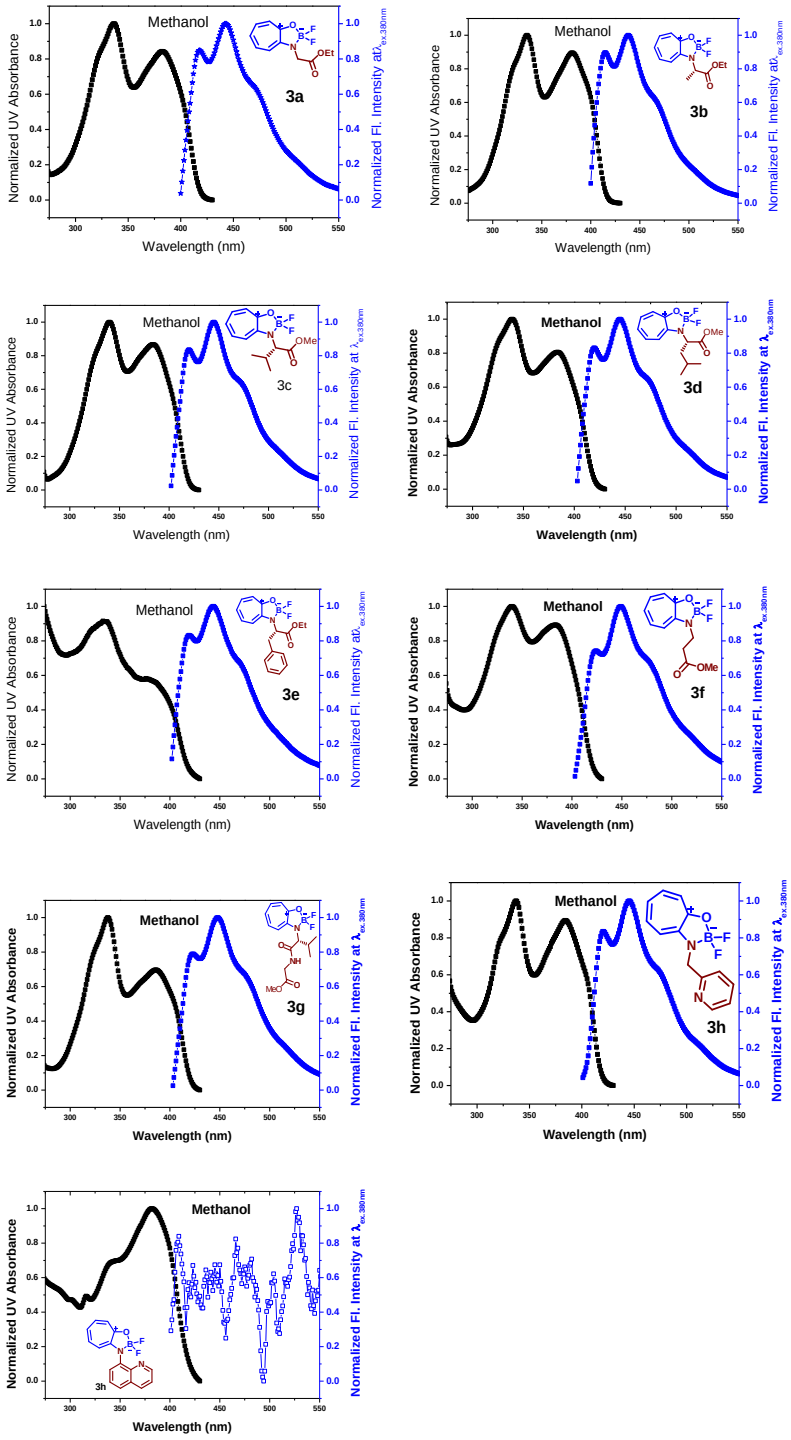

Figure S68: Normalized absorption-emission spectra of boron-aminotropone complexes (**3a-i**) in methanol at 50x10^{-5}M concentration.

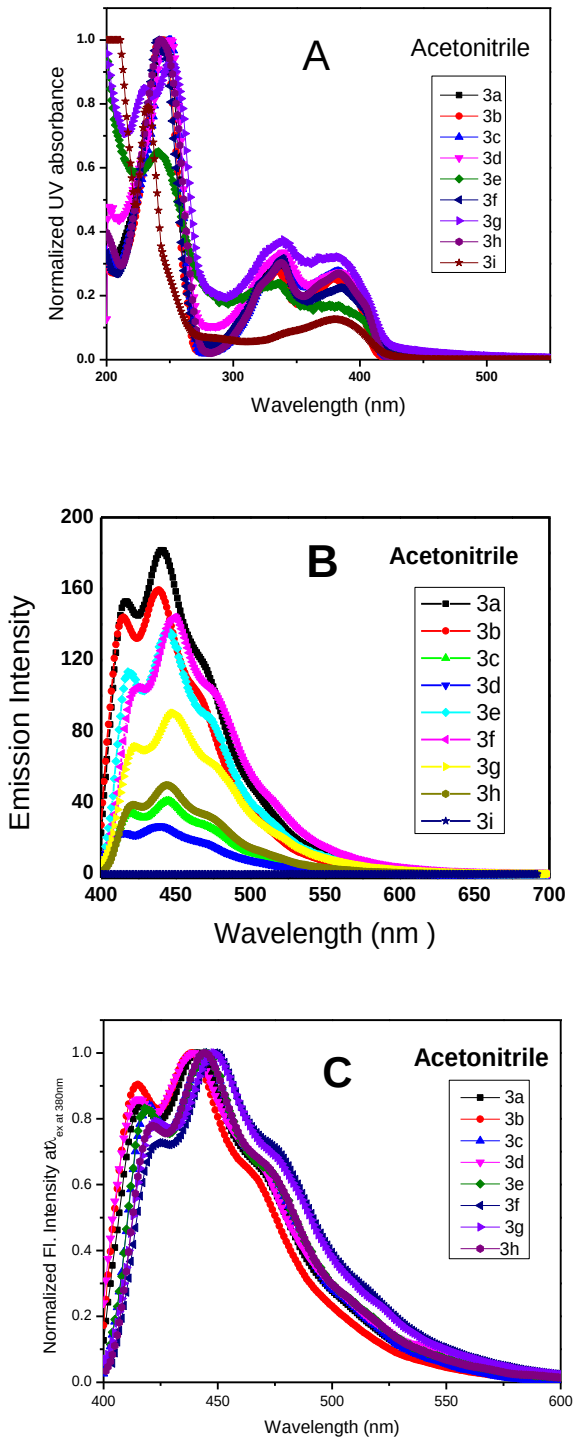

Figure S69: A) Normalized absorption B) Emission C) Normalized emission spectra of boron-aminotropone complexes (**3a-i**) in acetonitrile at $50x10^{-5}$M concentration.

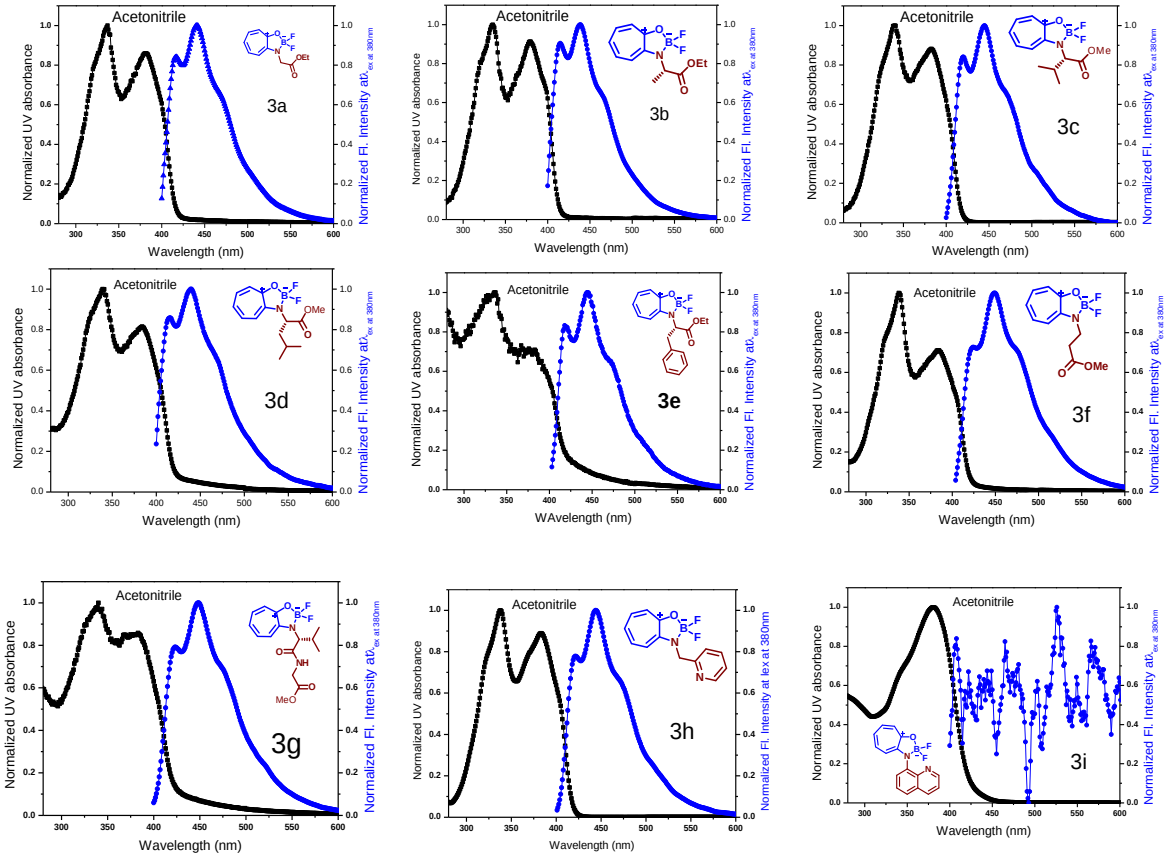

Figure S70: Normalized absorption-emission spectra of boron-aminotropone complexes (**3a-i**) in acetonitrile at $50x10^{-5}$M concentration.

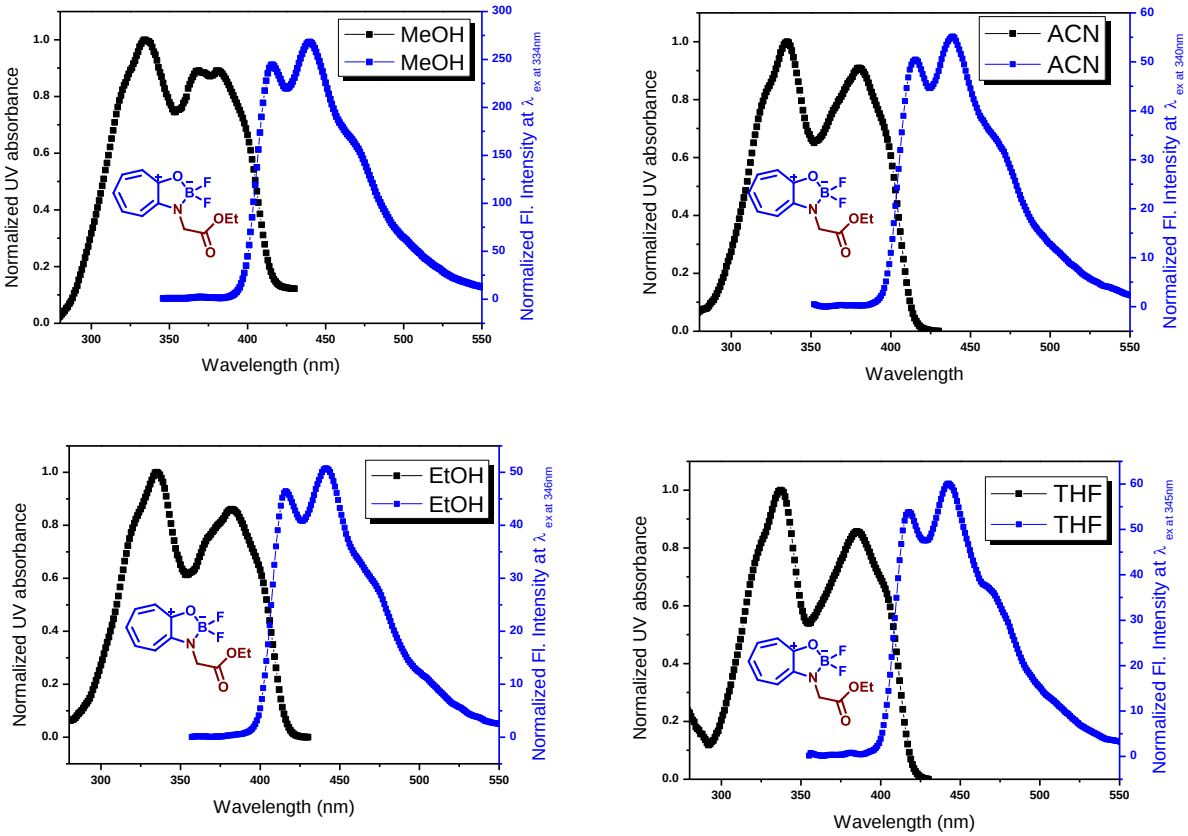

Figure S71: Normalized absorption-emission spectra of boron-aminotropone complexes (**3a)** in different solvent.

Table S4. Quantum yields of *boron-aminotropone* **(3a)**.

solvents	**λ_{abs} (nm)**	**Abs**	**λ_{em} (nm)**	**Stoke's Shift (nm)**	**OD/Abs (nm)**	**Φ_f**
Methanol	334, 380	0.06085	417,438	104	334	0.15
Acetonitrile	335,380	0.07202	415,441	106	340	0.14
Ethanol	335,382	0.08749	416,443	108	346	0.13
THF	337,385	0.08650	418,442	105	345	0.15

All measurements and quantum yields were determined for boron-complex **(4a)** by considering quinine sulfate in 0.1 M H_2SO_4 as standard reference.

Solid fluorescence of boron complexes

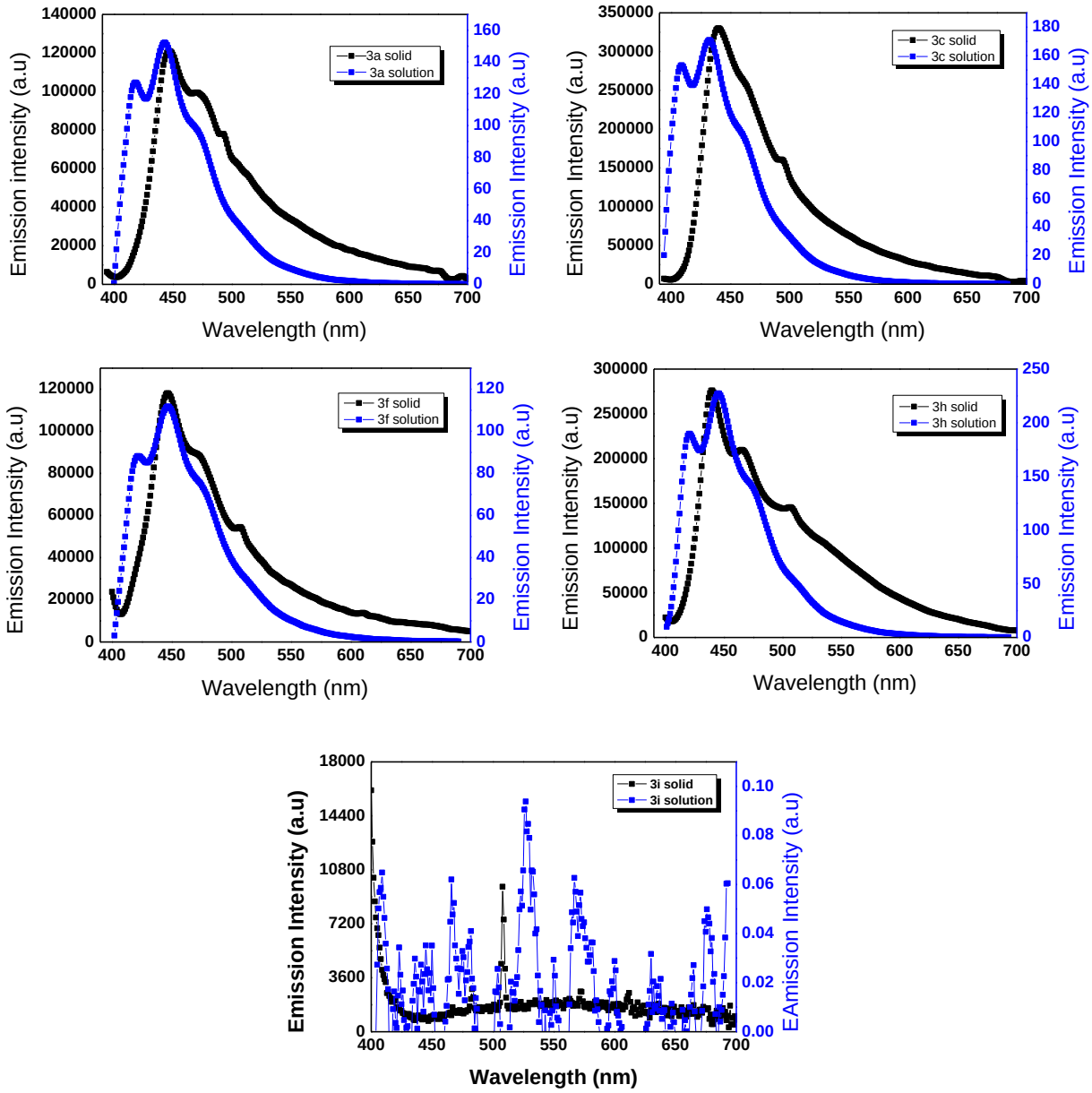

Figure S72: Comparision of Solid and Solution emission spectra of boron-aminotropone complexes (**3a, 3c, 3f, 3h, 3i)** in MeOH.

Table S5. Comparison of solid and solution fluorescence.

	MeOH			Solid	
Entry	λ_{abs} (nm)	λ_{em} (nm)	Φ_f (%)	λ_{em} (nm)	Φ_f (%)
1a	333, 381	417,438	15	447, 470, 492	4.94
1c	339,384	418,446	14	440, , 493	4.1
1f	339,384	423,448	9	447, 507,	0.73
1h	337,384	420,445	14	440, 465, 506	6.59
1i	381				0

Photostability of Boron complex **3a**:

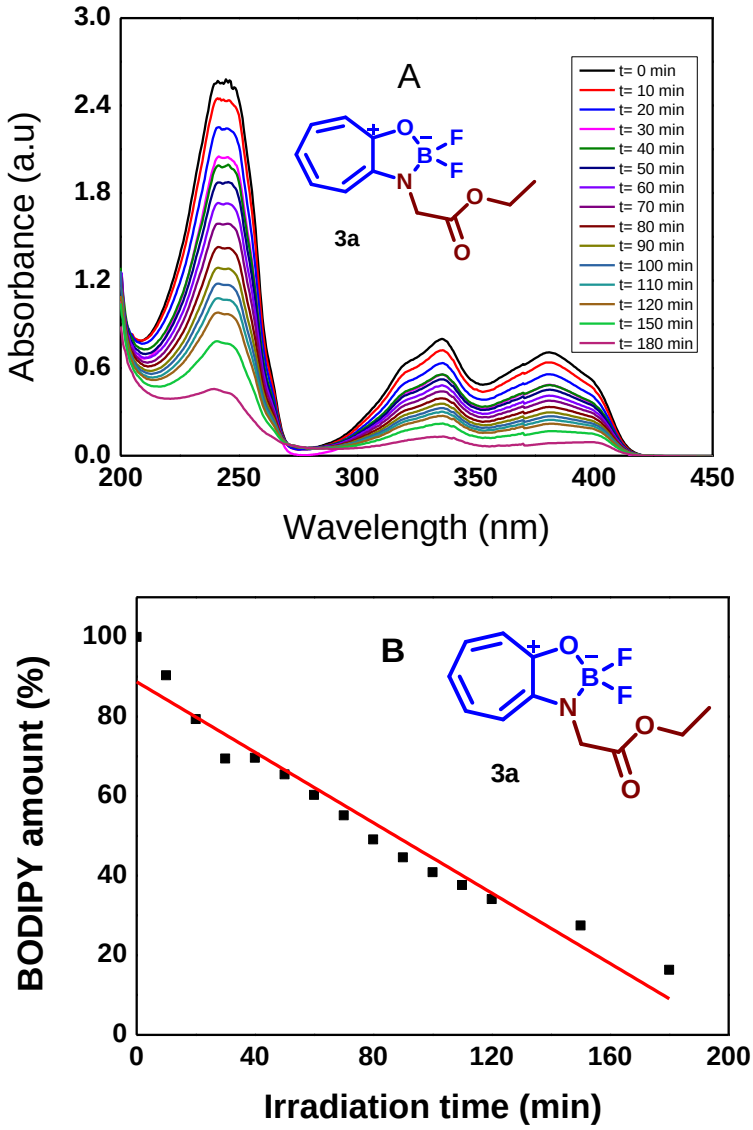

Figure S73: Photostability for boron-aminotropone complexes (**3a)** in MeOH A) Absorption spectra and B) Amount of decomposition with irradiation of UV ray at 265 nm.

Photostability of Boron complex **3c**:

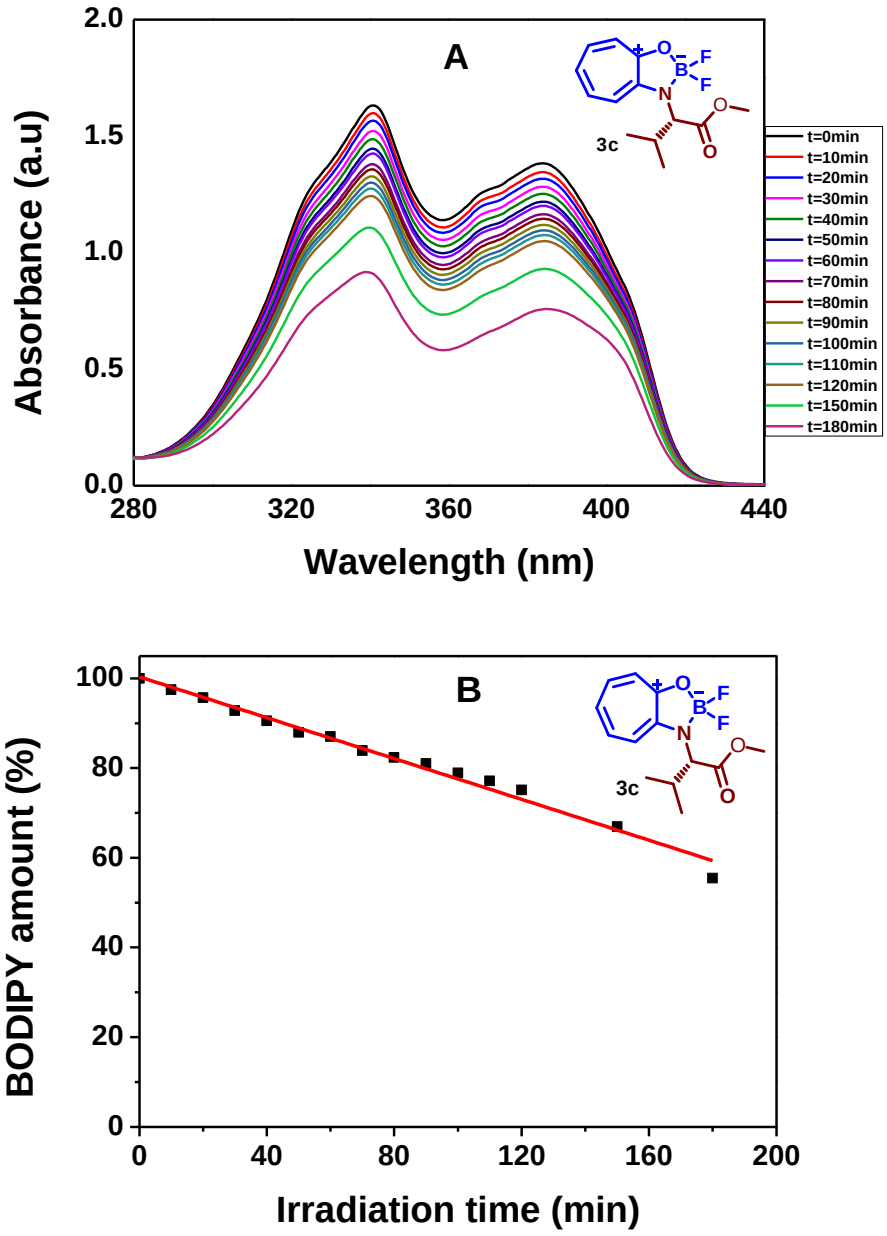

Figure S74: Photostability for boron-aminotropone complexes (**3c)** in MeOH A) Absorption spectra and B) Amount of decomposition with irradiation of UV ray at 265 nm.

Photostability of Boron complex **3h**:

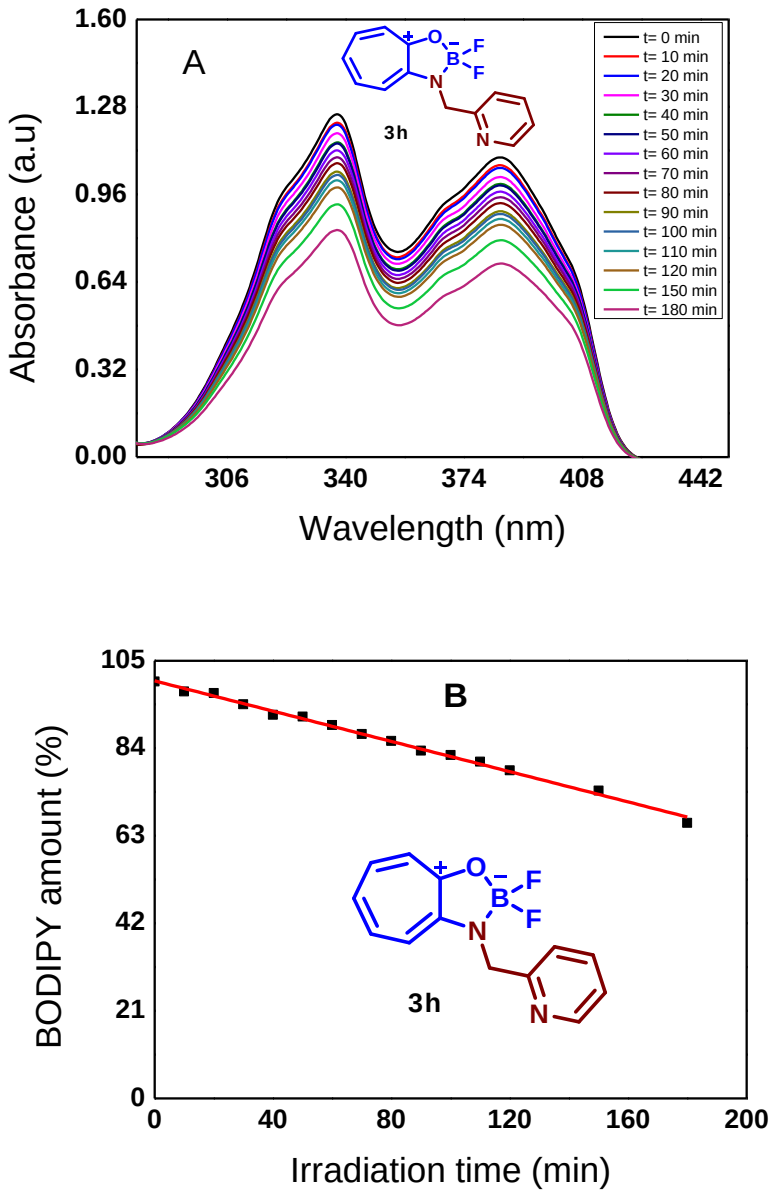

Figure S75: Photostability for boron-aminotropone complexes (**3c)** in MeOH A) Absorption spectra and B) Amount of decomposition with irradiation of UV ray at 265 nm.

22. Theoretical data

Cartesian coordinates of most stable structure for compound (**3a, 3a-OH, 3b, 3h, 3i**) has been calculated using **Gaussian 09 software** and B3LYP/6-31+G* level of theory in vacuum. Since all molecules are in their minimum energy level, no imaginary frequency was observed.

Coordinates and absolute energies of (**3a,3a-OH,3b,3h,3i**)

Table S6. Cartesian coordinates (Å) of Analogue **3a** optimized at the B3LYP/6-31+G* level

	X	Y	Z
C	-4.87177	-1.72318	-0.05083
C	-4.45226	-0.34044	-0.52486
O	-3.39031	0.20463	0.30857
C	-2.12257	-0.08436	-0.03367
O	-1.79169	-0.76565	-0.97946
C	-1.15622	0.53911	0.97800
N	0.17843	0.71859	0.46142
C	1.09042	-0.23869	0.30263
C	2.29809	0.39601	-0.23629
O	2.11755	1.68200	-0.41155
B	0.73424	2.11651	0.01380
F	0.79448	2.99838	1.08099
F	0.01895	2.64008	-1.04665
C	0.92744	-1.60888	0.60774
C	1.84943	-2.63724	0.49291
C	3.17975	-2.62199	0.03569
C	3.90513	-1.53119	-0.42609
C	3.51907	-0.18854	-0.55045
H	-0.05701	-1.89681	0.96227
H	4.25651	0.50897	-0.93890
H	1.47785	-3.61376	0.79824
H	4.92594	-1.74146	-0.73942
H	-1.15752	-0.09577	1.87617
H	-1.53902	1.51561	1.28370
H	3.69516	-3.57907	0.03980
H	-5.18149	-1.70013	0.99976
H	-5.72114	-2.07268	-0.65025
H	-4.05602	-2.44381	-0.16661
H	-5.26309	0.38398	-0.42150
H	-4.10475	-0.35540	-1.56042

Energy (a.u): -584574.8958440 hartree

Table S7. Cartesian coordinates (Å) of Analogue **3a-OH** optimized at the B3LYP/6-31+G* level

	X	Y	Z

C	-0.92316	-1.52578	-0.52396
C	-0.53643	-0.19147	-0.26949
N	0.69160	0.31129	-0.39321
C	1.86116	-0.41714	-0.81297
C	2.41764	-1.35208	0.25891
O	1.83426	-1.72879	1.24817
C	-2.18528	-2.09347	-0.43733
C	-3.41624	-1.52391	-0.06717
C	-3.66349	-0.20994	0.31161
C	-2.77791	0.87180	0.41750
C	-1.41087	0.90201	0.16648
O	-0.73782	2.01628	0.31203
B	0.72240	1.83996	-0.03539
F	1.06916	2.60465	-1.13737
F	1.53738	2.09927	1.04916
O	3.66864	-1.75032	-0.07141
H	-0.12347	-2.20124	-0.81139
H	-3.19073	1.82611	0.73380
H	2.63598	0.30435	-1.08615
H	1.66595	-1.01949	-1.71253
H	-4.69636	0.02182	0.56429
H	-2.22347	-3.15160	-0.68967
H	-4.27194	-2.19420	-0.07443
H	3.97890	-2.35738	0.62741

Energy (a.u): -535236.4094543 hartree

Table S8. Cartesian coordinates (Å) of Analogue **3b** optimized at the B3LYP/6-31+G* level

	X	Y	Z
C	1.77605	1.88664	-1.11423
C	1.09289	0.54381	-0.79937
N	-0.28418	0.71992	-0.36013
C	-1.16857	-0.27693	-0.29621
C	-0.95247	-1.61489	-0.70078
C	-1.83389	-2.68520	-0.67824
C	-3.16860	-2.76067	-0.24364
C	-3.94389	-1.73695	0.28642
C	-3.61281	-0.39426	0.51377
C	-2.41222	0.26122	0.26273
O	-2.29066	1.53378	0.53954
B	-0.92920	2.06594	0.15884
F	-1.05777	3.00176	-0.85703
C	1.89547	-0.25990	0.24510
O	3.15044	-0.47801	-0.19623
C	4.03124	-1.21582	0.69397
C	5.38523	-1.31834	0.01823
O	1.46670	-0.66564	1.30224
F	-0.26923	2.58031	1.25699
H	0.03975	-1.84188	-1.07697
H	1.10181	-0.05410	-1.72244
H	4.08327	-0.68007	1.64659
H	3.58712	-2.19845	0.88257
H	-1.41862	-3.61871	-1.05409
H	-4.38031	0.24298	0.94517
H	1.19936	2.43038	-1.86573
H	1.84899	2.51194	-0.22043
H	2.78032	1.69694	-1.49934
H	6.07587	-1.87216	0.66473
H	5.31111	-1.84753	-0.93800
H	5.80960	-0.32581	-0.16650
H	-3.64334	-3.73491	-0.32795
H	-4.95906	-2.00978	0.56844

Energy (a.u): -609244.5388150 hartree

Table S9. Cartesian coordinates (Å) of Analogue **3h** optimized at the B3LYP/6-31+G* level

	X	Y	Z
N	-2.65021	-1.12194	0.95526
C	-2.14854	0.03490	0.49533
C	-2.61818	0.65522	-0.67109
C	-3.65670	0.05034	-1.37642
C	-4.19170	-1.14821	-0.89724
C	-3.65233	-1.69148	0.26872
C	-1.03355	0.65929	1.32526
N	0.23354	0.78942	0.61184
B	0.81259	2.14554	0.08731
F	0.00706	2.70352	-0.89903
C	1.06033	-0.22012	0.34803
C	2.22772	0.33631	-0.34317
O	2.10673	1.63287	-0.50061
C	0.84183	-1.57802	0.68302
C	1.67147	-2.66403	0.45179
C	2.93130	-2.73422	-0.17246
C	3.66476	-1.69231	-0.72491
C	3.35859	-0.32495	-0.80501
F	1.04564	3.03871	1.11769
H	-0.90273	0.05803	2.23136
H	-1.31679	1.66973	1.63581
H	-2.16670	1.58270	-1.01070
H	4.08777	0.32292	-1.28445
H	1.27977	-3.61512	0.80829
H	4.62205	-1.96949	-1.16235
H	-4.04432	0.50837	-2.28279
H	-5.00395	-1.65221	-1.41326
H	3.37885	-3.72328	-0.22998
H	-0.10336	-1.79497	1.17269
H	-4.03492	-2.62603	0.67501

Energy (a.u): -571963.4580220 hartree

Table S10. Cartesian coordinates (Å) of Analogue **3i** optimized at the B3LYP/6-31+G* level

	X	Y	Z
F	-0.38384	2.36314	1.83873
O	-2.43208	1.58517	0.80808
F	-0.98285	3.20530	-0.24963
N	-0.41194	0.80442	-0.08576
N	1.19821	-1.33216	0.86758
C	0.96911	0.70660	-0.41554
C	1.77930	-0.35683	0.09349
C	-1.35999	-0.13331	-0.28180
C	3.18134	-0.36372	-0.20111
C	-1.19116	-1.34618	-0.98123
H	-0.20129	-1.51485	-1.37758
C	-2.60623	0.36255	0.28986
C	1.55177	1.71684	-1.16111
H	0.93279	2.53110	-1.50555
C	3.73828	0.67924	-0.98735
H	4.79869	0.66681	-1.20458
C	-3.84664	-0.24723	0.35554
H	-4.59971	0.34213	0.86146
C	3.95707	-1.42570	0.33805
H	5.01961	-1.45802	0.13329
C	-2.12399	-2.34019	-1.22216
H	-1.74988	-3.18323	-1.79183
C	2.93532	1.69734	-1.45143
H	3.35765	2.49993	-2.03988
C	1.96403	-2.30113	1.35822
H	1.46392	-3.04204	1.96804
C	3.35691	-2.38845	1.11730
H	3.92679	-3.20113	1.54459
C	-4.22931	-1.50143	-0.14148
H	-5.26303	-1.76965	0.04224
C	-3.47634	-2.43239	-0.84246
H	-3.98947	-3.33723	-1.14286
B	-1.00797	2.08140	0.61456

Energy (a.u): -643674.6435811 hartree

HOMO and LUMO orbitals calculation

DFT-B3LYP-6 Calculations of Boron-aminotropones:

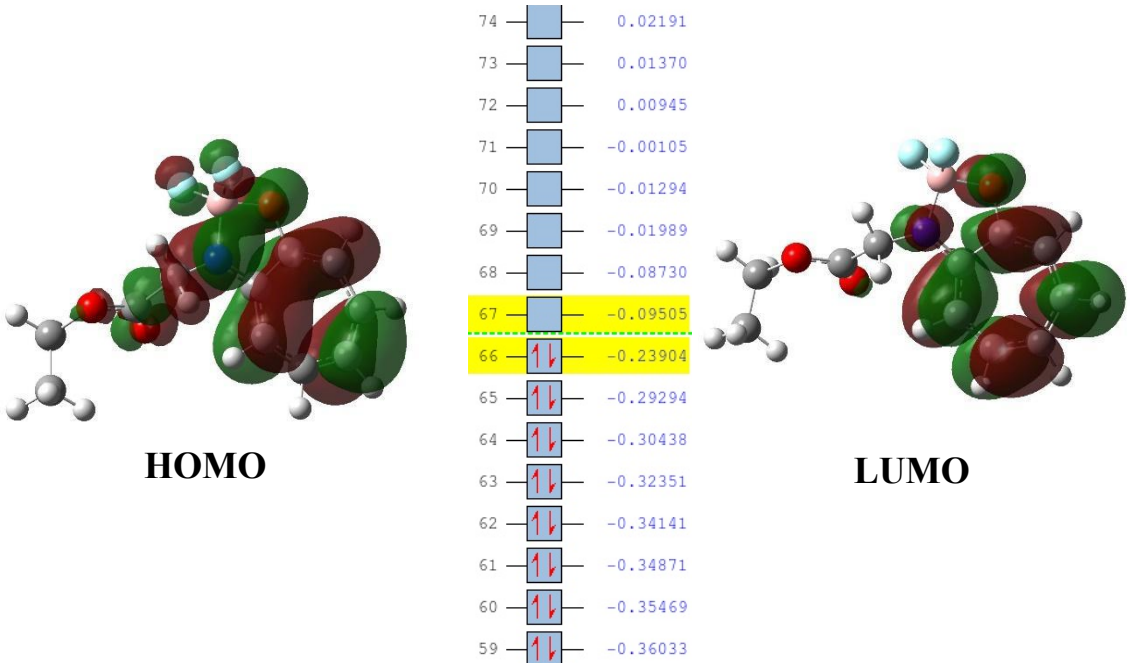

Figure S76: Optimized structure and HOMO- LUMO energy (atomic unit in hartree) of boron aminotropone (**3a**)

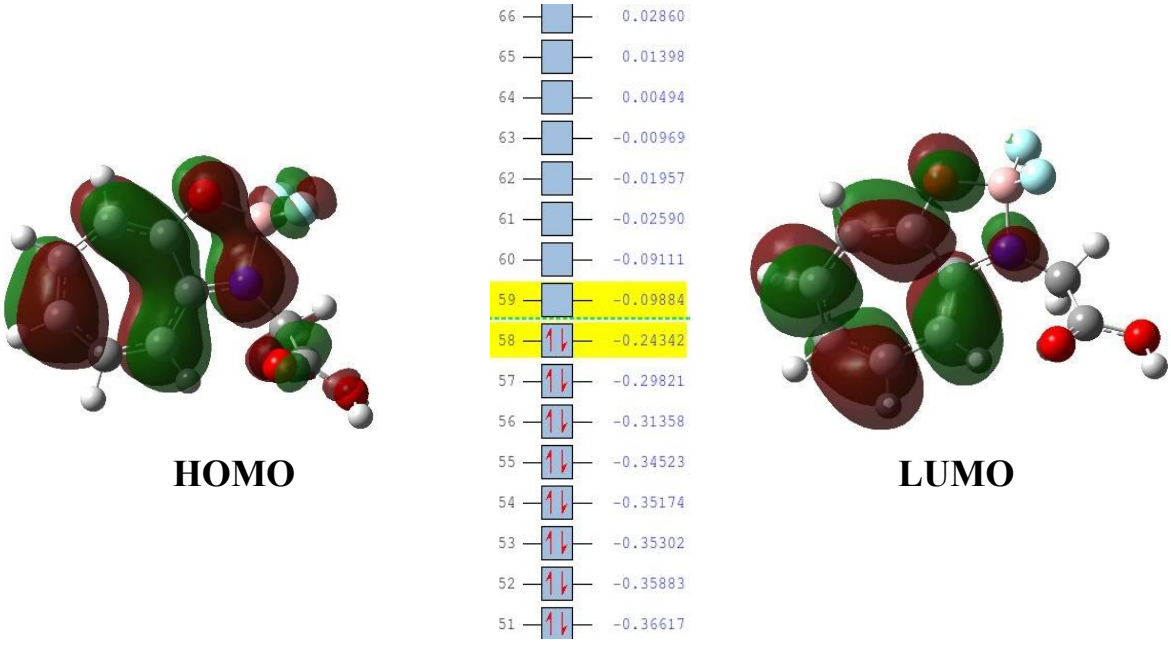

Figure S77: Optimized structure and HOMO- LUMO energy (atomic unit in hartree) of boron aminotropone (**3a-OH**)

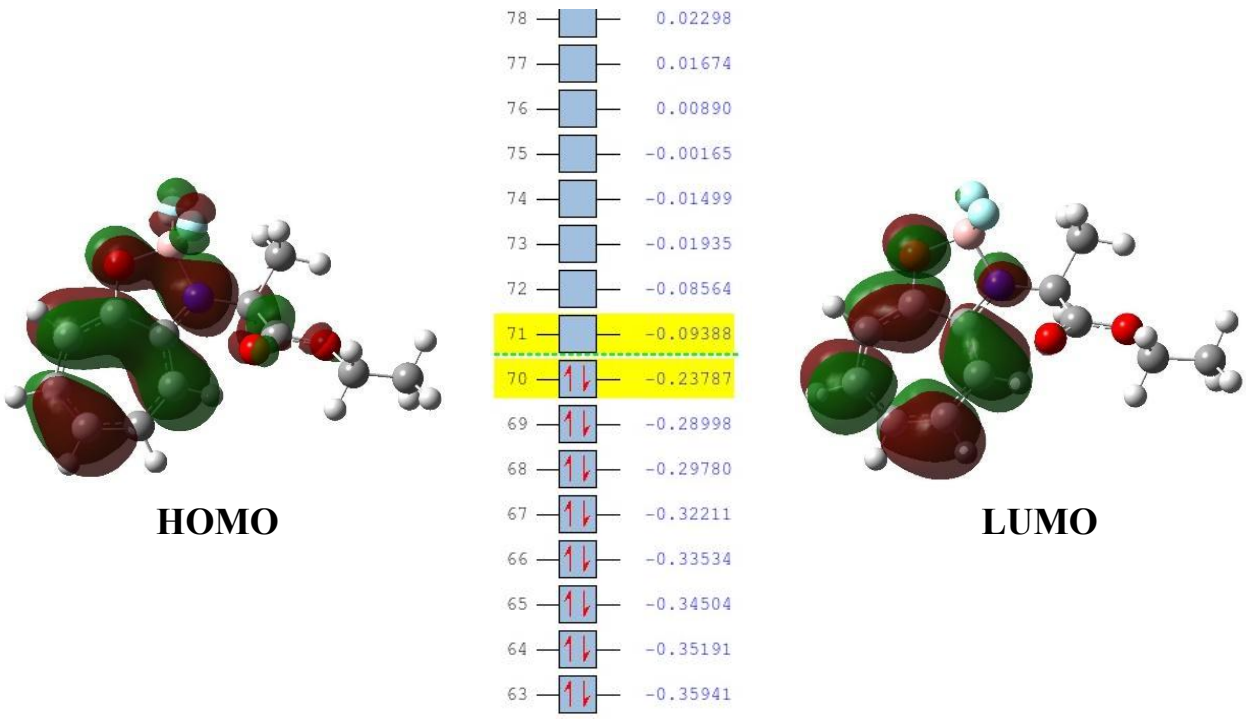

Figure S78: Optimized structure and HOMO- LUMO energy (atomic unit in hartree) of boron aminotropone (**3b**)

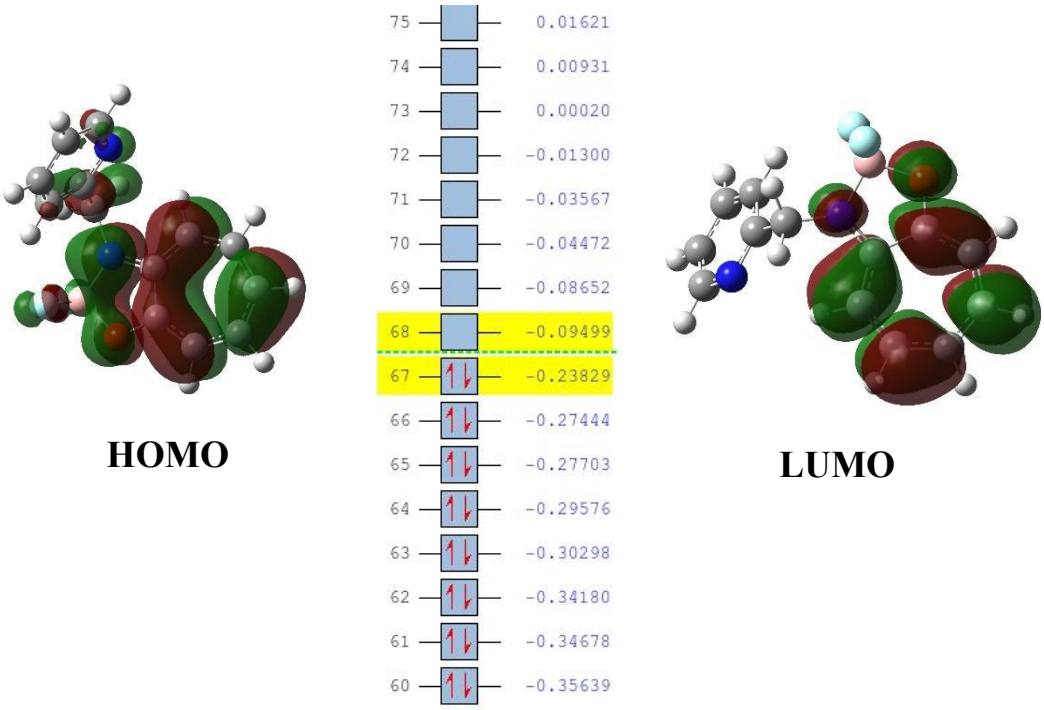

Figure S79: Optimized structure and HOMO- LUMO energy (atomic unit in hartree) of boron aminotropone (**3h**)

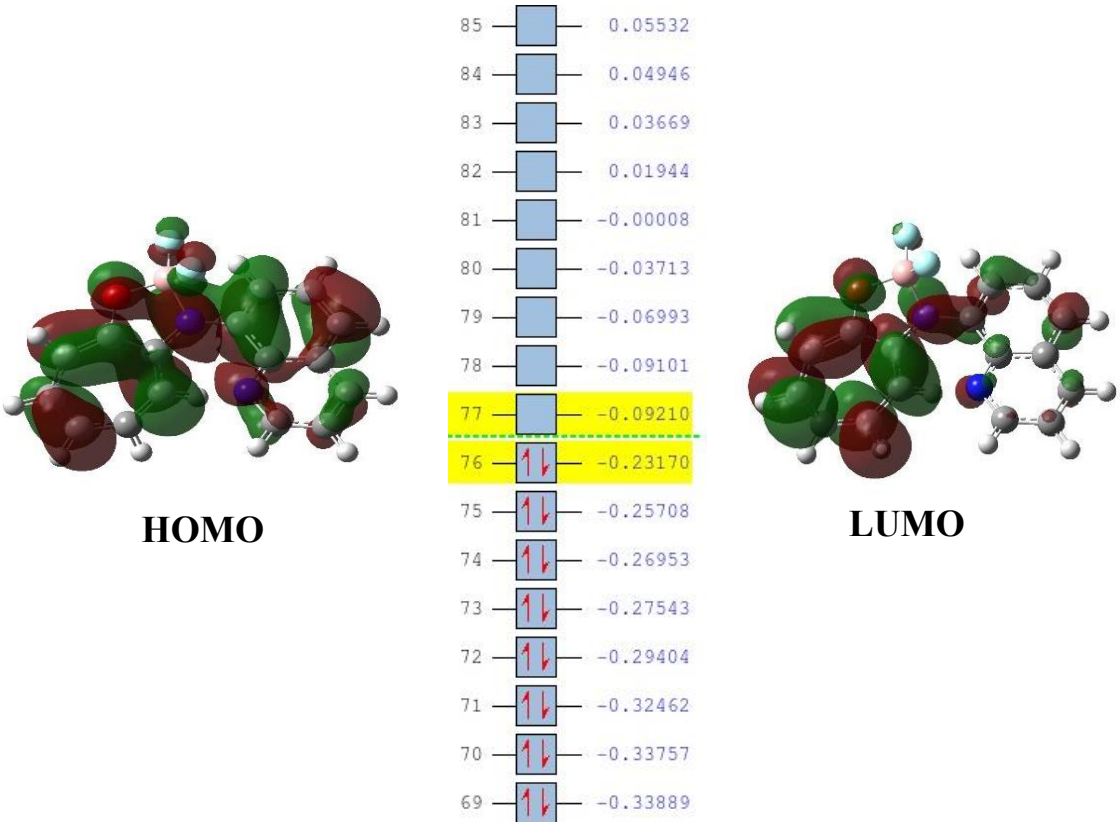

Figure S80: Optimized structure and HOMO- LUMO energy (atomic unit in hartree) of boron aminotropone (**3i**)

HOMO and LUMO orbitals DFT calculations

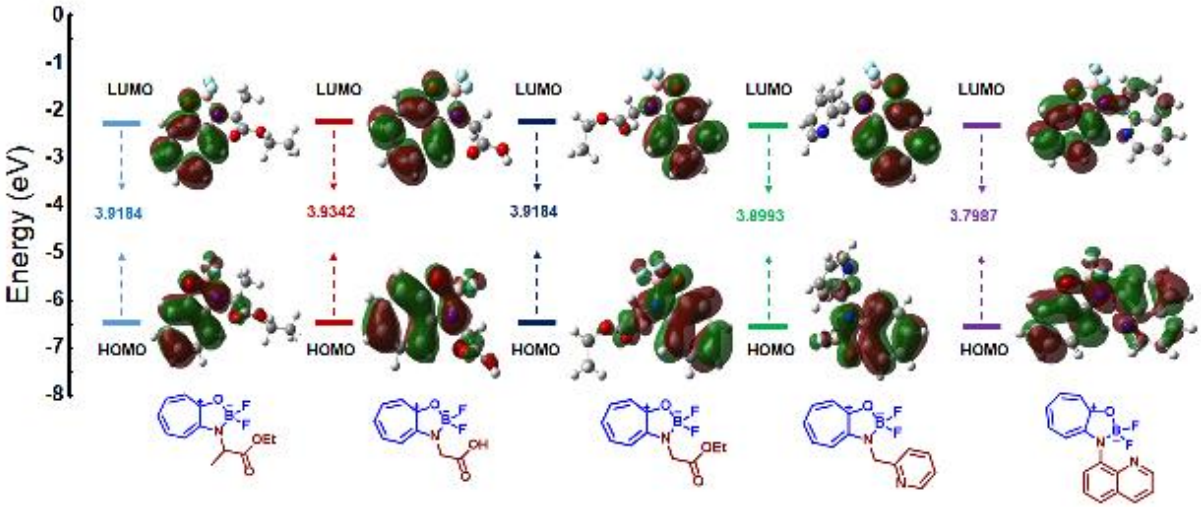

Figure S81: Optimized structure and HOMO- LUMO energy gap (atomic unit in eV) of boron aminotropone (**3a, 3a-OH, 3b, 3h, 3i**) at B3LYP/6-31+G* level of theory in vacuum.

Table-S11: Calculated HOMO and LUMO gap at B3LYP/6-31+G* level of theory in vacuum.

Analogue	Substituent	HOMO (eV)	LUMO (eV)	Δ (eV)	φ_f
3a	Gly	-6.5057	-2.5872	3.91844	0.15
3b	Ala	-6.4703	-2.5518	3.9184	0.13
3h	Picolylamine	-6.4831	-2.5837	3.8993	0.14
3i	AQ	-6.3048	-2.5061	3.7987	0
3j	Gly-OH	-6.6237	-2.6895	3.9342	0.02

23. Comparative N-B bond length studies

Table S12. Comparative bond length studies of compound 3a with reported BODIPY analogues.

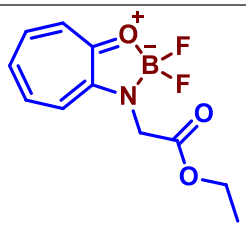

Synthesized compound

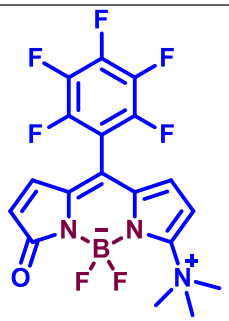

Model BODIPY

Chem. Commun., 2017, **53**, 1096-1099

3a	**Bond length(3a)**	**Model BODIPY**	**Bond length (M.B)**
N_1—B_1	1.5331Å	N_1—B_1	1.5265Å
O_1—B_1	1.4754Å	N_1—B_1	1.5797Å
B_1—F_1	1.3800Å	B_1—F_1	1.4046Å
B_1—F_2	1.3790Å	B_1—F_2	1.3808Å

24. Cyclic Voltammetry studies

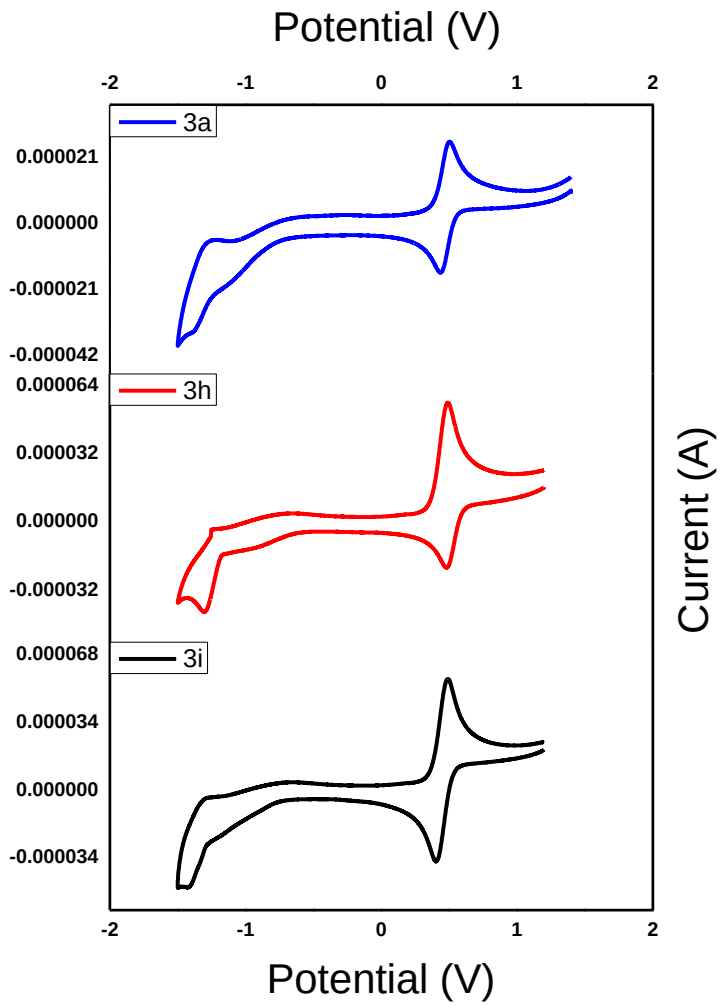

Figure S82. Cyclic voltammograms of 1mM (**3a**, **3h**, **3i**) measured in acetonitrile solution containing $TBPF_6$ as the supporting electrolyte and ferrocene as standard at room temperature. Glassy carbon electrode as a working electrode and scan rate 100mV.

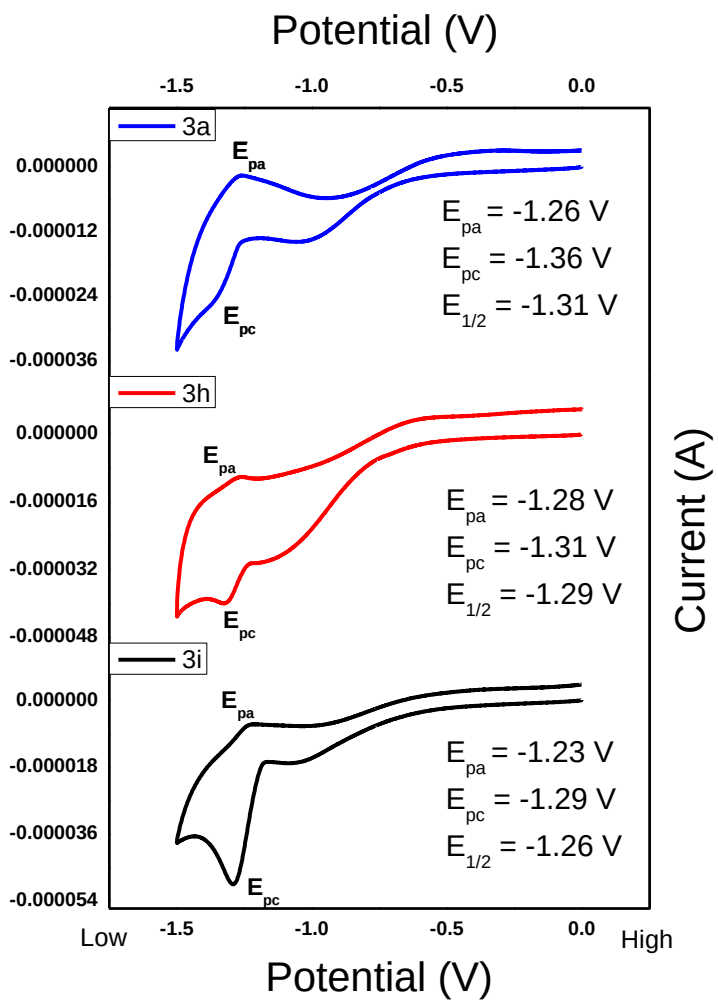

Figure S83. Cyclic voltammograms of 1mM (**3a**, **3h** & **3i**) measured in acetonitrile solution containing $TBPF_6$ as the supporting electrolyte at room temperature. Glassy carbon electrode as a working electrode and scan rate 100mV/s.